2019

Interactions among land cover, disturbance, and productivity across Arctic-Boreal ecosystems of Northwestern North America from remote sensing

BOSTON UNIVERSITY

GRADUATE SCHOOL OF ARTS & SCIENCES

Dissertation

INTERACTIONS AMONG LAND COVER, DISTURBANCE, AND PRODUCTIVITY ACROSS ARCTIC-BOREAL ECOSYSTEMS OF NORTHWESTERN NORTH AMERICA FROM REMOTE SENSING

by

JONATHAN ALEXANDER WANG

B.S., Brown University, 2010

Submitted in partial fulfillment of the

requirements for the degree of

Doctor of Philosophy

2019

Approved by

First Reader _____

Mark Friedl, Ph.D.
Professor of Earth and Environment

Second Reader _____

Curtis Woodcock, Ph.D.
Professor of Earth and Environment

Third Reader _____

Lucy Hutyra, Ph.D.
Associate Professor of Earth and Environment

ACKNOWLEDGMENTS

These studies were done as part of NASA's Arctic-Boreal Vulnerability Experiment (ABoVE). Resources supporting this work were provided by the NASA High-End Computing Program through the NASA Center for Climate Simulation at Goddard Space Flight Center. This material is based upon work supported by a National Science Foundation Graduate Research Fellowship under Grant No. DGE-1247312 and by NASA ABoVE grant Nos. NNX17AE74G and NNX15AU63A.

I cannot begin to enumerate all the friends, family, classmates, colleagues, kind strangers, administrative staff, and role models that have provided me the emotional, mental, and intellectual support necessary to complete this work. I have had countless incredible opportunities to grow as a scientist and as a person and I owe whatever success I have achieved to the myriad inspirations that my earnest and motivated colleagues have provided throughout this half decade. It's only by the generosity of those around me that I have this chance to participate fully in the scientific community and I will always be grateful for that. I especially appreciate the many mentors who have kindly taken time to share with me their experiences as I struggled over my career path. I particularly would like to acknowledge my loving family, my patient partner Carol Jin Jin Chiu, the ABoVE community, the Department of Earth and Environment at Boston University, the Biogeoscience program at Boston University, the Plants and Climate journal club at Harvard University, the 2015 class of Fluxcourse, the Student Airborne Research Program, my committee, and especially my main advisor, Mark Friedl, and the Land

Cover and Surface Climate research group. You're an eclectic and charming bunch. Thank you for your patience, inspiration, and support.

Furthermore, this work is built on the backs of countless IT professionals, systems engineers, field technicians, and bored programmers who contribute prolifically to stackoverflow.com. In particular, countless hours of assistance from the support staff the NASA's NCCS and BU's RCS groups have bridged the gaps between what I intend to do and what is possible with lots of computers. My work was made possible only through their heroic efforts.

INTERACTIONS AMONG LAND COVER, DISTURBANCE, AND PRODUCTIVITY ACROSS ARCTIC-BOREAL ECOSYSTEMS OF NORTHWESTERN NORTH AMERICA FROM REMOTE SENSING

JONATHAN WANG

Graduate School of Arts and Sciences, 2019

Major Professor: Mark Friedl, Professor of Earth and Environment

ABSTRACT

Arctic and Boreal ecosystems are experiencing accelerated carbon cycling that coincides with trends in the normalized difference vegetation index (NDVI), a widely used remotely sensed proxy for vegetation productivity. Meanwhile, a variety of processes are extensively altering Arctic-Boreal land cover, complicating the relationship between NDVI and productivity. Because high-quality information on land cover is lacking, understanding of relationships among Arctic-Boreal greenness trends, productivity, and land cover change is lacking.

Multidecadal time series of moderate resolution (30 m) reflectance data from Landsat and high resolution (<4 m) imagery were used to map annual cover and quantify changes in land cover over the study domain of NASA's Arctic-Boreal Vulnerability Experiment. Results identify two primary modes of ecosystem transformation that are consistent with increased high latitude productivity: (1) in the Boreal biome, simultaneous decreases in Evergreen Forest area and increases in Deciduous Forest area

caused by fire and harvest; and (2) climate change-induced expansion of Arctic Shrub and Herbaceous vegetation.

Land cover change imposes first-order control on the sign and magnitude of NDVI trends. Over a quarter of NDVI trends were associated with land cover change. Relative to locations with stable land cover, areas of land cover change were twice as likely to exhibit statistically significant trends in Landsat-derived NDVI. The highest magnitude trends were concentrated in areas of forest disturbance and regrowth and shrub expansion, while undisturbed land showed subtler, but widespread, greening trends. Based on Orbiting Carbon Observatory-2 data, sun-induced fluorescence, a proxy for productivity, reflected relationships among land cover, disturbance age, and productivity that were not fully captured in NDVI data.

In contrast with NDVI, time series of aboveground biomass provide physically-based measures of productivity in forests. Using Landsat-based land cover and reflectance and ICESat lidar data, aboveground biomass was mapped annually across the study domain. Most forests showed increasing biomass, with wildfires imposing substantial interannual variability and harvest imposing steady biomass losses. This dissertation provides new information on how disturbances are driving land cover and productivity change across Arctic-Boreal northwestern North America and reveals insights regarding the interpretation of remote sensing observations in these biomes.

TABLE OF CONTENTS

LIST OF TABLES

LIST OF FIGURES

LIST OF ABBREVIATIONS

ABoVE.....Arctic-Boreal Vulnerability Experiment

ABR .....Arctic-Boreal Region

AGB .....Aboveground Biomass

ASTER..... Advanced Spaceborne Thermal Emission and Reflection Radiometer

AVHRR..... Advanced Very High Resolution Radiometer

CO_2.....Carbon Dioxide

DF ..... Deciduous Forest

EF .....Evergreen Forest

EPA .....Environmental Protection Agency

ETM+..... Enhanced Thematic Mapper Plus

EVI..... Enhanced Vegetation Index

FPAR.....Fraction absorbed Photosynthetically Active Radiation

GBM .....Gradient Boosted Machines

GIMMS3g.....Global Inventory Modeling and Mapping Studies Third Generation

GLAS .....Geoscience Laser Altimeter System

GPP .....Gross Primary Productivity

Herb.....Herbaceous

ICESat..... Ice, Cloud, and Land Elevation Satellite

LAI..... Leaf Area Index

Lidar.....Light Detection and Ranging

MODIS.....Moderate Resolution Imaging Spectroradiometer

NASA.....National Aeronautics and Space Administration

NDVI.....Normalized Difference Vegetation Index

NEE.....Net Ecosystem Exchange

OCO-2..... Orbiting Carbon Observatory 2

PRI .....Photochemical Reflectance Index

RF.....Random Forest

SH .....Shrub

SIF.....Sun-Induced Fluorescence

SRTM..... Shuttle Radar Topography Mission

TM.....Thematic Mapper

XGBoost ..... Extreme Gradient Boosted Machines

INTRODUCTION

1.1 Background

Earth is experiencing substantial climate change due to steady increases in the atmospheric concentration of greenhouse gases (IPCC AR5 SPM). However, the climate of high northern latitudes is warming at a substantially higher pace via a system of physical climate feedbacks called "Arctic Amplification" (Chapin et al., 2005; Pithan and Mauritsen, 2014; Serreze et al., 2009; Xia et al., 2014). Because Arctic and Boreal ecosystems are critical and vulnerable components of the global climate system (Bonan, 2008; Bonan et al., 1992; Chapin et al., 2000), it is crucial to understand how changes in these high northern latitude biomes influence climatic processes. For example, aircraft measurements have reported a marked increase in the seasonality of atmospheric CO_2 in high northern latitudes over the last half century, which has been interpreted to reflect increases in northern ecosystem productivity (Graven et al., 2013; Keeling et al., 1996). Multiple mechanisms for this latitudinally-dependent shift in carbon exchange have been debated, including climate change, changes in vegetation cover, post-disturbance succession, land use, and CO_2 fertilization, among others (Forkel et al., 2016; Gray et al., 2014; Yuan et al., 2018; Zeng et al., 2014; Zhu et al., 2016; Zimov et al., 1999). Irrespective of the specific mechanisms causing this change, the observed trend toward increased CO_2 seasonality is likely broadly driven by increased photosynthetic rates, although some studies also suggest a role for increased rates of ecosystem respiration (Piao et al., 2008; Randerson et al., 1999; Thomas et al., 2016).

In addition to impacting the productivity of high latitude ecosystems, Arctic Amplification and warming also results in a variety of indirect changes to Arctic-Boreal ecosystems by altering disturbance regimes, which modify the demography of Boreal forests and Arctic tundra, and additionally by inducing shrub expansion in the Arctic tundra (Johnstone et al., 2010; Kasischke et al., 1995; Sturm et al., 2001; Tape et al., 2006). These land surface changes can substantially alter carbon uptake and biogeophysical feedbacks by influencing the extent and composition of vegetation types at continental scales (Elmendorf et al., 2012; Goulden et al., 2011; Randerson et al., 2006; Rogers et al., 2013; Zhang et al., 2013; Zimov et al., 1999). It is likely that all these land surface changes affect rates of large-scale ecosystem-atmosphere carbon exchange, although many of these impacts remain unquantified and therefore require more study.

Analyzing change in Boreal and Arctic ecosystem properties like land cover is challenging because of their vast geographic extent and remoteness, making field studies that can represent the domain relatively expensive and difficult to conduct. Therefore, technologies such as satellite remote sensing, which can characterize synoptic-scale processes over time, are crucial to improving our understanding of these ecosystems and how they are changing. However, interpretation of remote sensing data can be challenging since reflected or emitted electromagnetic radiation observed by spectroradiometers are only indirectly related to characteristics of interest on the ground, especially when relatively few sources of field data are available to calibrate and assess remote sensing-based observations of ecosystem properties and change. Understanding

and improving the information provided by satellite remote sensing is therefore important to address key open questions in Arctic-Boreal carbon and land change science.

1.2 Land Cover in Arctic-Boreal Biomes

Understanding the degree to which land cover changes impact how Arctic and Boreal ecosystems interact with the global and regional climate systems requires accurate quantification of the distribution and changes in land cover (Chapin et al., 2000). Current land cover products tend to be too spatially coarse, geographically limited, or do not provide sufficiently realistic information related to change (Bartsch et al., 2016; Song et al., 2018; Walker et al., 2005) to accurately characterize the highly dynamic and spatially heterogeneous landscapes of Arctic and Boreal biomes. Moderate spatial resolution land cover data (approx. 30 m) have been identified as sufficient to capture carbon dynamics in heterogeneous tundra systems (Treat et al., 2018), yet geographically extensive land cover products at this scale have yet to be produced with sufficient thematic detail (Bartsch et al., 2016). Efforts to map forest cover change often ignore forest phenological type (i.e., deciduous vs evergreen), which limits our understanding of how transitions in plant functional types might impact Boreal productivity (Hansen et al., 2013). Hence, there exists a fundamental knowledge gap in the nature, extent, and rate of land cover change in Arctic and Boreal ecosystems, particularly at a spatiotemporal resolution sufficient to capture both major and subtler cover changes, and the slow rates of growth.

Disturbance, defined here as any abrupt ecosystem process that results in a change in underlying land cover and ecosystem function, is widespread and common in high-

latitude ecosystems. Over 10% of Canada's Boreal forests have experienced logging, fire, or other disturbances over the last 30 years (White et al., 2017), while substantial areas of the Arctic tundra are undergoing shrub encroachment, the warming-induced proliferation of woody vegetation in previously herbaceous-dominated land (Elmendorf et al., 2012; Myers-Smith et al., 2011; Sturm et al., 2001; Tape et al., 2006). In areas of sporadic or discontinuous permafrost, thawing and degradation of permafrost has caused loss of evergreen forests and expansion of wetlands at a scale comparable to that of fire disturbance (Carpino et al., 2018; Gibson et al., 2018; Helbig et al., 2016). Following stand-replacing disturbances, forests continue to change via processes of recovery and succession (Johnstone et al., 2010).

In addition to modifying fire regimes, evidence suggests that climate warming is leading to increased frequency of insect infestations and drought-induced mortality in Boreal forests (Eamus et al., 2013, 2013; Hogg et al., 2008; Ma et al., 2012; Volney and Fleming, 2000). These disturbances afflict forests in two broad modes - as a gradual, or "press", disturbance, and as an abrupt, or "pulse" disturbance, both of which have very different potential impacts on carbon uptake and biomass accumulation (Grosse et al., 2011). In the aggregate, field and small-area studies throughout the Arctic-Boreal zone provide multiple lines of evidence that natural disturbance, human activity, and climate change are jointly causing substantial perturbations in land cover change across high-latitude ecosystems. Given that a growing body of evidence suggests that recent rates of fire in Boreal forests is significantly different from pre-historical rates, it is likely that the distribution of land cover across Boreal and Arctic ecosystems is out of steady state and

experiencing a fundamental shift in terms of the extend and geographic distribution of plant functional types (Boucher et al., 2017; Kelly et al., 2013).

Systematic changes in high latitude land cover have significant implications for coupled interactions between Arctic and Boreal ecosystems and both regional and global climate. To illustrate this, Table 1.1 highlights the range in seasonal land surface albedo, which influences regional climate by altering radiation budgets, and peak growing season net ecosystem exchange, which influence global climate via carbon cycle impacts, across key Arctic and Boreal land cover types. A shift of tundra herbaceous land cover to tundra shrubs is associated with a decrease in land surface albedo of approximately 18%, potentially creating a regional warming feedback (Loranty and Goetz, 2012; Zhang et al., 2018, 2013) while at the same time substantially increasing carbon storage by a factor of 5, which, in turn, would impose a negative feedback on warming on a global basis (Fox et al., 2008). Because these climate feedbacks are both substantial and opposite in sign, understanding the net climate forcing of tundra shrub expansion requires careful characterization of shrub expansion and the associated impacts on surface energy and carbon budgets. Similarly, Boreal deciduous forests cycle carbon at nearly twice the rate of Boreal evergreen forests, exhibit considerable seasonality in photosynthetic activity, and have a nearly 50% higher land surface albedo (Betts and Ball, 1997; Black et al., 2000; Dunn et al., 2007). These competing feedbacks occur at different scales (i.e. regional vs global), which complicates the evaluation of the net feedback of various land change processes. Further, disturbance and age structure in Boreal forests introduce

substantial variability to carbon exchange rates (Goulden et al., 2011; Pugh et al., 2019; Zimov et al., 1999).

Shifts in the demography and distribution of plant functional types resulting from disturbance, climate change, and human activity therefore have complex, multifaceted, and potentially large impacts on how Arctic and Boreal ecosystems influence the global climate system. Land cover, as a general construct, captures and abstracts a wide array of land surface properties into a single and easily understood description of the land surface. Models and algorithms that are used to assess changes in Earth's productivity generally utilize land cover as a fundamental input to parameterize a large number of surface properties (Bonan, 2008; Fisher et al., 2018; Myneni et al., 1997b; Running et al., 2004), so ignoring changes in high-latitude land cover, as most recent studies do, can substantially bias results (Chen et al., 2019; Zhang et al., 2008).

1.3 High-latitude Greening and Browning

One of the key changes observed in northern ecosystems is apparent widespread "greening" and "browning" over large areas that have been observed in time series of spectral vegetation indices such as the normalized difference vegetation index (NDVI) (Myneni et al., 1997a). Because spectral vegetation indices are correlated with important vegetation properties, indices such as the NDVI are commonly used as remotely-sensed proxies for productivity, leaf area, or biomass (Carlson and Ripley, 1997; Gamon et al., 1995; Myneni et al., 2001; Xiao, 2004), and observed changes in NDVI in northern

hemisphere ecosystems have been proposed as potential explanations for increased northern productivity (Bunn and Goetz, 2006; Myneni et al., 1997a).

However, as a tool for studying productivity, NDVI is fraught with complications. As an index, it does not have a unique physical relationship with productivity, but is widely used to parameterize light use efficiency models (Aber and Federer, 1992; Mahadevan et al., 2008; Running et al., 2004; Xiao, 2004) or in combination with field data that can be used for calibration (Berner et al., 2018; Park et al., 2016). NDVI measurements are also strongly affected by non-vegetated components of the land surface, such as surface water, which strongly reduces observed NDVI (Beget and Di Bella, 2007; Raynolds and Walker, 2016). Therefore, coarse spatial resolution pixels that include mixtures of land cover types present challenges for interpreting changes in NDVI (Badgley et al., 2017; Raynolds and Walker, 2016). Perhaps most significantly, different plant functional types vary substantially in terms of their NDVI values in ways that have little direct relationship with productivity (e.g. broadleaf forests and grasslands can have similar NDVI values but widely different productivity) (DeFries and Townshend, 1994). Finally, both anthropogenic and natural disturbance events, particularly those that result in changes in the underlying land cover, are relatively common at high latitudes and directly influence observed trends in NDVI (Sulla-Menashe et al., 2018). Because most studies that have examined trends in NDVI have used relatively coarse spatial resolution imagery (i.e., 100s of m to 10s of km), sub-pixel variation in land cover following disturbance (which substantially impacts observed NDVI trends) is often not accounted for, especially for smaller, but potentially widespread, forest disturbances like seismic

lines or permafrost thaw (Alcaraz-Segura et al., 2010; Beck and Goetz, 2011; Ju and Masek, 2016). The net impact of sub-pixel disturbance and land cover depends on the sensor and spatial resolution that is used, adding considerable uncertainty to NDVI trend interpretation (Alcaraz-Segura et al., 2010; Guay et al., 2014). Hence, the underlying land cover affects not only the absolute value of NDVI, but also the way it is interpreted in terms of climatic or ecological meaning, and uncovering these impacts requires careful characterization with sufficiently high spatial resolution imagery.

1.4 Alternatives to NDVI

Despite its heavy utilization, NDVI provides a highly simplified measure of ecosystem processes, particularly since its interpretation depends heavily on the underlying land cover. Research is ongoing to develop other remote sensing methods and proxies that capture ecosystem processes such as productivity at synoptic scales, including additional spectral indices (Gamon et al., 2016, 1992; Garbulsky et al., 2011), hyperspectral data (Schimel et al., 2015), multi-angle observations (Hall et al., 2008; Hilker et al., 2013), and derived land surface data products. Sun-induced fluorescence (SIF) from satellite remote sensing has recently emerged as a promising proxy of photosynthesis at synoptic scales (Damm et al., 2010; Frankenberg et al., 2014; Grace et al., 2007; Meroni et al., 2009), with particular ability to capture Boreal forest and Arctic tundra carbon dynamics (Luus et al., 2017; Walther et al., 2016). A key feature of SIF is that it provides measurements with physical units that quantify the flux of emitted

photons as a by-product of photosynthesis. Hence, values from SIF can be compared across biomes and land cover types in ways that NDVI and other spectral indices cannot.

1.5 Aboveground Biomass in Boreal Forests

One of the most direct ways of measuring carbon uptake in ecosystems with remote sensing is by estimating stocks and changes in aboveground biomass (AGB) (Lu, 2006). Because net accumulation of AGB is a direct realization of the combined effects of annual net productivity and disturbance, estimates of change in AGB can be used as direct indicators of changes in carbon balance (Botkin and Simpson, 1990). In recent years, advances in lidar remote sensing and machine learning techniques have enabled the use of surface reflectance time series to map AGB at synoptic scales and over time (Baccini et al., 2012, 2004; Lefsky et al., 2002; Wulder et al., 2012). Such multi-sensor techniques have been used in the tropics to estimate net carbon fluxes associated with processes such as deforestation and provide a valuable monitoring technique for understanding changes in ecosystem services in the world's forests (Baccini et al., 2017).

The carbon budget of Boreal forests is an important component of the global carbon cycle, but its interannual variability and total stocks remain highly uncertain (Malhi et al., 1999; Neigh et al., 2013). Most studies rely on long-term forest surveys, but these are hard to scale and rarely capture the influence of disturbances (Botkin and Simpson, 1990). Widespread drought-induced tree mortality, insect infestation, low-intensity fires, and partial logging impact Boreal forests in ways are difficult to capture by land cover classification or analysis of NDVI trends (Eamus et al., 2013; Hogg et al.,

2008; Kasischke et al., 1995; Ma et al., 2012; Volney and Fleming, 2000), and high quality information related to large scale dynamics in Boreal carbon budgets is lacking. Field data are essential for calibrating remote sensing-based models of biomass, but are usually limited in both extent and density due to the cost of conducting field studies in remote and vast areas like the Boreal forest. However, recent advances in the availability of lidar data and computational techniques have allowed researchers to connect field-based allometric information with lidar remote sensing data (Wulder et al., 2012), and have improved understanding of carbon stocks across Boreal forests derived from time series of remote sensing data (Matasci et al., 2018a, 2018b). At the same time, recent studies of Boreal forest biomass have not incorporated disturbance and land cover change explicitly, resulting in potential biases (Matasci et al., 2018a). Information on land cover and disturbance history are essential to mapping biomass because allometric equations that relate Boreal forest structure to AGB vary as a function of land cover properties such as by forest type or burned status (Asner et al., 2009; Drake et al., 2003; Neigh et al., 2013; Wang et al., 2013). Hence, there exists a need for methods that estimate dynamics in Boreal forest AGB that are informed by land cover and an understanding of the interactions among AGB, land cover change, disturbance.

1.6 Research Objectives and Dissertation Outline

Ignoring land cover change introduces substantial bias into the interpretation of remote sensing-based metrics of productivity. Land cover remains a fundamental input to algorithms and models in Earth System Science, yet studies utilizing models at large

scales often over-simplify land cover or ignore land cover change altogether. Recent advances in computational techniques have enabled efficient processing of large data volumes that are required to derive data products from moderate resolution data like Landsat. However, these advances have not been fully exploited to understand how land cover and carbon dynamics are changing in high latitude ecosystems. In this dissertation we address this need by using time series of moderate resolution remote sensing data from Landsat 5 and Landsat 7 to characterize annual land cover and multidecadal land cover change at continental scale and explore how these land cover changes inform our understanding of carbon dynamics in the Arctic-Boreal Region (ABR) of northwestern North America.

To address these objectives, this dissertation presents research conducted in the Core Study domain of NASA's Arctic-Boreal Vulnerability Experiment (ABoVE) across Alaska and northwestern Canada. The study region encompasses the Core Study Domain of ABoVE project, which includes the majority of Alaska and northwestern Canada and covers 4.76×10^6 km^2, the equivalent of 5.2×10^9 30 m Landsat pixels (Fisher et al., 2018) (Figure 1.1). To facilitate the analysis, all data were gridded into tiles (180 km on a side) with an Albers Equal Area projection centered on the ABoVE Core Study Domain. We used ecoregions mapped by the US Environmental Protection Agency to distinguish between Boreal and Arctic biomes and between ecoregions within the study domain (https://www.epa.gov/eco-research/ecoregions-north-america). Ocean pixels were excluded using a manually-edited land-ocean mask based on the 10 m ocean mask

from Natural Earth Data (Kelso and Patterson, 2010). This study domain defined the scope of all the work in this dissertation.

Following this introductory chapter, the dissertation is organized into four parts. In Chapter Two, we use a 31-year time series of Landsat data in combination with extensive high-resolution imagery to map annual 30 m land cover and estimate the extent of land cover changes across the spatiotemporal domain. In Chapter Three, we combine the land cover and land cover change information from Chapter Two to characterize how statistically significant greening trends, derived from time series of Landsa-based NDVI, are related in extent and magnitude to land cover, land cover change, and disturbance processes. In Chapter Four, we incorporate lidar data from the Geoscience Laser Altimeter System (GLAS) instrument to annually map 30 m aboveground biomass density and characterize the variability in time series of AGB as a function of ecoregion and disturbance process. In Chapter Five, we summarize the major findings of this research, identify key implications, and discuss future directions.

Table 1.1 | Variability in carbon and biophysical characteristics according to Boreal/Arctic land cover. Values are intended to provide rough order of magnitude estimates to demonstrate variability in land surface characteristics arising from differences in land cover. Values indicated are either averages derived from eddy covariance studies or values utilized in modeling studies. NEE refers to "Net Ecosystem Exchange", a measure of the flux of carbon between the atmosphere and the land surface; negative values refer to carbon uptake by the land surface. References: [1]Chapin et al. (2005); [2](Dunn et al., 2007); [3](Vourlitis and Oechel, 1999); [4] (Fox et al., 2008); [5](Black et al., 2000); [6](Betts and Ball, 1997)

Land Cover	Land Surface Albedo (Winter)	Land Surface Albedo (Summer)	Average Summer NEE (μmol CO_2 m^{-2} s^{-1})
Tundra Herbs	0.8(1)	0.17(1)	-0.545(3)
Tundra Shrubs	0.6(1)	0.15(1)	-2.813(4)
Deciduous Forest	0.182 (6)	0.156(6)	-5.025(5)
Evergreen Forest	0.132(6)	0.093(6)	-2.82(2)

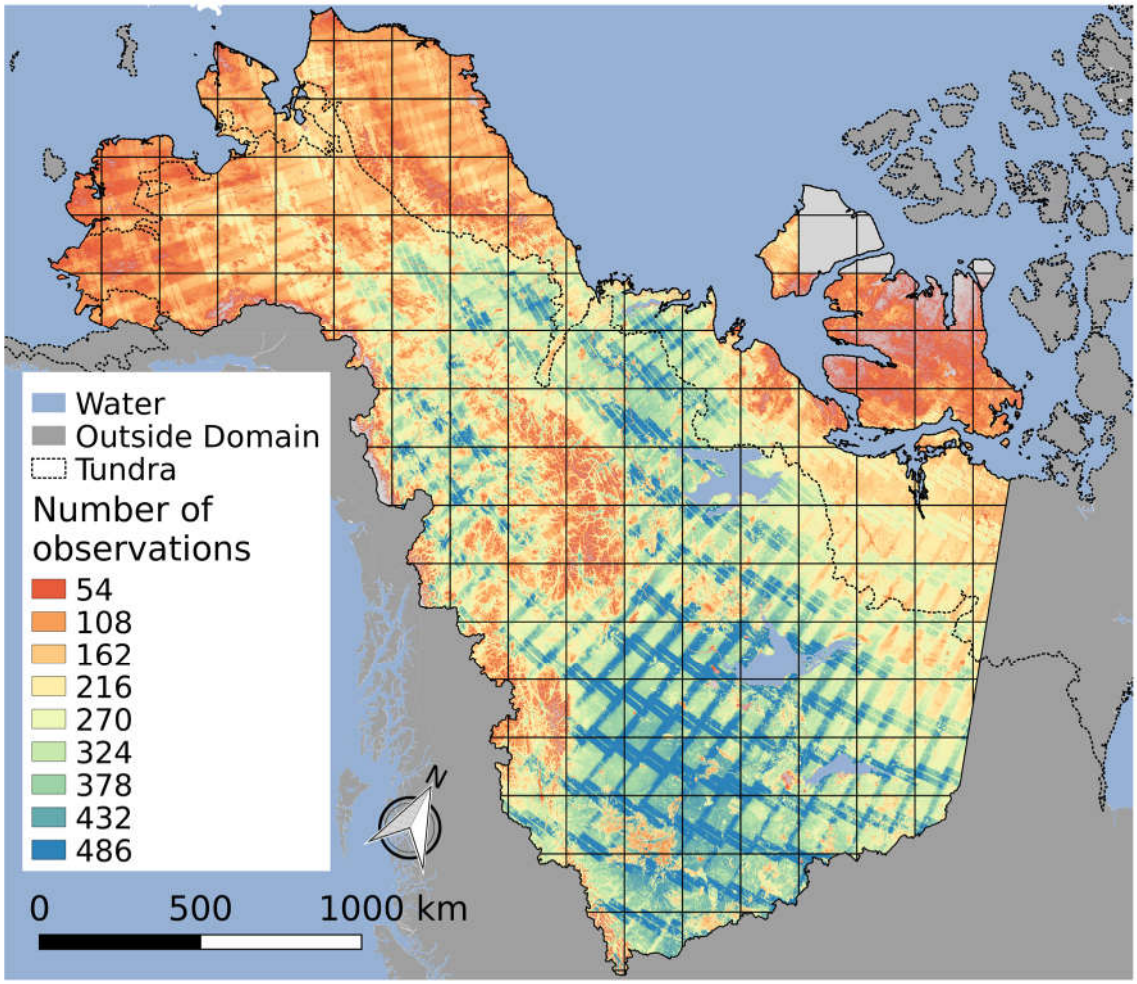

Figure 1.1 | Density of cloud-free and snow-free Landsat observations over the 1984-2014 period, as an average per 900 m^2 area in the Arctic-Boreal Vulnerability Experiment (ABoVE) Core Study Domain. Landsat observations are especially dense where multiple orbits overlap, resulting in additional observations in a given location per 16 day orbital repeat period. The orbital overlaps increase in frequency near the poles, where the orbits converge. The orbital convergence compensates for substantial cloud coverage at high latitudes and snow coverage in mountainous areas.

WIDESPREAD PLANT FUNCTIONAL TYPE TRANSITIONS ACROSS THE ARCTIC-BOREAL REGION OF NORTHWESTERN NORTH AMERICA CAUSED BY DISTURBANCE AND CLIMATE CHANGE.

2.1 Introduction

Rapid climate warming is changing the structure and composition of Arctic and Boreal biomes, influencing land cover both directly (e.g., via warming-induced shrub growth) and indirectly (e.g., by altering disturbance regimes) (Soja et al., 2007). In the Boreal biome, changes in climate and fire regimes, in addition to resource extraction, infrastructure development activities, and permafrost degradation, are inducing tree mortality and triggering successional processes (Carpino et al., 2018; Helbig et al., 2016; Williams et al., 2013). In the Arctic tundra, climate change, including warming and growing season length enhancement, is inducing woody shrub cover expansion (Elmendorf et al., 2012; Tape et al., 2006). These processes substantially change Arctic and Boreal land cover and, by extension, climate-ecosystem interactions in the Arctic-Boreal Region (ABR) via changes in albedo (Randerson et al., 2006), carbon exchange (Goulden et al., 2011; Zimov et al., 1999), and snow and permafrost dynamics (Zhang et al., 2013). For example, flask measurements collected from aircraft have shown that seasonality in atmospheric CO_2 in the mid- and high-latitude Northern Hemisphere has increased substantially over the last half century, suggesting large-scale changes in biome-wide ecosystem production (H. D. Graven et al., 2013; Keeling et al., 1996; Randerson et al., 1999). These measurements coincide with widespread increases in high-

latitude land surface greenness (a proxy for productivity) derived from remote sensing (Beck and Goetz, 2011; Myneni et al., 1997a). However, it is unclear to what degree these greening changes reflect changes in biomass or leaf area versus large scale transitions in the distribution of plant functional types. Given extensive and frequent disturbances in this region (White et al., 2017), a key factor that limits understanding of ecosystem change in the ABR is the lack of high quality land cover and land cover change data. Land cover products that are too coarse tend to mischaracterize changes resulting from disturbances (Ju and Masek, 2016) and those not designed for the Arctic tundra or too short in timescale are likely to misclassify slow changes in the Arctic tundra (Bartsch et al., 2016; Hermosilla et al., 2018). The Canadian Forest Service land cover products lack information on Alaska, which is a substantial portion of the ABoVE Core Study Domain (Wulder et al., 2008). Incomplete information on forest cover type (i.e. deciduous versus evergreen) precludes our ability to quantify the loss, regrowth, and transitions between evergreen and deciduous tree species in the Boreal forest biome at large spatial scales (Hansen et al., 2013; Song et al., 2018), which may be driving substantial changes in northern productivity (Augusto et al., 2015; Kimball et al., 2007, 2000).

Many studies have attempted to characterize land surface changes across the ABR using temporal trends of spectral indices like the normalized difference vegetation index (NDVI), but these techniques are unable to capture the multi-dimensional changes associated with shifts in dominant plant functional type, like changes in light use efficiency, seasonality, or albedo. Changes in land cover imply substantial potential

changes in these land surface characteristics. Analyses are likely to mischaracterize land surface changes if the underlying plant functional type has shifted due to disturbance or regrowth, but most studies assume constant land cover type. The potential regional-scale impacts of such changes are difficult to quantify without land cover information at the appropriate geographic extent, spatial resolution, or temporal domain.

Here, we use time series of medium spatial resolution (30 m) Landsat remote sensing data to classify annual land cover and land cover change (between 1984 and 2014) over the Core Study Domain of NASA's Arctic-Boreal Vulnerability Experiment (ABoVE), a 4.76 x 10^6 km^2 area of Alaska and northwestern Canada. These climate-sensitive areas are representative of the vulnerable forest and tundra ecosystems of northern high latitudes that are rapidly transforming in response to substantial climate change (Fisher et al., 2018). We incorporate spectral changes, climate, topography, and permafrost information to characterize annual land cover to understand how land cover has changed over the ABR in response to disturbances and climate change. Additionally, we incorporate manual interpretation of high resolution (<4 m) imagery to characterize the accuracy of our maps and quantify the uncertainty around change estimates over the domain. Using these data, we address the following questions:

(1) In the Boreal biome, what is the extent and spatial variability of forest loss, forest growth, and net shifts in forest phenological types (i.e. evergreen vs. deciduous) between 1984 and 2014?

(2) In the Arctic biome, what is the extent and spatial variability of Shrub and Herbaceous replacement of Barren land between 1984 and 2014?

(3) To what extent do certain major disturbance types (e.g. fires or logging) drive these plant functional type changes?

2.2 Methods

2.2.1 Overview

Our analysis used surface reflectance imagery from the Landsat 5 Thematic Mapper and Landsat 7 Enhanced Thematic Mapper+ to detect land cover change, classify land cover type, and to characterize change across NASA's Arctic-Boreal Vulnerability Experiment (ABoVE) study region, encompassing northwestern Canada and Alaska. Our workflow includes four main components: (1) break detection in time series of land surface reflectance to identify, per pixel, land cover change and time segments with stable land cover; (2) a semi-supervised classification approach that combines unsupervised clustering with supervised classification to maximize spectral separability and map statistical clusters across the domain; (3) interpretation of field photography and very high resolution imagery to assign land cover labels to statistical clusters; and (4) accuracy assessment using a design-based sample to correct for biases in area estimation arising from classification error. We estimate disturbance dates using the Continuous Change Detection and Classification (CCDC) algorithm (Zhu and Woodcock, 2014) and map land cover using our semi-supervised approach applied to 31 years (1984 – 2014) of remote sensing data. Using this framework, we map land cover for each year and net

land cover change over the study period (1984-2014), focusing on expansion and contraction in the area occupied by Evergreen Forests, Deciduous Forests, Shrublands, and Herbaceous land cover.

2.2.2 Model Input Data

The primary source of data for land cover and disturbance mapping is time series of surface reflectance and brightness temperature from Landsat 5 Thematic Mapper and Landsat 7 Enhanced Thematic Mapper+ (Woodcock et al., 2008). The data were atmospherically corrected and screened for clouds and snow using the *Fmask* algorithm (Zhu and Woodcock, 2012). In addition, we included auxiliary data sources, including long-term average climate data from Worldclim (Fick and Hijmans, 2017), the Permafrost Zonation Index (PZI) (Gruber, 2012), elevation and slope information from the Advanced Spaceborne Thermal Emission and Reflection Radiometer (ASTER) (Tachikawa et al., 2011), and surface water status (Pekel et al., 2016). These data sources were used to complement Landsat imagery by capturing the unique climatic and permafrost conditions of the northern high latitudes. Disturbance and change detection were performed solely using time series of Landsat surface reflectance data, while the auxiliary datasets (climate, PZI, elevation, surface water) contributed to land cover predictions.

2.2.3 Disturbance Detection and Feature Modeling

The minimum mapping unit and unit of analysis were 30 meter Landsat pixels. For each pixel, we used CCDC to estimate statistical breaks in the time series of Landsat data and model surface reflectance as a function of time. Between each pair of breaks is a time segment that is assumed to represent relatively stable land cover with characteristic spectral signatures, and each pixel contains a sequence of one or more time segments (Figure 2.1). CCDC estimates harmonic models at each pixel that can be used to provide synthetic data that bridges gaps (e.g., caused by clouds) and reduces noise from outliers. Using these models, we derived a set of seasonal-spectral features for each time segment that include the median value for each season (e.g. pixel-specific peak summer or early spring), difference between subsequent seasons, and annual metrics like minimum, maximum, and amplitude, across all Landsat bands and several spectral indices, including the normalized difference vegetation index (NDVI), enhanced vegetation index (EVI), normalized burn ratio (NBR), and tasseled cap indices (brightness, greenness, wetness), among others (Crist and Cicone, 1984) (Appendix Table A.1.1). The seasonal-spectral features characterize the seasonality of land surface reflectance, enabling us to capture the variability between forest phenological types (i.e. deciduous versus evergreen) that may not be sufficiently captured by peak growing season values alone (Figure 2.2) (Pasquarella et al., 2018). These features provide the basis for both the unsupervised clustering and the supervised *Random Forest* land cover model.

Because the snow-free seasons were very short, it was not feasible to rely on model coefficients as input factors for land cover classification (Zhu and Woodcock,

2014). When growing seasons were very short, there was considerable variability in which coefficients were non-zero, making reliable mapping of clusters based on the model coefficients inconsistent. To control for this, we developed our prediction features based on seasonal metrics of the synthetic reflectance. We defined the seasons for the spectral-temporal features as a function of the long-term mean snow-free season inferred from *Fmask.* For example, the start spring was defined as the day of year corresponding to 25% into the snow-free season, where the beginning of the season is defined by the long term mean date of snow melt (the 5th percentile of *Fmask* day of year) and the end of season is defined by the long term mean date of snow fall (95th percentile of *Fmask* day of year) while peak summer was defined as 50% into the season. At each pixel, we estimated the start and end of the growing season, and took median synthetic reflectance values at 5% (winter), 20% (spring), 35% (spring-summer), 50% (peak summer), 65% (summer-autumn), 80% (autumn), and 95% (winter) into the relative season as our key spectral-temporal metrics. We also used these synthetic reflectance values to determine annual metrics for each time segment, including mean, median, and amplitude, as well as the difference between seasons (e.g. per-day change between spring and spring-summer).

2.2.4 Semi-supervised Classification

The extent of our region and uniqueness of Arctic and Boreal land cover types (e.g., dwarf shrubs, tundra, or forested permafrost peat plateaus) made it difficult to decide *a priori* what Boreal and Arctic classes can be mapped with high accuracy from Landsat imagery. Further, the generation of high-quality training sites appropriate for a

large, heterogeneous region is labor intensive, making it desirable to rapidly produce training sites with a more automated, data-driven approach. To overcome these challenges, we performed an unsupervised clustering on the spectral reflectance and seasonal features from a sample of Landsat pixels (n = 19,682) training sites to identify spectrally-distinct statistical clusters and characterized those with visual interpretation of a select number of high-resolution images. The training sites were selected based on existing field photography and samples from existing static land cover datasets and were paired with extensive high-resolution imagery (see below). To perform the clustering, we utilized the R (Team and others, 2013) package *treeClust* to calculate a dissimilarity matrix between all point-wise pairs of samples based on their spectral and spatial features described above (Buttrey, 2016). A tree-based clustering method was used because it captures differences arising from non-linear relationships, benefits from automatic variable selection, and efficiently handles combinations of continuous and categorical data. We then used the *Partitioning Around Medoids* (PAM) clustering algorithm from the R package *cluster* (Maechler et al., 2017), applied to the site-by-site dissimilarity matrix estimated using *treeClust,* to identify a set of distinct clusters (k = 55) that capture the set of sub-classes with unique spectral-temporal, climatological, and topographical properties that are evident in the dataset (Kaufman and Rousseeuw, 1990). We chose 55 clusters with the expectation that the same land cover class should occur in several separate, smaller clusters that are specific to geographic regions, and that these clusters representing sub-classes would be aggregated into more general land cover classes in the final land cover legend. We based this framework on the land cover types included in the

Earth Observation for Sustainable Development (EOSD) land cover map of Canada for the year 2000, and hypothesized that 18 classes (taken from EOSD's legend, excluding No Data, Cloud, Shadow, and Ice classes and combining the Rock and Exposed Land classes as a more generic "Barren" class) would be uniquely represented in each of three major ecoregions (tundra, taiga, and northern Boreal forests), yielding a total of k = 54 clusters to represent land cover across the ABoVE Core Study Domain. We added one additional cluster to represent shoreline and shallow water (shallows), which is not included in the EOSD legend but was evident in the field photos of the Old Crow Flats.

We trained a supervised *Random Forest* model to predict the statistical clusters identified from the *treeClust / PAM* algorithms using the same sample of Landsat pixels and spectral-seasonal features used in the clustering (Breiman, 2001). These predicted clusters represent the unique classes across the ABoVE Core Study Domain that would be later aggregated to the broader land cover classes. Relying on the statistical clusters, rather than direct land cover prediction, allowed us to more accurately predict land cover based on region-specific spectral signatures across the large area of the ABoVE Core Study Domain and to let the data drive the precise definitions of our training data. We used the implementation of *Random Forest* from the package *Ranger,* which is a fast implementation of *Random Forest* for high dimensional data (Wright and Ziegler, 2017). *Random Forest* is an ensemble supervised algorithm that has been used extensively in remote sensing and land cover applications (Breiman, 2001; Gislason et al., 2006). Similar to our clustering algorithm *treeClust*, this algorithm allows for non-linear relationships among response and predictor variables, handles high-dimensional and

correlated predictors, and is robust to noise and outliers. Our *Random Forest* model mapped clusters that were then assigned land cover labels and aggregated to ten land cover classes on the basis of visual interpretation of high-resolution imagery (Table 2.1).

2.2.5 High Resolution Imagery and Training Sites

Considerable high-resolution imagery and field photographs were utilized to assign land cover classes to statistical samples. We generated training sites by sampling from the ABoVE Core Study Domain via stratified random sampling from existing 30 m land cover maps for Alaska (Jin et al., 2017) and Canada (Wulder et al., 2008) circa 2000, ensuring coverage across a range of climatic conditions, spectral feature space, and ecosystem types (n = 15,628 sites). We opportunistically augmented these sites with additional sites based on geolocated oblique aerial and ground-based photographs. These photographic data sets include publicly available photos from the EarthScope earthquake sensor network (n = 135) from across Alaska and the Yukon (Meltzer, 2003), photos taken during a field campaign in July 2017 in the Northwest Territories (n = 63), and oblique aerial photos taken in the Old Crow Flats, a wetland complex in the Yukon, in 2008 and 2009 (n = 1,355). We also included training sites from a stratified random sample extracted from existing very high-resolution land cover maps (0.2 – 10 m resolution), which provided high-quality training samples for wetland classes (Chasmer et al., 2014) and tundra-specific herbaceous and shrub classes (Greaves, 2017). In total, the training data set included 15,628 sampled from the Canadian and Alaskan land cover datasets (Jin et al., 2017; Wulder et al., 2008), 1,531 sites from Chasmer et al.'s 10 m

Scotty Creek land cover map (Chasmer et al., 2014), 970 sites from Greaves et al.'s 0.20 m Toolik Lake tundra vegetation map (Greaves, 2017), and 1,553 sites from field photographs for a total of 19,682 training sites. For some of these sites (n = 10,136), we visually interpreted high resolution (<4 m resolution) images based on available satellite imagery (copyright DigitalGlobe) derived from the satellites IKONOS, Geo-Eye, QuickBird, Worldview-2, and Worldview-3 and, when available, geotagged field photographs. Our visual interpretations provide the basis for characterizing statistical clusters and assigning land cover labels to mapped statistical clusters. For each site, there were between 1 and 24 high-resolution images across multiple seasons and years.

2.2.6 Post-processing

To create the final annual land cover maps, we performed several post-processing steps to correct artifacts in the data. First, within each pixel, consecutive time segments with the same land cover were merged into single time segments to eliminate spurious land cover class transitions. Second, to reduce the incidence of spurious land cover changes due to short-term climate variability or noise, sequences of short time segments that repeatedly changed between two classes were all assigned to a single class corresponding to the initial land cover class at the pixel. For example, a time segment series that had the sequence of land cover [Forest, Fen, Forest, Fen, Forest] was assumed to be changing due to sensor noise, was redefined as a series of a single time segment, [Forest], and was not considered a pixel of land cover change. Third, because topographic shadows were widely confused with water bodies, particularly in forested

mountain areas with substantial topography, we attempted to detect and correct shadowed land spuriously classified as water. To do this, we compared our mapped land cover predictions with topographic slope and an existing global 30 m surface water map (Pekel et al., 2016), which uses Landsat to quantify the seasonality and extent of surface water across the globe. If a pixel had non-zero slope and was classified as water or shallows, but Pekel et al. predicted the pixel to have no surface water, we assigned the pixel to the second most-likely class (i.e., after the water classes) based on class-conditional likelihoods generated by the *Random Forest* model for each time segment at each pixel.

2.2.7 Land Cover and Land Cover Change

Based on the procedures described above, we originally mapped fifteen classes (Appendix Table A.2.1). For the purposes of change analysis, however, we simplified the land cover legend to reduce the number of change trajectories we would estimate. The simplified legend was created by aggregating similar classes in the full land cover legend (e.g. Woodlands and Evergreen Forests were combined into Evergreen Forests). The maps we publish on the Oak Ridge National Laboratory Distributed Active Archive Center (ORNL DAAC; https://doi.org/10.3334/ORNLDAAC/1691) include these more detailed and more numerous classes, as well as the simplified land cover legend used here.

Using the annual maps of land cover, we assigned a stable land cover class or a 1984-2014 land cover change class to each pixel in the domain. Rather than exhaustively mapping every possible combination of paired land cover transitions, we focused on

specific land cover change trajectories related to our primary science questions (e.g. forest dynamics and Arctic shrub expansion). Because reference data collection for accuracy assessment and area estimation is resource intensive and scales with the number of change classes estimated, we limited our mapped land cover change classes to facilitate sampling, area estimation, and production of reference data over the domain (Olofsson et al., 2014). We mapped seven change classes that characterize land cover change trajectories between 1984 and 2014: Evergreen Forest Loss, Shrub Loss, Deciduous Forest Gain, Evergreen Forest Gain, Herbaceous Gain, Shrub Gain, and Other Change, which includes all changes not described by the previous six class changes (Table 2.1; Appendix Table A.3.1). We specifically defined the beginning and end points of each of these change classes to prevent clashes between definitions (e.g. Evergreen Forest becoming Shrub is Evergreen Forest Loss and not Shrub Gain). We limited the change analysis to the end points of the Landsat time series to maximize detection of relatively slow land cover change processes (e.g. shrub encroachment) and because a dearth of observations in Alaska in the 1990s prevented precise detection of disturbance at less than multidecadal scale. Because our analysis is agnostic to disturbance type (e.g., fire or permafrost degradation), we estimate changes in plant functional type stemming from all possible causes.

We did not analyze classes with negligible mapped areas of change, defined here as those mapped over less than 1 % of the study domain. These include Herbaceous Loss and Deciduous Forest Loss. The estimated area of change associated with each of these transitions were generally not different from zero, and thus were not estimated explicitly,

but grouped together into the Other Change class. The combined Other Change stratum accounted for 1.7 % of the study domain. We did not estimate changes in water/wetland areas explicitly, and changes in wetland and water extent are included in the combined Other Change class. To avoid double counting areas of conflicting transitions (e.g. an area of forest loss could also be defined as herbaceous gain), we devised a specific set of transitions that do not allow for clashes (Appendix Table A.3.1). This ensures that each pixel in the net change (1984-2014) map is only classified once, allowing us to design our stratified random sample for accuracy assessment and area estimation.

2.2.8 Accuracy Assessment and Area Estimation

We performed an accuracy assessment of the land cover and land cover change maps to correct bias in mapped areas that is introduced by classification errors (Olofsson et al., 2011; Stehman, 2000). Our accuracy assessment used a design-based sample for area estimation that includes estimation of variance and confidence intervals and was conducted by: (1) drawing a stratified random sample of points from the mapped areas of change; and (2) developing a reference data set at each of these points by visual interpretation of additional samples of high-resolution imagery and time series of Landsat data.

Following the methodology recommended by Olofsson et al. (2014), we use a stratified design and estimation approach, with stratified random sampling used to target sampling of areas of specific land cover change trajectories (Cochran, 1977; Olofsson et al., 2013). We draw a probability sample (n = 1,299) from the 1984 – 2014 change maps

by stratifying along the ten stable and seven change classes (total 17) in order to generate a reference data set and characterize accuracy (Table 2.1). Our reference sample was designed to provide high precision in estimated evergreen forest loss and targeted a standard error of 2.5% (equivalent to 6,071 km^2 or an 95% confidence interval of ± 12,142 km2) (Cochran, 1977). To generate our reference validation dataset, we analyzed the 1,299 sites using additional high-resolution imagery from Digital Globe in combination with time series of Landsat data to catalogue land cover from 1984 to 2014 for each 30 m Landsat pixel assessment unit. To do this, we visually estimated break points from time series of Landsat surface reflectance and interpreted Digital Globe imagery and Landsat imagery to determine land cover between identified break points. Our reference dataset thus includes a land cover label for every year between 1984 and 2014 at each reference site, which we use to estimate per-year areas of individual land cover. We used the reference sample to generate unbiased estimates of areas of land cover and land cover change, as well as unbiased variance estimators.

2.3 Results

2.3.1 Accuracy Assessment

Based on our accuracy assessment, our era-wide (1984-2014) map of land cover and land cover change had an accuracy of 76.1 % (Table 2.2), and our annual land cover maps have an overall accuracy of 84.1 ± 4.1 % (mean and 95 % confidence interval over 31 years). After aggregating all change classes and comparing them to the aggregated stable classes, we estimated land cover change over 1984-2014, more generally, with an

accuracy of 86.6%. There was considerable variability in the accuracy of various classes, with the most common confusion occurring between stable Shrub and Shrub Loss (21 cases) as well as stable Deciduous Forest and Deciduous Forest Gain (12 cases). There was also considerable confusion between the Other Change class and many other classes, particularly the stable Shrub and Fen classes. Based on our accuracy assessment, the mapped areas of Bog, Shallows/littoral, and most change classes (except Evergreen Forest Loss) were considerably biased low (between -15.5 and -66.8%), while stable Deciduous Forest, Herbaceous, Sparse, and Shrub classes mapped areas were moderately biased high (between +1.5 and +157%) relative to the estimated areas (Appendix Table A.3.2). These biases were corrected and uncertainty was estimated for the final estimates of land cover change.

2.3.2 Overall Land Cover Change

Our results reveal widespread and systematic changes in the distribution of land cover of the ABoVE Core Study Domain (Figure 2.3). A total of $0.647 \pm 0.061 \times 10^6$ km^2, equivalent to 13.6 ± 1.3 % of the study domain, experienced a transition in dominant plant functional type between 1984 and 2014. We did not identify significant trends in the overall rate of change as a function of time over the course of the 31-year time series (results not shown), likely resulting from the high interannual variability in burned area per year over the 31-year timespan of our study.

2.3.3 Boral Forest Dynamics

In absolute area, Evergreen Forest cover experienced substantial losses while Deciduous Forest cover experienced more moderate gains. On a relative basis, both Evergreen Forest net losses and Deciduous Forest gains were substantial. Evergreen Forest Loss occurred in 259,949 ± 34,996 km^2 (-19.6 ± 2.6 %, relative to 1984 Evergreen Forest area) and Evergreen Forest Gain occurred over 63,975 ± 18,688 km^2 (+4.8 ± 1.4 %), resulting in a net loss of Evergreen Forest of 195,974 ± 39,673 km^2 (-14.8 ± 3.0 %) (Figure 2.4). Concurrently, Deciduous Forest cover expanded by 50,244 ± 17,467 km^2 (+15.4 ± 5.2 %), primarily in the southern portion of the Boreal biome. Evergreen Forest Loss significantly outpaced Evergreen Forest Gain, while Deciduous Forests expanded alongside negligible Deciduous Forest Loss, suggesting a broad shift from evergreen dominated forests to increased deciduous forest cover. The majority of Evergreen Forest Loss occurred in highly localized patches, primarily related to the occurrence of fires within the study domain throughout the Boreal forest (Appendix Figure A.4.1). The occurrence of Evergreen Forest Gain and Deciduous Forest Gain were less concentrated into small patches. The type of forest gain varied considerably by latitude, with Evergreen Forest Gain occurring more commonly further north, with Deciduous Forest Gain occurring primarily in the southern portion of the domain.

We found that the areas of different forest types changed monotonically, with Evergreen Forest steadily decreasing and Deciduous Forest steadily increasing over the 31-year timespan (Figure 2.5). The changes in Evergreen Forest area were driven mostly by losses, which showed some interannual variability due to stochasticity in burned area.

Meanwhile, the Deciduous Forest areas were more moderate and steadier in their increase over time.

To better understand the drivers of forest changes across the ABoVE Core Study Domain, we compared our land cover change data with historical fire perimeters from the Alaskan Large Fire Database (Kasischke et al., 2002) and the Canadian National Fire Database (Stocks et al., 2002). Fire-related losses accounted for the majority (165,078 km^2; 63.5 %) of Evergreen Forest Loss area in the study domain, while pre-1984 fires were associated with substantial portions of both Evergreen Forest Gain (41,949 km^2; 65.5 %) and Deciduous Forest Gain (17,906 km^2; 35.4 %) (Table 2.3). Successive fire events occurring over multiple decades create heterogeneous landscapes where landscape composition at any disturbed location is largely explained by the time since the last fire, and where high-resolution imagery is required to characterize land cover and detect land cover changes. Figure 2.6, for example, shows a 42,077 km^2 region in British Columbia where known fires accounted for 78.7% of all forest cover changes, including 1,664 km^2 of Evergreen Forest Loss, 1,150 km^2 of Deciduous Forest Gain, and 1,551 km^2 of Evergreen Forest Gain. All recent burned areas resulted in Evergreen Forest Loss, but the longer-term post-fire regrowth varied as either Evergreen Forest Gain or Deciduous Forest Gain. This fire-dominated landscape is representative of much of the ABoVE Core Study Domain, and the changes we map suggest that large-scale shifts in forest types, from Evergreen Forest to Deciduous Forest, are broadly occurring throughout the ABoVE Core Study Domain in response to the cumulative impact of repeated fire events.

Timber harvest in the study region accounted for relatively small areas of forest cover changes, including 18,053 km^2 (6.9%) of Evergreen Forest Loss and 640 km^2 (1%) of Evergreen Forest Gain (Table 2.3). While harvest only occurred in 0.57% of the study domain, it was associated with a significant portion (7,117 km^2, or 14.1 %) of growth of Deciduous Forest, suggesting a significant role of harvest in forest successional processes. We attribute the remaining 76,818 km^2 (29.6 %) of Evergreen Forest Loss to a combination of other forest loss processes, including insect infestations (Volney and Fleming, 2000), permafrost thaw-induced forest mortality (Carpino et al., 2018; Helbig et al., 2016), and resource exploration (Williams et al., 2013). Conversely, we attribute 21,416 km^2 (33.5 %) of Evergreen Forest Gain and 25,548 km^2 (50.5 %) of Deciduous Forest Gain to tree line expansion and regrowth following unrecorded fires. Studies focused on more granular mapping of disturbance types are required to better understand these land cover shifts.

2.3.4 Arctic Shrub Expansion

In contrast to the changes we document in the Boreal biome, Arctic areas above the tree-line experienced gradual, but widespread, encroachment of short herbaceous and woody vegetation into areas previously occupied by Barren and Sparse Vegetation land (Figure 2.3). Shrub Gain (75,843 ± 20,860 km^2, or +13.3 ± 3.6 % of 1984 shrub cover) substantially exceeded Shrub Loss (42,154 ± 21,051 km^2; -7.4 ± 3.7 %) (Figure 2.4). Herbaceous Loss was negligible, but Herbaceous Gain (104,871 ± 31,699 km^2; +18.4 ± 5.6 %) was sizeable in both the Canadian high tundra (particularly on Banks and Victoria

Islands) and in agricultural areas of Alberta (Appendix Figure 3.2). Net combined Shrub and Herbaceous Gain, most of which occurred in the Arctic biome replacing Barren or Sparse Vegetation areas, totaled 138,560 ± 37,947 km^2 (+7.3 ± 2.0 %) (Figure 2.4). A notable portion of Shrub Gain (27,057 km^2, or 25.8 %) occurred in areas of fire (Table 2.2), which likely represent areas that were burned before the start of the time series but grew slowly enough that they did not transition to forests by the end of the time series. Growth of new shrubs is outpacing loss of shrubs (e.g., due to permafrost degradation), and herbaceous vegetation is expanding into previously barren land areas in response to climate warming.

Slow growth rates and spatial heterogeneity in tundra landscapes make changes in shrub cover challenging to detect from satellite imagery (Bartsch et al., 2016). However, mapped shrub expansion is borne out by *in situ* observations. For example, Figure 2.7 shows land cover changes that we map on Qikiqtaruk-Herschel Island, Yukon Territory, a small (136 km^2) tundra island off the northern coast of Canada, along with photos collected across a 27-year timespan (1987-2014) on the island (Myers-Smith et al., 2019). The photos confirm pronounced increases in shrub cover and height in locations that were previously dominated by herbaceous vegetation (Myers-Smith et al., 2019). Qikiqtaruk-Herschel Island experienced an increase in Shrub cover of 9.67 km^2 (+59.5% relative to 1984) and reductions in Sparse Vegetation and Barren land of 4.69 km^2 (-36.6% relative to 1984). These changes coincide with a 2.5 - 4º C increase in air temperature, earlier snowmelt, and decreased frost frequency over the island (Myers-Smith, In Press), suggesting that climate warming is the key driver behind shrub

expansion. More generally, our findings of increased vegetation cover and reduced bare ground cover (Figure 2.5) are consistent with field-based studies across the Arctic (Elmendorf et al., 2012; Myers-Smith et al., 2019). However, repeat photography of Arctic vegetation is difficult to obtain, so considerable uncertainty remains in Arctic shrub expansion rates.

Additional notable changes in land cover include a reduction in Sparse Vegetation area (by 64,824 ± 64,489 km^2; -13.2 ± 13.1 %) in mountain and Arctic regions, and expansion in the area covered by Fen, Bog, and Shallows wetland ecosystems (by 18,768 ± 52,188 km^2; +10.2 ± 28.5 %) throughout the taiga. However, the area of change associated with each of these land cover types is highly uncertain, and additional work is required to more fully and accurately characterize these changes and their drivers.

2.4 Discussion

2.4.1 Overall Land Cover Change

The shifts in forest type and changes in forest and shrub coverage we report for the ABoVE Core Study Domain are broadly consistent with those expected from climate change and attendant changes in disturbance regimes. In particular, our findings of a net loss in conifer forest are consistent with a shift toward a more active fire regime in Boreal forests relative to the last several millennia, which would tip the overall balance of evergreen forest loss and post-fire regrowth out of steady state (Kelly et al., 2013), and our findings of Arctic shrub expansion are consistent with numerous field studies

reporting the proliferation of woody shrubs in the Arctic tundra (Elmendorf et al., 2012; Myers-Smith et al., 2011) .

The estimation efforts in this study focused on a few specific land cover change types, since a comprehensive effort to map each potential transition would have been infeasible given our resources. Thus, we focused our change analysis on just a few key changes that were focused on our scientific questions and were occurring frequently enough at 30 m resolution scale to be detectable and estimated. While our analysis was agnostic to the specific driver of land cover change, the fact that it was defined only in terms of net land cover change means that our map effectively captures, without attribution, all potential change drivers. This includes rarer and less studied changes, such as the loss of forests due to permafrost degradation in the Taiga Plains (Carpino et al., 2018), insect infestation, or shifts in surface water coverage. We do not limit our analysis to just the most extensive change processes (e.g. fires), and instead attempt to capture changes that occur at different rates in different ecoregions and quantify the relative impacts of drivers for which sufficient data exist. There currently is a lack of mapped information on the rate and extent of other drivers of forest loss, though some smaller scale studies suggest some non-fire effects are similar in magnitude to fires, such as permafrost degradation (Helbig et al., 2016).

2.4.2 Changes in Forest Cover

Fires usually change the underlying land cover of the burned area by eliminating the vegetation in the area, with post-fire recovery being a relatively stochastic process. In

some places, over the course of several decades, Boreal forests regenerate after a fire, with significant impacts on ecosystem productivity and land surface characteristics while it returns to its pre-disturbed state (Bolton et al., 2017). One might expect that over a large enough area and period that the loss of forest cover in one area would be compensated by the regrowth from older disturbances in other areas. The results from this study suggest that land cover dynamics in Arctic and Boreal biomes of northwestern North America are not in steady state, ostensibly as a result of changing disturbance regimes and climate, resulting in systemic shifts in plant functional type composition. We find that the time between a stand replacing fire and regrowth of forest is generally between 40 and 50 years, but the incidence of deciduous forest gain primarily occurs in the south (Figure 2.8). The northern fires result primarily in forest recovery as Evergreen Forest, and southern fires were split between returning as Deciduous Forest or as Evergreen Forest.

While harvest was not a dominant factor in our study region (0.58 %), we found a fair amount of Deciduous Forest Gain (14 %) occur in areas that were harvested (Table 2.2). Most forest harvest occurs in evergreen forests; this suggests timber harvest has the potential to shift Boreal forest demography towards deciduous forests. Harvesting typically occurred in the southern part of the domain; similarly, post-fire deciduous forest gains occurred in the southern portion of the domain (Figures 2.4 and 2.8). As the southern portion of the domain is generally warmer, this suggests a climate-driven backdrop towards successional trajectories, triggered by disturbances, towards Deciduous Forest rather than Evergreen Forest. However, determining the factor that drives this

variability in phenological type in forest regrowth will require a more systematic and extensive analysis of other fire characteristics that may drive successional trajectories, such as fire severity (Johnstone et al., 2010).

2.4.3 Boreal Expansion of Shrubs and Herbs

The Shrub and Herbaceous Gain change classes are meant specifically to capture the increase of shrubs, herbaceous, and sparsely vegetated land from previously less-vegetated land (e.g. non-forest turns to shrub or barren turns to sparse vegetation). Broadly, we see that the majority of the shrub and herb gain classes are occurring in the northern tundra, where there are plot-based reports of shrub encroachment and greening trends. However, noticeable amounts of these new growth changes do occur in the southern part of the domain. Boreal Shrub Gain likely represent partial time series of forest loss and regrowth (i.e. a forest disturbance occurs before 1984 and we capture a portion of the regrowth). A longer time series might reveal these areas to be transitioning to forest and would be mapped as forest regrowth, in reality, rather than the increase of shrub cover analogous to tundra shrub encroachment. Southern herbaceous gain is likely a result of the extensive agriculture that occurs in Alberta and British Columbia. Areas that lie fallow in the beginning of the time series are initially mapped as Sparse Vegetation or Barren, and will be mapped as Herbaceous gain if they become planted later. The influence of agriculture should not be interpreted as a long-term conversion towards additional herbaceous land, as agricultural practices typically involve cycling between fallow and planted seasons and does not represent a similar ecological shift as

vegetation expansion in the Arctic. Agriculture does not comprise a substantial portion of our study domain, so specific measures were not made to correct for this. Due to the mid-successional shrub growth and the artifacts in agricultural herbaceous expansion, our mapping estimates for these processes should be considered an upper bound.

2.4.4 Potential Impacts on Biogeochemistry and Land Surface Characteristics

These land transformations, especially the transition between forest types, have important implications for key land surface properties such as albedo and for coupled ecosystem-atmosphere interactions related to carbon, energy, and water exchange at high latitudes (Augusto et al., 2015). For example, younger, deciduous forests are considerably more productive and more seasonal than evergreen forests (Goulden et al., 2011; Randerson et al., 2006; Zimov et al., 1999) and the transition from Evergreen Forests to Deciduous Forests in Boreal ecosystems, as well as the increased Shrub and Herbaceous cover in both Boreal and Arctic biomes (Figure 2.4), is consistent with increased seasonality in net ecosystem production (Graven et al., 2013; Zhang et al., 2013). Similarly, expansion of shrubs in the Arctic has the potential to alter climate-ecosystem interactions by increasing ecosystem productivity and reinforcing warming by via positive feedbacks from changes in albedo and snowpack (Zhang et al., 2013).

A shift towards deciduous forest cover relative to evergreen forest cover in the Boreal forest translates to a substantial increase in average summer carbon uptake; hence, the results here suggest a substantial increase in the seasonality and magnitude of carbon exchange in the Boreal forests. Similarly, transitions from Herbaceous tundra to Shrub

tundra suggest a substantial increase of mean summer carbon uptake. Interactions with climate (e.g. via environmental stressors like drought) further complicate this relationship.

Similarly, seasonal albedo values are likely to vary considerably as a result of these land cover changes. Deciduous Forests have higher albedo values than Evergreen Forests across both winter and summer, while Shrub tundra have lower albedo than Herbaceous, Sparse Vegetation, and Barren tundra (Table 1.1). Changes in Arctic albedo have the potential to considerably increase global temperatures more than increased CO_2 concentrations would (Chapin et al., 2005). While the increased shrub cover would decrease albedo in both summer and winter in the tundra, the increased Deciduous Forest would substantially increase albedo in both summer and winter in the Boreal biome, resulting in opposite biophysical climate forcing effects. These changes in albedo influence the nature of net climate forcing caused by land cover changes in the ABR.

2.5 Conclusions

Our results provide a comprehensive characterization of systematic and widespread transitions in plant functional types across a large area of northwestern North America that were not previously documented because land cover dynamics in the ABR region vary over relatively short spatial scales, and so were not detectable from coarse spatial resolution imagery used in previous studies (Song et al., 2018). Shifts in Boreal forest types and Arctic shrub extent are extensive and have significant potential impacts on global carbon-climate feedbacks. The results presented here fill a critical gap in

understanding the shifting character of northern ecosystems in light of rapid climate change and disturbances and provide a substantial improvement in our ability to model and understand land surface changes across this climate-sensitive region.

Table 2.1 | Description of the major land cover and land cover change strata mapped over the ABoVE Core Study Domain. Included are the areas for each stratum (W_i, in % of ABoVE Core Study Domain) and sample allocation (n_i) used for stratified random sampling for area estimation. Non-italics indicate stable land cover classes, while italics indicate land cover change classes (separated by horizontal line).

Stratum	Description	W_i (%)	n_i
Evergreen Forest	Forests dominated (>50 %) by evergreen conifer trees	24.9	233
Deciduous Forest	Forests dominated (>50 %) by deciduous broadleaf trees	5.4	102
Shrub land	Areas dominated (>50 %) by shrubs of any stature (short or tall) and of any phenological habit	8.6	140
Herbaceous	Areas dominated (>50 %) by herbaceous vegetation	8.8	81
Sparse Vegetation	Areas with 20 – 50 % coverage of any vegetation, primarily underlain by rock	13.5	83
Barren	Areas with less than 20 % of any vegetation, primarily rock or exposed land	9.7	73
Fen	Hydrologically-connected, sedge-dominated wetlands	2.3	62
Bogs	Ombrotrophic, shrub- and *Shagnum* moss-dominated wetlands	0.2	50
Shallows/littoral	Shallow lakes, wetlands with unclear dominant vegetation, or mixed water/land shoreline	0.6	44
Water	Lakes, rivers, oceans, and other open bodies of water	8.8	83
Everg Forest Loss	Areas changing from Everg.Forest to Shrub, Herb., Sparse Veg., Barren, Fen, Bog, Shallows, or Water	5.0	66
Shrub Loss	Areas changing from Shrub to Herb., Sparse Veg., Barren, Fen, Bog, Shallows, or Water	1.6	58
Decid Forest Gain	Areas changing from Everg. Forest, Shrub, Herb., Sparse Veg., Barren, Fen, or Bog to Decid. Forest	1.4	44
Everg Forest Gain	Areas changing from Deciduous Forest, Shrub, Herb., Sparse Veg., Barren, Fen, or Bog to Everg. Forest	2.6	40
Herbaceous Gain	Areas changing from Barren land to Sparse Veg. or Herb., or areas changing from Sparse Veg. to Herb.	2.2	39
Shrub Gain	Areas transitioning from Herb., Sparse Veg., or Barren land to Shrub	2.6	49
Other Change	All other transitions not captured above	1.9	52

Table 2.2 | Accuracy Assessment results indicating classification and reference data for the changes in mapped areas spanning 1984-2014. Due to space constraints, Evergreen Forest is abbreviated as EF, Deciduous Forest as DF, Shrub as SH, Herbaceous as Herb, Shallows as Shall., and Other as Oth. Reference data indicated in columns and mapped classification data indicated in rows, total n = 1299. Producer's accuracies (Prod. Acc) indicate the rate of errors of omission, while user's accuracies (User Acc) indicate the rate of errors of commission, in units of %. Overall accuracy: 76.1% (sum of the diagonal divided by the total sample); Accuracy of annual land cover maps: 84.1 ± 4.1%, estimated from the set of accuracies across all mapped years (1984-2014, n = 31).

	EF	DF	SH	Herb	Sparse	Bare	Fen	Bog	Shall.	Water	EF Loss	SH Loss	DF Gain	EF Gain	Herb Gain	SH Gain	Oth.
EF	199	5	10	0	0	1	3	3	1	1	8	0	1	0	0	0	1
DF	2	95	4	0	0	0	0	0	0	0	0	0	1	0	0	0	0
SH	7	9	109	8	0	0	2	0	0	0	0	4	0	1	0	0	0
Herb	0	0	1	76	2	0	0	0	0	2	0	0	0	0	0	0	0
Sparse	1	0	3	4	69	1	0	0	0	0	0	1	0	0	3	0	1
Bare	0	0	0	0	5	64	1	0	1	2	0	0	0	0	0	0	0
Fen	3	5	5	0	0	0	45	1	1	0	1	0	1	0	0	0	0
Bog	5	0	0	0	0	0	2	43	0	0	0	0	0	0	0	0	0
Shall.	2	0	0	3	2	0	1	0	33	2	1	0	0	0	0	0	0
Water	1	0	0	0	0	0	0	0	7	75	0	0	0	0	0	0	0
EF Loss	2	0	1	0	0	0	2	0	1	0	57	0	1	0	0	2	0
Shrub Loss	1	1	21	7	3	0	7	0	0	0	0	16	0	1	1	0	0
DF Gain	2	12	2	0	0	0	3	0	1	0	1	0	22	1	0	0	0
EF Gain	3	2	5	0	1	0	5	0	3	0	0	0	0	21	0	0	0
Herb Gain	0	0	0	6	4	1	0	0	0	0	1	0	0	0	26	0	1
Shr Gain	0	0	5	8	1	0	6	0	0	0	0	0	0	0	2	26	1
Other	0	4	8	2	6	0	9	1	2	2	1	1	1	0	1	1	13
Prod. Acc	87.3	71.4	62.6	66.7	74.2	95.5	52.3	89.6	66	89.3	81.4	72.7	81.5	87.5	78.8	89.7	76.5
User Acc	85.4	93.1	77.9	93.8	83.1	87.7	72.6	86	75	90.4	86.4	27.6	50	52.5	66.7	53.1	25

Table 2.3 | Distribution of land cover changes occurring in areas associated with fires and with harvesting. Proportions indicate the proportion of domain-wide area of land cover change class that occurs within fire or harvest areas (i.e. 63.5% of all Evergreen Forest Loss occurred in fire perimeters). Mapped fired areas are derived from the Alaskan Large Fire Database and the Canadian Fire Database. Mapped harvested areas are derived from time series of Landsat data across Canada. There was negligible timber harvest occurring in the Alaskan portion of our study domain (Smith, 2002).

Land Cover Change	Mapped Area in Fires (km^2)	% in Fire Area	Harvested Area (km^2)	% in Harvest Area
Everg. Forest Loss	165,078	63.5	18,053	6.9
Shrub Loss	16,505	39.2	406	< 1
Decid. Forest Gain	17,906	35.4	7,117	14.1
Everg. Forest Gain	41,919	65.5	640	1.0
Herbaceous Gain	7,185	6.9	167	< 1
Shrub Gain	27,057	36.2	575	< 1

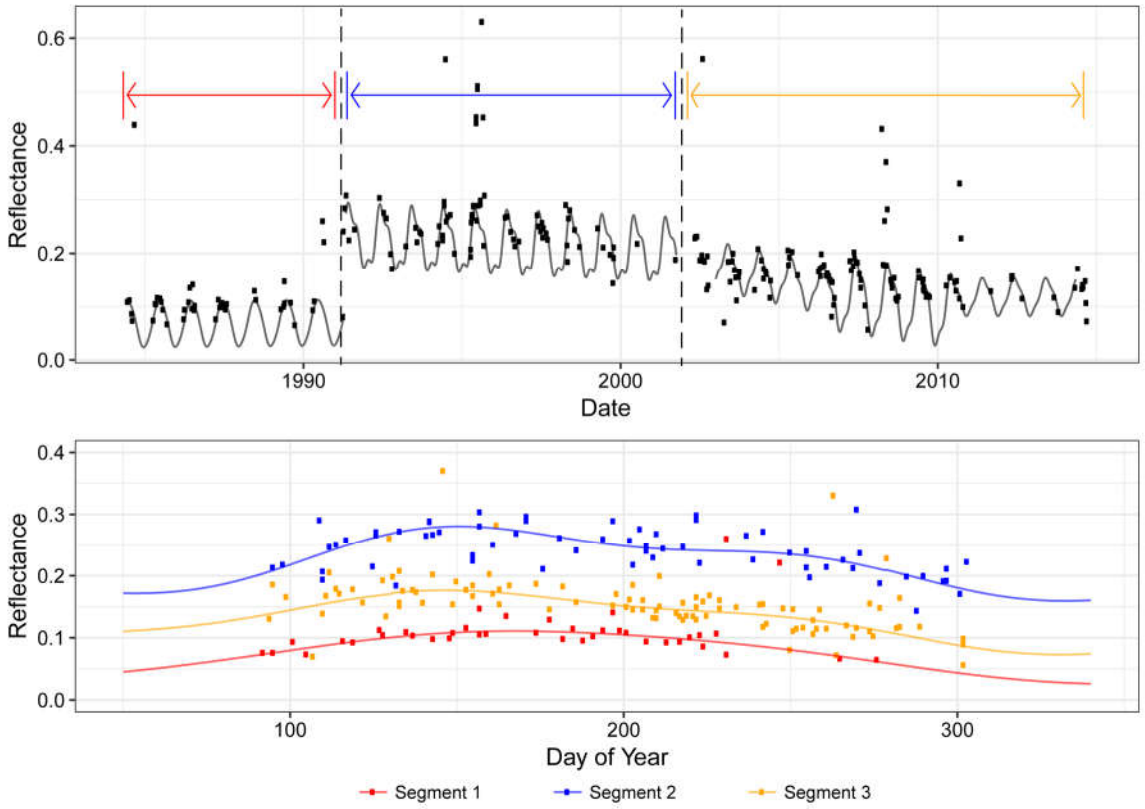

Figure 2.1 | Example of time series and disturbance detection for one Landsat band and one pixel using the Continuous Change Detection and Classification (CCDC) algorithm. In this example, surface reflectance for Landsat band 5 (shortwave-infrared) is shown; however, CCDC is used on all six surface reflectance bands in Landsat data. Top panel: points are time series of observations reflectance, grey lines are fitted harmonic models, dashed vertical lines are the approximate timing of breaks in land cover, and colored horizontal lines and arrows indicate between-break time segments of stable land cover. The occurrence of outlier pixels are likely cloudy pixels that were missed by the cloud screening algorithm; however, CCDC detects and removes outliers in its model fits. Bottom panel shows characteristic seasonal cycle (as day of year stacked across years) of the time segments indicated in the top panel, color coded to match the horizontal lines in the top panel. Colored points indicate observations falling within the correspondingly colored time segments and lines indicate the harmonic model fit across those values, averaged across all years within the time segment.

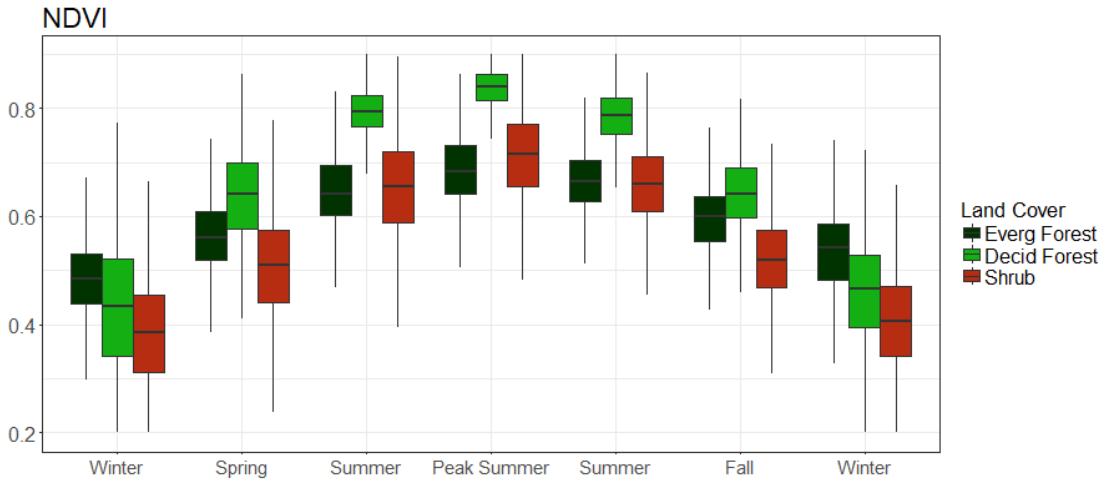

Figure 2.2 | Example of spectral-seasonal features used to distinguish classes. Shown is the distribution of seasonal values of the normalized difference vegetation index (NDVI) for evergreen forests, deciduous forests, and shrubs from a sample of time segments (n = 10,000) across the study domain. Relative values of NDVI are highly dependent on season for each land cover class, and these relative differences are used to distinguish the land cover classes. For example, shrubs and evergreen forest have similar peak summer values, but evergreens have higher winter and shoulder season values of NDVI than shrubs do.

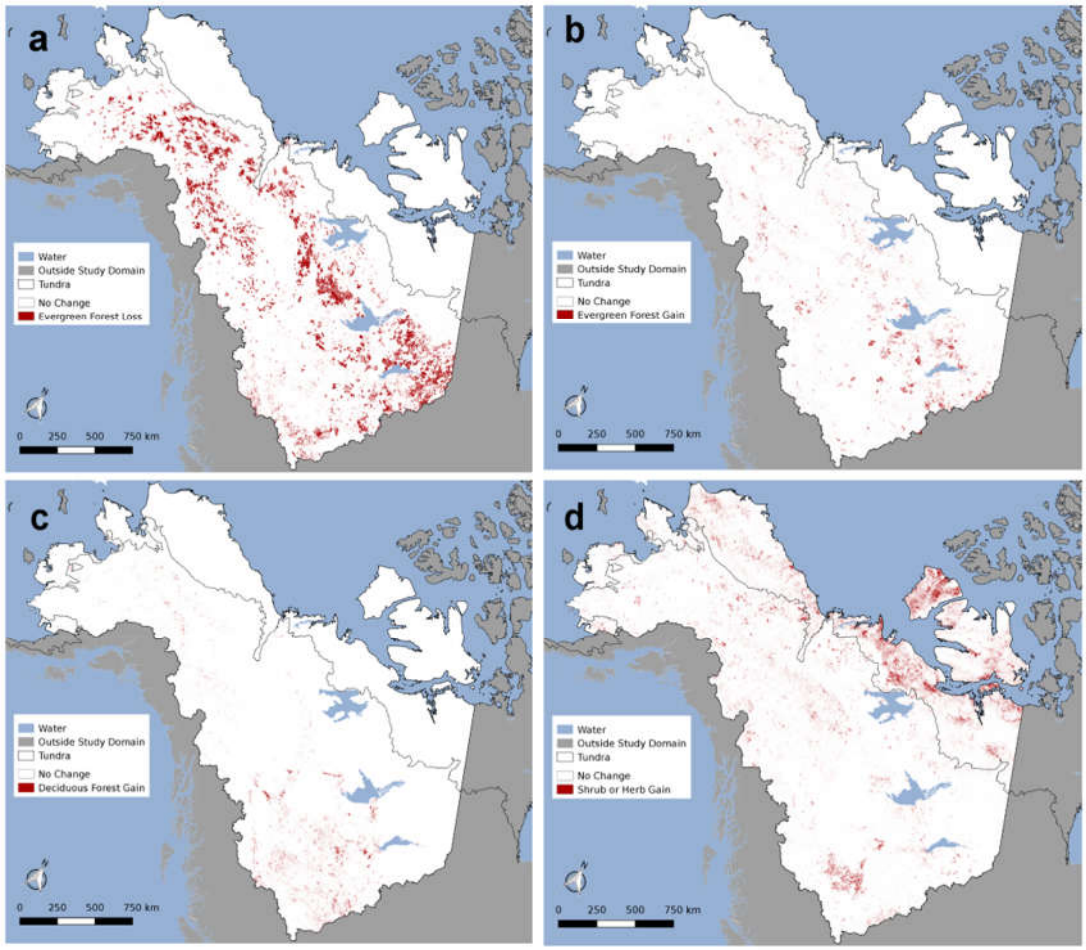

Figure 2.3 | Domain-wide maps showing land cover and specific land cover change classes across the ABoVE Core Study Domain, rescaled to 900 m pixels and showing areas with majority coverage of change class a) Spatial distribution of Evergreen Forest Loss over 1984-2014 b) Evergreen Forest Gain c) Deciduous Forest Gain d) Shrub Gain and Herbaceous Gain. Further maps, including land cover and additional land cover change classes, are shown in Appendix Figure A.4.2. Dotted line displays the treeline, which serves as our boundary of the tundra.

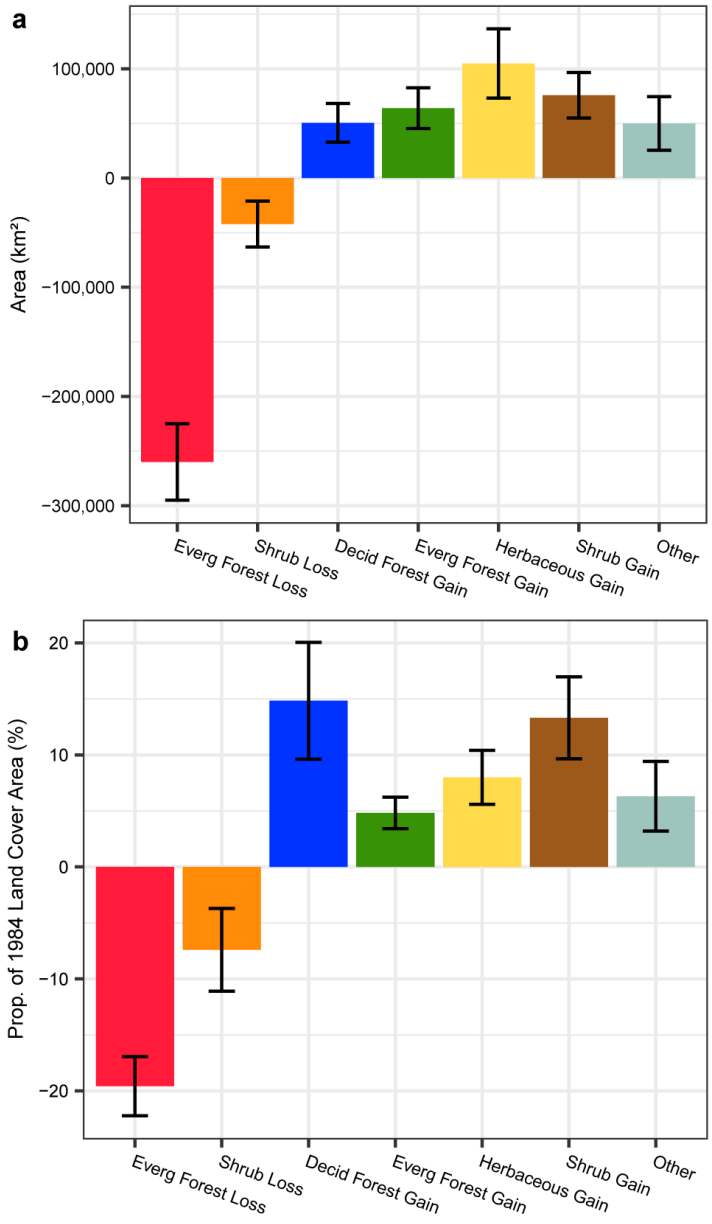

Figure 2.4 | Total estimated areas with confidence intervals of land cover change over the ABoVE Core Study Domain. (a) Absolute area (b) and proportional change relative to the initial 1984 land areas for each of the seven change classes estimated across the entire study domain over 1984-2014. Relative changes in (b) are specific to each land cover change class's key land cover, e.g. Evergreen Forest Loss area is equivalent to approx. 20% of Evergreen Forest area in 1984. Error bars indicate 95% confidence intervals based on variances derived from a probabilistic sample (see methods).

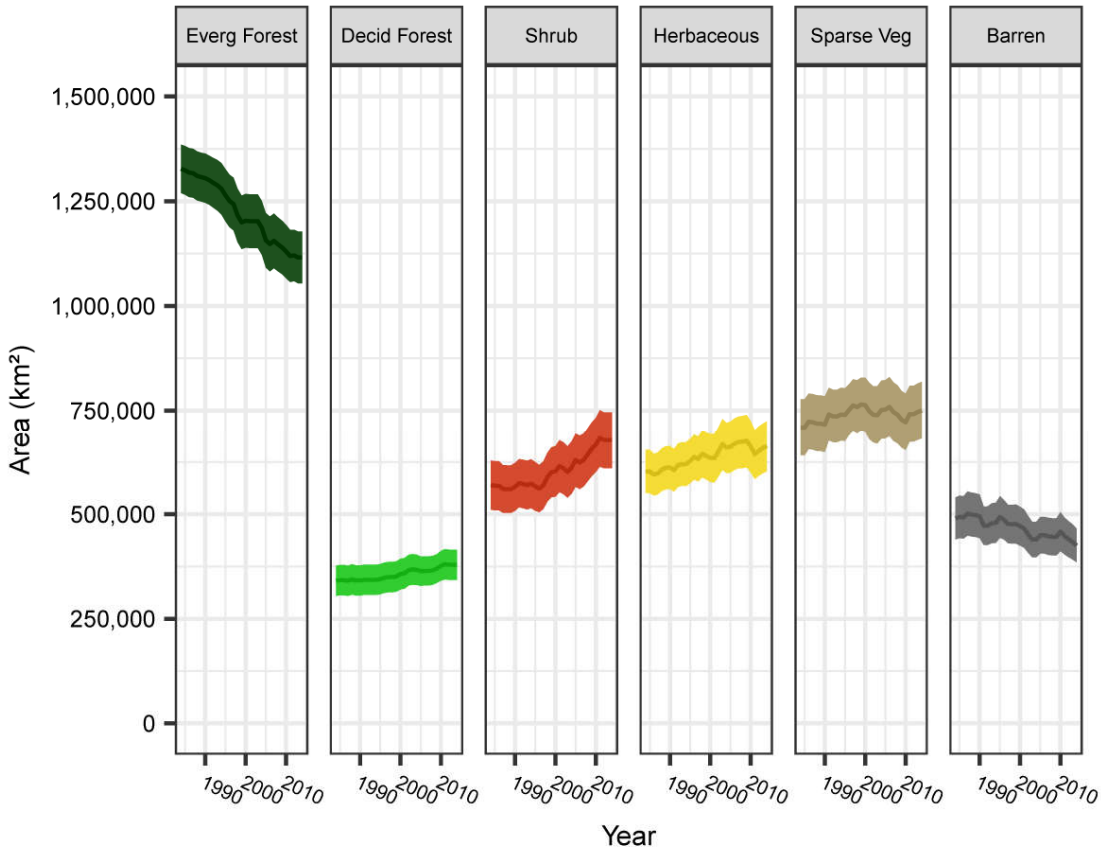

Figure 2.5 | Time series of area land cover change across the ABoVE Core Study Domain. Lines indicate estimated area means and ribbons indicate 95% confidence intervals over the mean, with variances estimated from a probabilistic sample (see methods). Not shown are the time series curves for Fen, Bog, Shallows/littoral, or Water, which did not exhibit significant change over time.

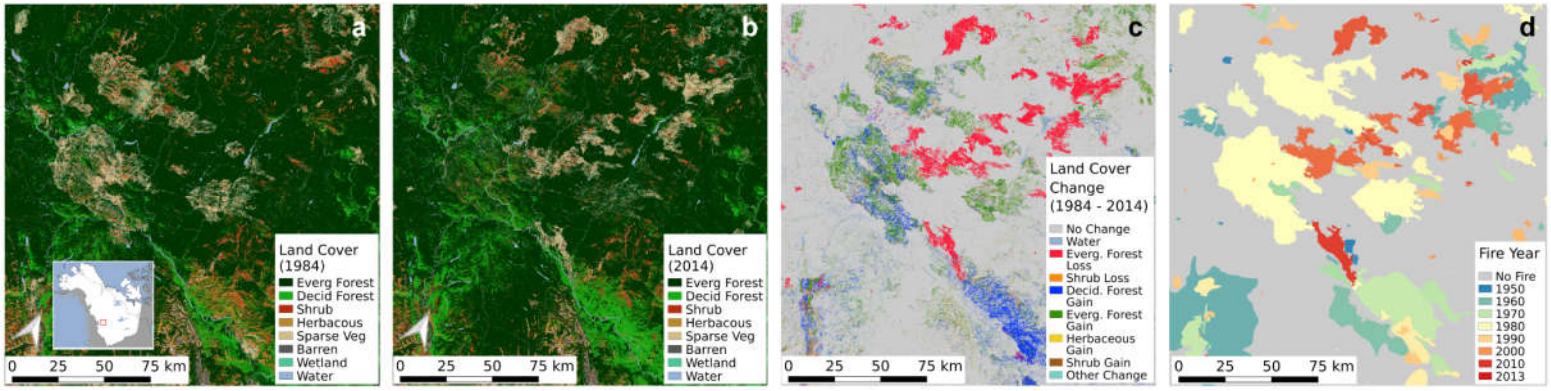

Figure 2.6 | A detailed example of the control of old and young fires on forest regrowth in British Columbia, Canada. a) Land cover in 1984 b) land cover in 2014, following forest growth and loss c) the net change in land cover over these areas and d) the perimeters of fires from the Canadian Fire Database in the area with colors indicating time of the fire. The spatial patterns of forest loss and growth are highly associated with the occurrence of young and old fires.

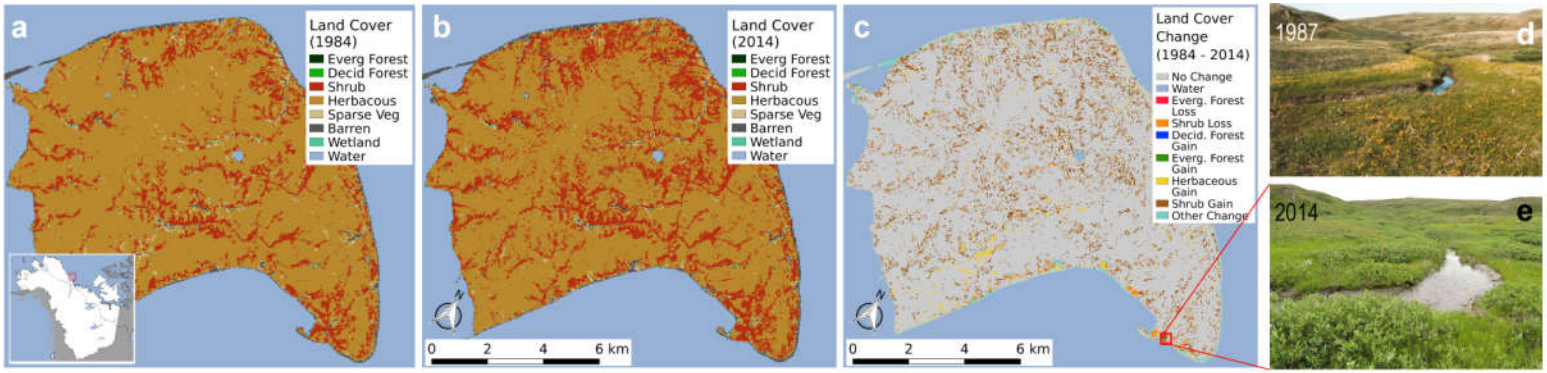

Figure 2.7 | A detailed example of the impact of climate change on the coverage of shrubs in the high tundra at Qikiqtaruk-Herschel Island, Yukon, Canada. a) Land cover in 1984 b) land cover in 2014, following substantial shrub growth c) the net change in land cover d) a field photo taken in 1987 showing primarily grass tundra and e) a field photo taken in 2014 showing substantial *in situ* increases in both height and coverage of *Salix richardsonii* shrubs (Myers-Smith et al., 2019). Inset shows detailed spatial pattern of shrub cover dynamics for the area surrounding the pair of photographs.

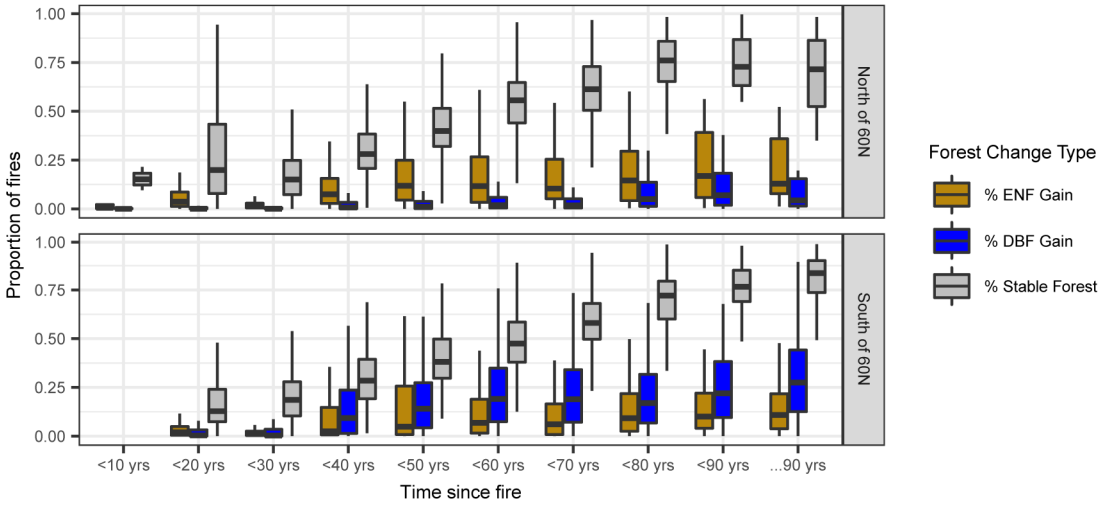

Figure 2.8 | The proportion of fire perimeters experiencing forest recovery as a function of time between fire and mapped land cover change and geography. ENF Gain refers to Evergreen Forest Gain and DBF Gain refers to Deciduous Forest Gain. Stable Forest refers to areas of both Evergreen Forest and Deciduous Forest that did not experience change. Southern forest fires more frequently result in Deciduous Forest Gain, whereas northern fires result in Evergreen Forest Gain. Forests that were stable within 1984-2014 tended to occur mostly in fire perimeters more than 40 years old.

THE INFLUENCE OF DISTURBANCE AND LAND COVER CHANGE ON SATELLITE-DERIVED MEASURES OF PRODUCTIVITY IN ARCTIC AND BOREAL ECOSYSTEMS

3.1 Introduction

Climate change is occurring most rapidly in the high northern latitudes, particularly in Boreal and Arctic ecosystems where warming is happening at twice the rate compared to the rest of the planet (Pithan and Mauritsen, 2014). Concomitant with this warming, numerous studies have observed an increase in the seasonal amplitude of atmospheric [CO_2] (H. Graven et al., 2013; Keeling et al., 1996) and so-called greening of land surfaces at mid- and high-latitudes, as observed from time series of satellite remote sensing data (Beck and Goetz, 2011; Ju and Masek, 2016; Myneni et al., 1997a). Trends in the seasonal amplitude of atmospheric carbon dioxide (CO_2) have significant implications for global carbon-ecosystem feedbacks since they imply changes in the underlying productivity of Northern Hemisphere ecosystems. However, the mechanisms behind enhanced carbon cycling in high northern latitudes are not well understood. Modeling and observations studies suggest a suite of potential drivers, including an increase in leaf area index (Zhu et al., 2017), CO_2 fertilization (Zhu et al., 2016), and land use (Gray et al., 2014; Zeng et al., 2014), but precise attribution is still lacking.

Land cover is a fundamental input for many algorithms and models that are used to simulate and understand ecosystem dynamics at high latitudes. In particular, plant functional type provides a first order characterization that is used to parameterize

vegetation properties in both remote sensing-based products (e.g., the MODIS LAI, FPAR, and GPP products) and ecosystem models that are extensively used to study high latitude ecosystems (Luus and Lin, 2015; Myneni et al., 1997a; Zhang et al., 2008; Zhu et al., 2017). Arctic-Boreal land cover experiences frequent and extensive changes due to anthropogenic and natural processes, so understanding how land cover dynamics interact with remotely sensed metrics of ecosystem properties like productivity is essential to appropriate interpretation of both model- and remote sensing-based studies of high latitude change

3.1.1 Trends in Land Surface Greenness

Trends in land surface greenness, commonly inferred by statistical analysis of satellite-derived spectral vegetation indices such as the normalized difference vegetation index (NDVI), are often interpreted to be indicative of changes in vegetation dynamics in Arctic and Boreal ecosystems (Myneni et al., 1997a; Pastick et al., 2019). Changes in productivity associated with trends in remotely-sensed measurements may help to explain observed changes in the seasonality of atmospheric CO_2 and have been used to infer the presence of significant environmental stressors in Boreal and Arctic ecosystems, such as insect infestations and drought (Parent and Verbyla, 2010; Rogers et al., 2018; Verbyla, 2011; Zhang et al., 2008). However, recent studies have cast doubt on previous interpretations of high-latitude NDVI trends. Specifically, the relatively low radiometric quality of NDVI derived from the Advanced Very High Resolution Radiometer (AVHRR) (Guay et al., 2014; Ju and Masek, 2016), the dependence of NDVI trends on

the timing and severity of fire disturbance (Sulla-Menashe et al., 2018), and confounding perturbations in land surface properties such as changes in surface water (Cooley et al., 2019; Raynolds and Walker, 2016) all impact the potential meaning of a change in NDVI. Further, NDVI, as a proxy for biomass, leaf area index, or productivity, has diminished sensitivity to change at high values (Buermann et al., 2002; Carlson and Ripley, 1997), which adds significant uncertainty to interpretation of trends (or the lack thereof). Hence, it can be difficult to interpret the importance or impact of NDVI trends without a complete understanding of the land surface history, particularly in dynamic landscapes such as those found in Arctic and Boreal biomes.

3.1.2 Arctic-Boreal Land Cover Change

Land cover in Arctic and Boreal ecosystems is highly dynamic and results from a combination of climate change, fires, permafrost degradation, drought, insect disturbance and land use (Helbig et al., 2016; Hogg et al., 2008; Ma et al., 2012; Myers-Smith et al., 2011; White et al., 2017). However, despite the strong impact of disturbance on the biophysical properties of high-latitude land surfaces, most studies analyzing changes in biophysical properties such as leaf area index or land surface greenness do not consider the role of land cover change, potentially biasing interpretation of apparent trends (Park et al., 2016). At global scales, some studies have found land cover change to have a relatively small impact on greening trends (Zhu et al., 2016). However, the extent and magnitude of disturbance in high-latitude biomes is significantly higher than the global average, with frequent and widespread fires exerting first-order control the demography,

successional stage, and carbon dynamics of Boreal forests (Bond-Lamberty et al., 2007; Kasischke et al., 1995; Soja et al., 2007). Remote sensing data sources used in many previous studies of NDVI trends at high latitude have shown substantial disagreement, suggesting substantial uncertainty in the Arctic-Boreal productivity. These differences may arise from sensor-specific characteristics, such as poor radiometric quality in AVHRR) and relatively coarse resolution from both AVHRR and the Moderate Resolution Imaging Spectroradiometer (MODIS) that does not resolve fires, harvests, and other sub-pixel disturbances (Alcaraz-Segura et al., 2010; Ju and Masek, 2016; Stow et al., 2007).

Recent work has begun to clarify many of these issues using remotely sensed imagery with higher spatial resolution that provide substantially improved thematic detail (Bartsch et al., 2016; Greaves, 2017; Treat et al., 2018), and which therefore capture land cover dynamics in Arctic and Boreal ecosystems (Hermosilla et al., 2018). Ju and Masek (2016) used Landsat imagery to identify NDVI trends resulting from small-scale disturbances that were not captured by the widely used GIMMS3g NDVI dataset. In a similar study, Sulla-Menashe et al. (2018) showed that the strength and direction of NDVI trends over 1984-2011 in Canadian Boreal forests is strongly controlled by the timing of disturbance. Specifically, forest disturbances that occurred later in the NDVI time series (i.e. later than 1990) were associated with strong negative trends, and disturbances that occurred earlier in the time series (i.e. between 1970 and 1990) were associated with positive trends. Pastick et al. (2019) demonstrated that Alaska is experiencing large areas of changes in NDVI and land surface wetness that are related to

a variety of land change processes that operate at both large (e.g. 100s of km) and small spatial scales (e.g. 10s of m). However, their work does not explicitly account for land cover change, and only characterize land change processes within the context of spectral indices, which can be hard to interpret without extensive visual interpretation of very high-resolution imagery. Land cover change processes require sufficient spatial resolution to be resolved and to therefore be characterized with respect to large scale ecosystem change.

Alternatives to NDVI as a proxy for land surface productivity or biomass have been an active area of research, resulting in the conception of other spectral indices such as the enhanced vegetation index (EVI; Huete et al., 2002) or the photochemical reflectance index (PRI; Gamon et al., 1992; Garbulsky et al., 2011) that attempt to improve upon or complement the information provided by NDVI. Considerable recent research has investigated the measurement and application of sun-induced fluorescence (SIF), a remotely-sensed proxy of photosynthesis (Meroni et al., 2009; Sun et al., 2017). Because fluorescence is more directly related to photosynthetic rate (Damm et al., 2010), does not appear to saturate across a range of land covers (Zhang et al., 2014), and has direct physical meaning related to productivity (Krause and Weis, 1991), it may provide a suitable next generation over NDVI for the remote sensing of land surface productivity. Studies of fluorescence have typically occurred at coarse spatial scales (Guanter et al., 2014) and focused on the impact of environmental stressors on fluorescence yields (Verma et al., 2017). There is still considerable research to be done to confirm that the influences of disturbance and successions on productivity, which are well-known from

eddy covariance studies (Goulden et al., 2011; Zimov et al., 1999), are captured in measurements of fluorescence.

To address this issue, we explore the role of land cover dynamics in controlling land surface greenness, as expressed in remotely sensed NDVI. Specifically, we explore how changes in land cover due to disturbance, climate change, and land use impact temporal dynamics and trends in NDVI across multiple decades. We utilize maps of land cover produced earlier in this dissertation to characterize continental scale land cover change over the period 1984-2014 and compare how areas of land cover change overlap with areas of significant trends in NDVI. The results we report here build upon and extend previous efforts from the literature, focusing on trends in NDVI in northwestern Canada and Alaska and their relationship with land cover and land cover change, as derived from Landsat, as well as an exploratory analysis into the relationships of sun-induced fluorescence, land cover, and time since disturbance. Specifically, we aim to answer the following questions:

1) What proportion of trends in NDVI are related to changes in land cover change?
2) How does the nature of the land cover and land cover change control the sign and magnitude of trends in NDVI?
3) Can Landsat resolution (30 m) capture landscape-scale dynamics of land cover change and NDVI trends?
4) How does land disturbance history impact our interpretation of trends in productivity from NDVI and other remotely sensed proxies (e.g., SIF)?

3.2 Methods

3.2.1 Land Cover and Land Cover Change Maps

Our analysis relies heavily on two medium spatial resolution datasets that cover the ABoVE Core Study Domain: (1) annual land cover and land cover change maps from Chapter 1 spanning 1984-2014; and (2) NDVI time series and trends from Ju and Masek (2016). Both data sets are derived from time series of Landsat 5 Thematic Mapper and Landsat 7 Enhanced Thematic Mapper imagery, are geometrically registered using the same projection and tiling system at 30 meter spatial resolution, and are publicly available.

The land cover and land cover change data set are described in the previous chapter, which show that 13.6 ± 2.6% of the Arctic and Boreal Region in northwestern North America has experienced land cover change over the last 30 years. This dataset was generated using a semi-supervised algorithm that combines unsupervised clustering of seasonal-spectral features, visual interpretation of high-resolution imagery, and machine learning-based classification. Prior to classification, periods of stable land cover and land cover change events were identified at each pixel using the Continuous Change Detection and Classification algorithm (Zhu and Woodcock, 2014). The resulting land cover and land cover change data base spans the period from 1984-2014 and provides annual maps of both land cover and land cover changes for the ABoVE Core Study Domain. For this work, we used these data to distinguish areas with stable land cover from those that experienced land cover change, to characterize the nature of land cover change where present, and to compute the time since change prior to each change event.

The land cover change dataset provides maps of ten stable land cover types and seven modes of land cover change (Table 2.1). Stable land cover classes include Evergreen Forests, Deciduous Forests, Shrubs, Herbaceous, Sparse Vegetation, Barren, Fens, Bogs, Shallows, and Water. Because they are the primary vegetation types in the domain and their relatively large proportional coverage of the domain, we focused on just six classes: Evergreen Forests, Deciduous Forests, Shrubs, Herbaceous, Sparse Vegetation, and Barren land. Land cover change classes identified transitions between specific groups of land cover types between 1984 and 2014. We considered major six change classes: Evergreen Forest Loss, Shrub Loss, Deciduous Forest Gain, Evergreen Forest Gain, Herbaceous Gain (from previously Sparse Vegetation or Barren), and Shrub Gain (from Herbaceous, Sparse Vegetation, or Barren). These land cover change types were selected to identify the most important changes that potentially drive trends in productivity (Augusto et al., 2015; Elmendorf et al., 2012; Zhang et al., 2013; Zimov et al., 1999), and only included change classes that covered more than 1% of the study domain, by area.

3.2.2 Landsat-based Greening and Browning data

To analyze NDVI trends, we used data created by Ju and Masek (2016), which was extracted from time series of Landsat 5 and 7 surface reflectance imagery for the period 1984-2012 and spans most of Canada and Alaska. In Ju and Masek's trend dataset, the 1984-2012 NDVI trend at each pixel was calculated by fitting an ordinary least squares linear model against the peak summer NDVI values as a function of year.

Statistically significant trends ($\alpha = 0.05$) were included in the analysis. For this work, we restricted the NDVI trend data to the ABoVE study domain to match the land cover and land cover change data. The datasets represent slightly different time periods (1984-2014 for the land cover dataset, 1984-2012 for the NDVI trends dataset), but differences arising due to land cover change occurring late in the time series (i.e. occurring in 2013 or 2014) are assumed to be negligible. Both datasets were projected to the same Albers Equal Area projection and tiled according to the system used by the ABoVE project.

The study domain excludes areas that are mapped as water. Furthermore, the extent of Ju and Masek's NDVI trend dataset does not fully overlap the ABoVE domain. The total studied area, after excluding water and non-mapped areas from the NDVI trend dataset, covered 3.86×10^6 km^2.

3.2.3 Disturbance Drivers

To support our analysis of how disturbance type influence trends in NDVI, we used several existing datasets that catalogue the occurrence of fires and harvesting throughout the study domain. To characterize fire disturbance, we combined the Alaskan Large Fire Database (Kasischke, Williams, & Barry, 2002) and the Canadian Fire Database (Stocks et al., 2002) to produce a unified database of fire perimeters for the ABoVE Core Study Domain that spans the period from 1917-2012. In additional, we used Landsat-derived datasets for the timing and location of timber harvest in Canada (White et al., 2017). There was no reported timber harvest in the Alaskan portion of the study domain (Smith, 2002).

Because the disturbance driver data are at relatively high spatial scale (e.g. 30 m) that matches the NDVI trend and land cover dataset, it is possible to directly compare spatial patterns between the two. Ju and Masek (2016) showed that AVHRR-scale patterns in NDVI trends are likely biased due to their inability to capture fine scale disturbance and land cover change. We focus on several areas of considerable landscape disturbance to consider the viability 30 m Landsat data for characterizing both land cover change and changes in NDVI.

3.2.4 Sun-Induced Fluorescence Preprocessing

As a complementary source of remotely sensed information related to productivity, we used data from the Orbiting Carbon Observatory-2 (OCO-2), which measures sun-induced fluorescence (SIF) in both the 757 nm (SIF_757) and 771 nm (SIF_771) bands, across the ABoVE domain between 2014 and 2017. We used OCO-2 SIF Lite version 8 files, which have been bias-corrected and quality screened and include a daily correction factor to account for variation in sun-sensor geometry (Sun et al., 2017). We filtered SIF measurements for the peak growing season, defined as occurring between day of year 180 and 240 (June 29 – August 28); this growing season definition matches that used by Ju and Masek (2016) for deriving their peak NDVI trend data. Because our land cover time series dataset ends in 2014, we assume that land cover did not change significantly between 2014 and 2017 across the OCO-2 samples. To explore relationships among land cover and SIF, we intersected OCO-2 retrieval footprints (1.3 x 2.1 km^2) with 30 m land cover from 2014, assigning the land cover class with the highest

percent coverage within each footprint. We only analyzed SIF measurements where its footprint had a relatively homogenous land cover composition – that is, if the majority vegetation type covered at least 67% of the footprint. In addition, to evaluate the impact of land cover history, we computed the mean time since disturbance within each OCO-2 footprint.

To reduce noise in the SIF retrievals, we performed several preprocessing steps, following the guidelines in the SIF Lite files user guide. First, we averaged both SIF_771 (SIF at 771 nm) and SIF_757 (SIF at 757 nm) across multiple simultaneously retrieved footprints, including adjusting each combined footprints' land cover and age distribution as the weighted average of the underlying footprints. We then applied the daily solar zenith angle-based correction factor to each combined footprint's mean SIF_771 and SIF_757 values. To further reduce noise, following the user guide, we multiplied SIF_771 by 1.5 to match the scale of SIF_757, and took the average of the two SIF measurements.

We additionally compared SIF measurements with peak growing season NDVI occurring near the end of the time series collocated within OCO-2 footprints. Due to the relatively short length of the record of OCO-2, it was not possible to create a long time series to estimate trends and compare with greening trends directly. Therefore, instead of analyzing NDVI changes over time, we analyzed absolute values of NDVI, informed by information on disturbance timing, to compare with observations of SIF. To minimize changes in NDVI that might occur due to land cover change, we focused on growing season values of NDVI in a limited timespan that was close in timing with the available

2014-2017 OCO-2 SIF data (i.e. the end of the time series). Within each OCO-2 retrieval footprint, we calculated the mean growing season NDVI value, and to minimize the impact of interannual variability in climate, greenness, and cloudiness, we averaged annual peak NDVI from 2010 to 2014. Hence, the resulting NDVI values represented the mean growing season NDVI for each pixel and land cover at the end of the Landsat time series used for this work. Over each ABoVE tile and year between 1984 and 2014, the peak growing season NDVI was estimated as the per-pixel maximum NDVI occurring between day of year 180 and 240 (June 29 – August 28) (Sulla-Menashe et al., 2018).

We additionally considered the relationship between NDVI and NIRv, the product of NDVI and the land surface reflectance in the near infrared. The NIRv has recently been proposed as an alternative to NDVI that captures the spatial and temporal variability of sun-induced fluorescence at monthly and 1-degree grid cell scales (Badgley et al., 2017).

3.2.5 Analysis

Our analysis is organized into four parts: (1) characterizing the amount of overlap of areas of land cover status and NDVI trends, (2) characterizing the distribution of NDVI trend magnitude (i.e. the slope of the trends) associated with each land cover and land cover change type, (3) mapping example areas of heterogeneous land cover change and NDVI trends and (4) characterizing the relationship between SIF, NDVI, and land cover.

To determine the areas of land cover change associated with NDVI trends, each 30 m pixel in the study domain was flagged with land cover, disturbance, and NDVI trend sign and magnitude, and each pixel was counted into domain-wide and ecoregion-wide area totals. We used this flagged dataset to analyze the areas of intersection and change and to generate maps of NDVI trends filtered for land cover status. We performed this analysis on both the broad land cover change statuses (i.e. stable versus change classes) and on individual land cover and land cover change classes.

To estimate the magnitude of NDVI trends associated with each land cover and land cover change class, we randomly sampled 1.5% of the study domain. We filtered our sample to statistically significant trends and a subset of the land covers, which focuses on shifts in vegetation types that we discuss throughout this paper (i.e. we excluded water and wetlands). We did not stratify our sample according to land cover, but our sample was large enough to capture the variability of NDVI trends across land covers (n = 3,670,464, smallest land cover n = 37,883). This sample was used to characterize the distribution in NDVI trend magnitudes across land cover and land cover change types.

We mapped some detailed examples to demonstrate the spatial heterogeneity in both land cover and NDVI trends captured by 30 m Landsat data. The detailed examples are shown for both an area with extensive logging in British Columbia, Canada and for an area with extensive and repeated fires in the Northwest Territories. We filtered the areas for land cover change status to demonstrate the spatial patterns of NDVI trends associated with land cover change and those associated with stable land covers.

To characterize the SIF measurements according land cover, we classified each SIF measurement during the growing season according to the underlying land cover in 2014 within the measurement footprint. Because of the resulting lack of mostly homogenous footprints covering certain land covers, we limited our analysis to four land covers – Evergreen Forest, Deciduous Forest, Shrub, and Herbaceous. We calculated the mean time since disturbance within each SIF footprint using our land cover and land cover change dataset, as well. If the majority of a SIF footprint had no land cover change in our dataset, it was classified as ">25 years since disturbance". In the ABoVE domain, 642,698 peak growing season SIF retrievals were acquired between 2014 and 2017; after the averaging procedures described above, and filtering for quality control, there were 60,807 observations. Of these combined footprints, 25,298 included a land cover class that covered more than 67% of the footprint, which were used for our analysis.

3.3 Results

3.3.1 Large-scale Patterns in Greening and Browning

Of the 3,861,514 km^2 in the ABoVE Core Study Domain for which Landsat NDVI trends were estimated by Ju and Masek (2016), 1,648,210 km^2 (42.7%) showed statistically significant trends, of which 1,309,937 km^2 (33.9%) were positive ("greening") and 338,272 km^2 (8.8 %) were negative ("browning") (Figure 3.1). Concurrently, 816,148 km^2, equivalent to 21.2% of the area of Ju and Masek's NDVI trend data within ABoVE study domain, experienced net land cover change between 1984-2014. Greening and browning were spatially widespread, but the highest magnitude

trends tended to occur in localized patches associated with areas of land cover change (Figure 3.2). Additionally, a substantial amount of the greening and browning are highly associated with the areas of fires throughout the domain (Figure 3.2c). Of areas with significant NDVI trends, just over a quarter (454,630 km^2; 27.6%) experienced a net land cover change from 1984-2014.

The rates and magnitudes at which greening and browning trends occurred varied widely as a function of land cover change status. For both changed and unchanged pixels, the distribution of trends tended to be bi-modal, with distinct modes of browning and greening in each case (Figure 3.1). In areas with stable land cover, 37.8% of pixels showed significant trends in NDVI, of which 83% were positive with a median increase of $+0.0023 \pm 0.0015$ yr^{-1} (median and interquartile range) and 17% were negative trends with a median decrease of -0.0021 ± 0.0019 yr^{-1} (Figure 3.1). In contrast, NDVI trends were roughly 50-100% larger in magnitude and more variable in areas with land cover change than in stable land cover areas (c.f., Figure 3.2a, b; Figure 3.1). The majority of pixels with land cover change (55.7%) showed statistically significant NDVI trends, of which 67.3% were greening trends, with a median trend of $+0.0034 \pm 0.0028$ yr^{-1}, and 32.7% of pixels showed browning trends with a median trend of -0.0048 ± 0.004 yr^{-1} (Figure 3.1b). Nearly half (43.9%) of browning pixels and nearly a quarter (23.3%) of greening pixels were associated with land cover change, even though land cover change occurred only over 21.2% of the study domain. Notably, a substantial portion of land cover change areas (44%) did not experience a significant trend in NDVI.

Consistent with results from Sulla-Menashe et al. (2018), our results suggest that spatial patterns of NDVI trends are strongly, but not exclusively, influenced by land cover change and disturbance processes (Figures 3.2 & 3.3). Broadly speaking, both land cover and land surface greening are changing significantly across the study domain. However, not all areas with land cover change are experiencing NDVI trends, and not all areas with significant NDVI trends are associated with land cover change. When excluding areas of land cover change, the regional patterns of NDVI trends are more widespread, but of lower magnitudes relative to trends in disturbed locations (Figure 3.3). Conversely, locations with the largest magnitude trends (both greening and browning) tend to be co-located with spatially coherent patches of land cover change, primarily Evergreen Forest Loss (Figure 3.2).

3.3.2 Greening and Browning Across Stable and Changing Land Cover Classes

Beyond the land cover change-specific variability in greening and browning trends, we observed substantial variability in the proportional area and magnitude of trends as a function of specific land cover and land cover change classes (Figure 3.4). Except for Sparse Vegetation, the majority of the area of stable land cover classes were not greening or browning, though there was considerable variability in the greening proportions across classes. The largest magnitude NDVI trends among the stable land cover classes occurred in the Shrub, Herbaceous, and Barren land cover classes (Figure 3.5), which is consistent with previous studies suggesting recent widespread increase in the fractional vegetation cover and overall growth of these land cover types (Elmendorf

et al., 2012). In general, pixels with stable land cover tended to have positive NDVI trends, although some browning occurred in Deciduous Forests (11.7%), Evergreen Forests (7.5%), and Sparse Vegetation (6.9%). All other stable land cover types experienced browning in less than 5% of their total area. Median greening trends across stable land cover types were of relatively lower magnitude, ranging from a low of $+0.0018 \pm 0.0014$ yr^{-1} in Deciduous Forests (median ± interquartile range) to a high $+0.0030 \pm 0.0017$ yr^{-1} in Herbaceous (Figure 3.5). Browning trends were similarly low magnitude, ranging from a low of -0.0017 ± 0.0010 yr^{-1} in Deciduous Forests to a high of -0.0022 ± 0.0029 yr^{-1} in Barren. Given the relative rarity of browning in stable land cover classes, the browning trend magnitudes for stable land cover reported here are unlikely to characterize much of the domain.

Land cover change classes, on the other hand, showed NDVI trends that tended to have larger magnitudes and were proportionally more frequent relative to pixels with stable land cover (Figure 3.4b). With the sole exception of the Shrub Loss class, the majority of the area for each land cover change class was greening or browning (Figure 3.4). Median greening trends across land cover change classes were generally of higher magnitude than in stable land cover classes, ranging from $+0.0029 \pm 0.0018$ yr^{-1} in Shrub Loss areas to $+0.0040 \pm 0.0029$ in Evergreen Forest Loss areas (Figure 3.5). Only Evergreen Forest Loss, Shrub Loss, and Evergreen Forest Gain had substantial areas (> 5%) of browning trends. Browning trends ranged from -0.0025 ± 0.0024 yr^{-1} in Evergreen Forest Gain pixels to -0.0055 ± 0.0037 yr^{-1} in Evergreen Forest Loss pixels. Intuitively, the largest browning trends occurred in the Evergreen Forest Loss and Shrub

Loss classes, while the largest greening trends occurred in the Deciduous Forest Gain, Evergreen Forest Gain, and Evergreen Forest Loss classes. Evergreen Forest Loss had, by far, the largest proportional area (43.7%) of browning. At the same time, 20.6% of Evergreen Forest Loss exhibited greening, which may relate to regrowth following forest loss occurring early in the Landsat time series. Somewhat counterintuitively, some areas mapped as Evergreen Forest Gain (7.1%) showed browning. Otherwise, NDVI trends for land cover "gain" change classes were dominated by greening.

When mapped, there were clear patterns in greening and browning trends according to specific land cover change classes. The largest magnitude trends were located in spatially coherent patches of forest and shrub loss in higher-latitude regions of the Boreal forest ecoregion (e.g., browning in Central Alaska and greening in the Northwest Territories) (Figure 3.6). At higher latitudes above the tree line, growth of new shrubs and herbaceous vegetation creates a more uniform, geographically extensive, and more subtle greening trend, particularly in the Canadian Arctic (Figures 3.1 & 3.2).

3.3.3 Spatial Heterogeneity of Logging and Fire-driven Greening Trends

The 30 m spatial resolution provided by Landsat supports analysis of how specific land cover change and disturbance processes (e.g., logging and fire) influence NDVI trends at multiple scales in a way that is not feasible from 8-km AVHRR or 500-m MODIS imagery. For example, figure 3.7 demonstrates the high spatial heterogeneity in greening trends due to timber harvest in a small area in British Columbia. The impact on NDVI trends of timber harvesting, which is primarily located in southern regions of the

Boreal biome, is variable in regard to both the sign and magnitude of NDVI trends at short (100s of m) spatial scales (Figure 3.7). High magnitude negative trends are most common in areas where timber harvest occurred later in the time series (e.g. after 1995), mapped as Evergreen Forest Loss where replacement of Evergreen Forests by Barren or Sparse Vegetation land covers creates a sharp drop in NDVI at the end of the time series. Locations with positive trends, on the other hand, are most common where timber harvest occurred early in the time series (e.g. before 1995) to allow for substantial regrowth, and are mapped as either Evergreen Forest Loss that occurred before 1995, or as either Evergreen Forest Gain or Deciduous Forest Gain. If land cover change is excluded from the trends in NDVI, the remaining trends in stable land covers are relatively subtle and sparse (Figure 3.7d). The greening trends associated with these early or pre-time series harvest events are mostly signals of forest regeneration.

In contrast to timber harvest, which was concentrated in the southern portions of the study domain, fire disturbance impacts ecological processes and landscape structure throughout the entire Boreal forest biome. As illustrated in Figure 3.8, areas experiencing significant fire disturbance tend to be characterized by more spatially complex mosaics with both positive and negative NDVI trends of varying magnitude. The complexity and heterogeneity of NDVI trends shown in Figure 3.8 are representative of patterns we observe throughout the Boreal forest, where the timing of fire disturbance exerts first order control on the sign and magnitude of NDVI trends. For example, some areas experience greening even though they are associated with Evergreen Forest Loss – these tend to be related to fires occurring on or after 1990. Meanwhile, forest regrowth,

represented either by the Evergreen Forest Gain class or a greening NDVI trend, are associated with fires occurring earlier in the time series (earlier than 1990). In contrast to the logging-dominated area shown in Figure 3.7, areas with stable land cover in Figure 3.8 show widespread greening in locations where fire events occurred before the start of the Landsat time series. This suggests post-fire recovery continuing beyond the re-establishment of the pre-fire land cover.

Overall, fire events occurred in 5.5% of pixels with positive trends across the study area and in 24.4% of pixels with negative trends, while harvesting occurred in 1% of pixels with positive trends and 3.4% of pixels with negative trends. Together, these fire and logging events represent important drivers of greening and browning in the Boreal biome. The largest magnitude trends were generally associated with these sources of stand replacing disturbance, and we find no material difference in the nature and magnitude of NDVI trends between areas that experienced fires versus those that experienced timber harvest. Pixels with land cover change not attributable to either fire or harvest account for 19% of positive trends and 24.0% of negative trends, suggesting that many other disturbance processes may be influencing greening trends in the study domain. However, data at comparable spatial resolution does not yet exist for these other drivers (e.g. insect infestation, drought, and permafrost degradation).

3.3.4 Land Cover- and Disturbance controls on Fluorescence and Greenness

To understand how greening and browning trends reflect changes in land cover and productivity, we analyzed SIF and NDVI as a function of land cover and time since

disturbance. In the Arctic biome, SIF varied linearly with NDVI across land covers across the range of observed mean NDVI (Figure 3.9). The vast majority of SIF observations occurred in Herbaceous land cover, though the Shrub land cover had the highest values of both SIF and NDVI. The range of SIF was considerably less pronounced (varying between 0 and 0.5 mW m^{-2} sr^{-1} nm^{-1}) than the range of NDVI (varying between 0.4 and 0.8). Meanwhile, in the Boreal biome, Deciduous Forests had the highest values of both NDVI and SIF, while Evergreen Forests had moderate values for NDVI and lower values for SIF, about half of Deciduous Forests SIF values. Boreal Herbaceous land cover spanned the whole range of observed NDVI and SIF. SIF and NDVI varied linearly across both biomes, except at very high NDVI (greater than 0.8), where the relationship saturated for Boreal Herbaceous and Deciduous Forests (Figure 3.9). This suggests a loss of sensitivity in NDVI at high values of SIF. Assuming SIF is linearly related to photosynthetic rate, this non-linearity in NDVI is consistent with studies showing a loss of sensitivity in NDVI to productivity and leaf area (Carlson and Ripley, 1997). This saturation of NDVI only occurs in the Boreal biome, where productivity is generally higher.

To understand more about productivity and SIF at the high ranges of NDVI, we explored the hypothesis that forest age is a significant control on productivity (Goulden et al., 2011; Pugh et al., 2019). We stratified values of SIF as a function of age, land cover, and ecoregion (Figure 3.10). In the Boreal biome, median SIF values over Evergreen Forests were roughly half as large as those observed over Deciduous Forests, and increased monotonically with age, from 0.6 for Evergreen Forests less than 10 years old

to 0.9 mW m^{-2} sr^{-1} nm^{-1} for Evergreen Forests older than 25 years. In contrast, SIF values over Deciduous Forests were maximum for forests of intermediate age (1.5-2.0 mW m^{-2} sr^{-1} nm^{-1} for Deciduous Forests 10-25 years after disturbance) and were lower for younger (1.2 mW m^{-2} sr^{-1} nm^{-1} for Deciduous Forests <10 years since disturbance) and older (0.9 mW m^{-2} sr^{-1} nm^{-1} for Deciduous Forests >25 years after disturbance) forests. In other words, there was a local optimum in SIF for Deciduous Forests as a function of age.

The values for SIF were considerably more variable for Shrubs and Herbs, and their values were not significantly different from those of Evergreen Forests. In the Boreal biome, only Deciduous Forests had significantly different values for SIF. In the Arctic, SIF values were generally higher over areas dominated by woody shrubs (median SIF values 0.4 – 0.8 mW m^{-2} sr^{-1} nm^{-1}) relative to areas dominated by herbaceous vegetation (0.2-0.4 mW m^{-2} sr^{-1} nm^{-1}), but there was substantial overlap suggesting that Shrub and Herb productivity do not vary too widely in the Arctic. We find no meaningful pattern in SIF with respect to time since land cover change in the Arctic.

In comparison, mean growing season NDVI showed clearer variation as a function of land cover type than that observed for SIF, and different patterns with respect to time since disturbance (Figure 3.10). In the Boreal biome, similar to patterns observed in SIF, NDVI was highest over Deciduous Forests and lowest over Herbaceous land cover. There was a weak positive relationship between NDVI and age for Deciduous Forests, but no discernible relationship between time since disturbance and NDVI within any of the other classes. The relationship between time since disturbance and NDVI for Deciduous Forests is in marked contrast with the relationship between time since

disturbance and SIF for Deciduous Forests, which experienced a noticeable mid-age maximum. In tundra regions above the tree line, NDVI was higher over Shrub land than over Herbaceous land, which is consistent with the general pattern observed in SIF. The difference between Shrub and Herb NDVI, however, was larger than the difference between Shrub and Herb SIF. Arctic Herbaceous land had a noticeable relationship for NDVI as a function of age, with NDVI reaching a minimum in middle-aged Herbs, while Arctic Shrubs did not show a noticeable relationship between NDVI and age.

The NIRv, calculated as the product of NDVI and near-infrared reflectance, has recently been proposed as an alternative to NDVI that captures the spatial and temporal variability of sun-induced fluorescence at monthly and 1-degree grid cell scales (Badgley et al., 2017). The patterns of NIRv we observed do not capture the same patterns of SIF but rather mimicked the patterns found in NDVI, suggesting that NIRv is not a substantial improvement over NDVI as an indicator of ecosystem productivity (results not shown).

3.4 Discussion

A growing body of research suggests that the ecology and productivity of high-latitude ecosystems is changing in response to climate change. Remote sensing studies have identified areas of both greening and browning (Beck and Goetz, 2011; Guay et al., 2014; Myneni et al., 2001; Parent and Verbyla, 2010), measurements of atmosphere chemistry have shown that the seasonality of atmospheric CO_2 is changing (Graven et al., 2013; Keeling et al., 1996), and model-based studies point to enhanced productivity in

Boreal and Arctic systems (Forkel et al., 2016; Luus et al., 2017). Because the relationship between NDVI and productivity is non-linear and depends on plant functional type, NDVI trends and landscape-scale changes in productivity must be interpreted in the context of concomitant changes in land cover. In the previous chapter, we showed that substantial portions of Arctic-Boreal northwestern North American have experienced changes in land cover due to both natural and anthropogenic disturbances. However, the manner in which landscape-scale land cover and land cover changes across the Arctic-Boreal Region contribute to large scale ecosystem changes has not been examined in detail.

3.4.1 Greening in Areas of Land Cover Change

Our results suggest a significant overlap between areas of land cover change and areas of greening and browning – roughly a quarter of pixels with significant trends in NDVI are associated with land cover change over the same time period. Not only is land cover change responsible for a large area of NDVI trends, but they are responsible for most of the highest magnitude trends for both greening and browning. Evergreen Forest Loss was the most extensive driver of trends, and it was responsible for both greening and browning, depending on the timing of disturbance. This suggests considerable uncertainty in the interpretation of NDVI trends – an area may be greening because of a loss of forest and an increase in high-NDVI Herbaceous cover, which would have very different implications for productivity and other biophysical land surface characteristics than an area greening due to steady forest growth.

Because of these competing effects different processes that change NDVI, it is important to characterize land cover change and NDVI trends using the spatial scale at which these disturbances occur. The detailed maps of harvest and fire presented here demonstrate the high spatial heterogeneity present for both the sign and magnitude of greening and browning trends in highly disturbed areas. These heterogeneous NDVI trends tend to cancel each other over small distances, and aggregating these changes to a coarser resolution results in a loss of sensitivity to these gains and losses of land surface greenness. Ju and Masek (2016) suggested that the coarse spatial resolution (8 km) and compositing methodology of AVHRR data inhibits realistic characterization of greening and browning trends in disturbed Boreal forests. While coarse spatial resolution instruments such as MODIS and AVHRR unquestionably provide valuable sources of image time series, the scale and complexity of variation in landscape processes at high latitudes limits the utility of these two data sources for studies attempting to understand how multiple agents (natural disturbance, human disturbance, climate change, etc.) that operate at multiple scales are driving change in high latitude ecosystems. It is beneficial to use Landsat data, as described in this study, to establish the context and interpretation of greening and browning trends in light of extensive and frequent land cover change at landscape scale.

Counterintuitively, there were many areas that had significant land cover change, but did not exhibit an NDVI trend. It might be expected that areas of stable land cover exhibit no trend or slight positive trends, reflecting gradual growth; however, land cover change often entails a large-scale shift in underlying plant cover, which would imply a shift in

NDVI. What we find, however, recapitulates the findings of Sulla-Menashe et al. (2018) – disturbances occurring in the middle of the time series will exhibit little trend. Studies using solely simple linear regressions of time series of NDVI are likely to miss substantial significant land changes and must be carefully evaluated with detailed land cover information (Pastick et al., 2019).

In the Boreal zone, where disturbance is common, NDVI trends reflect complex mosaics of disturbance history. In particular, a substantial portion of browning was associated with Evergreen Forest Loss due to abrupt disturbance. Boreal browning may also reflect gradual disturbances, such as drought (Hogg et al., 2008; Ma et al., 2012), insect infestation (Verbyla, 2011; Volney and Fleming, 2000), permafrost degradation (Helbig et al., 2016), or forest decline (Rogers et al., 2018) more generally. Counterintuitively, Boreal browning was observed in some areas Deciduous Forest and Evergreen Forest Gain – we hypothesize that these areas represent forest successional processes that are causing a shift from deciduous tree species with high NDVI to evergreen tree species with low NDVI. This pattern is also reflected in reduced productivity, as measured by SIF, in later aged Deciduous Forests (Figure 3.10). This may reflect recruitment of conifer tree species into areas initially colonized by deciduous trees after disturbance, which would reduce the average productivity. Extending the time series into the future may show these areas transition to Evergreen Forest. Importantly, each of these processes (succession, drought, and insects) would manifest as browning, but have substantively different implications for the long-term health and productivity of Boreal forests. However, limitations in disturbance datasets, both in terms of disturbance

type (e.g. insects) and relatively short time period (30 years) limit our ability to further explain greening and browning trends as a function disturbance.

3.4.2 Greening in Areas of Stable Land Cover

In contrast to the areas of land cover change, around 33 % of the stable land cover areas exhibited modest, but statistically significant, greening, primarily in the Arctic but evident throughout the study domain. By removing the areas of land cover change, the tendency for NDVI trends is to be of lower magnitude and generally not browning. The exact mechanisms behind observed greening in stable land cover cannot be inferred from this work, but they may reflect a combination of increased fractional vegetation cover or height (Berner et al., 2018), reduced surface water area (Raynolds and Walker, 2016), and shifts in community composition toward more deciduous species. These changes are largely indicative of widespread increases in vegetation productivity throughout the ABoVE study domain over the last 30 years. Incorporating land cover information provides additional context for understanding the drivers of greening and browning trends.

In Arctic ecosystems, disturbance was rare and land cover change was mostly limited to expansion of woody shrubs and herbaceous land cover. The vast majority of pixels showed increases in NDVI, again suggestive of increased productivity. Only a small proportion of pixels in Arctic ecosystems that showed statistically significant greening trends also showed land cover change, which we interpret as the areas of most dramatic shrub encroachment. This suggests that expansion of herbaceous vegetation and woody

shrubs is occurring at rates sufficient to be captured in 31-year time series of Landsat NDVI, but insufficient to cause a change in land cover over this period, especially in the Alaskan tundra where Shrub Gain and Herbaceous Gain-specific greening was not detected (Figure 3.6).

3.5.3 Interpretations of Productivity from Greenness

The implications of these results with respect to ongoing changes in high latitude ecosystem function and productivity, as well as the use of remote sensing to infer these changes, are numerous. A few studies have considered how disturbance impacts greening and browning trends, but either assume constant land cover or only examine large disturbances (Beck and Goetz, 2011; Hicke et al., 2003; Ju and Masek, 2016; Sulla-Menashe et al., 2018). The results presented in this paper demonstrate that recent and ongoing land cover change strongly influences the relationship between remotely sensed measures of productivity such as the NDVI and ecosystem change at high latitudes. For example, Evergreen Forest Gain and Deciduous Forest Gain exhibit similar trends in NDVI (Figure 3.5) but they are not equivalent in terms of their impact on carbon cycling and are parameterized differently in ecosystem models (Augusto et al., 2015; Zimov et al., 1999). Furthermore, the land cover and age-dependent structure of SIF measurements shown in Figure 3.10, as well as previous chronosequence studies of Boreal forest productivity, suggest that both carbon uptake and respiration in forests vary as a function of time since disturbance (Goulden et al., 2011). For example, Deciduous Forests had highest productivity at moderate ages and reductions in late aged Deciduous Forests, as

evidenced by the age-dependent patterns of SIF. Hence, characterizing the relationship between NDVI values and ecosystem productivity (and by extension, sensitivity to climate change) requires more complete representation of both land cover type and time since disturbance. As disturbance regimes change (Andela et al., 2017; Kelly et al., 2013; Soja et al., 2007), it's likely that significant Arctic-Boreal land cover will become even more variable in terms of land cover and age demography.

3.5 Conclusions

The results presented in this study demonstrate that studies focused on characterizing and explaining greening and browning trends in high latitude ecosystems must go beyond simple explanations that equate changes in NDVI with changes in productivity. We found that nearly one third of the greening trends in the ABoVE Core Study Domain were associated with land cover changes, suggesting a substantial bias in the interpretation of changes in NDVI as changes in productivity across the Arctic-Boreal biomes. The largest changes in NDVI occurred in areas of land cover change; ignoring land cover change therefore would overestimate the increases in ecosystem productivity implied by greening trends. Multiple lines of evidence suggest that ecosystem composition, structure, and function in high latitude terrestrial ecosystems has been changing over the last several decades. Remote sensing-based studies showing high-latitude greening and browning support this conclusion. However, excessive reliance on NDVI as a direct surrogate for productivity is fraught by over-simplification of their underlying relationship. Understanding land cover composition and history is therefore crucial to interpreting

observed trends in remotely sensing NDVI time series, and by extension, understanding the changes in ecosystem productivity and coupled ecosystem-atmosphere feedbacks to the climate system that NDVI trends are capturing.

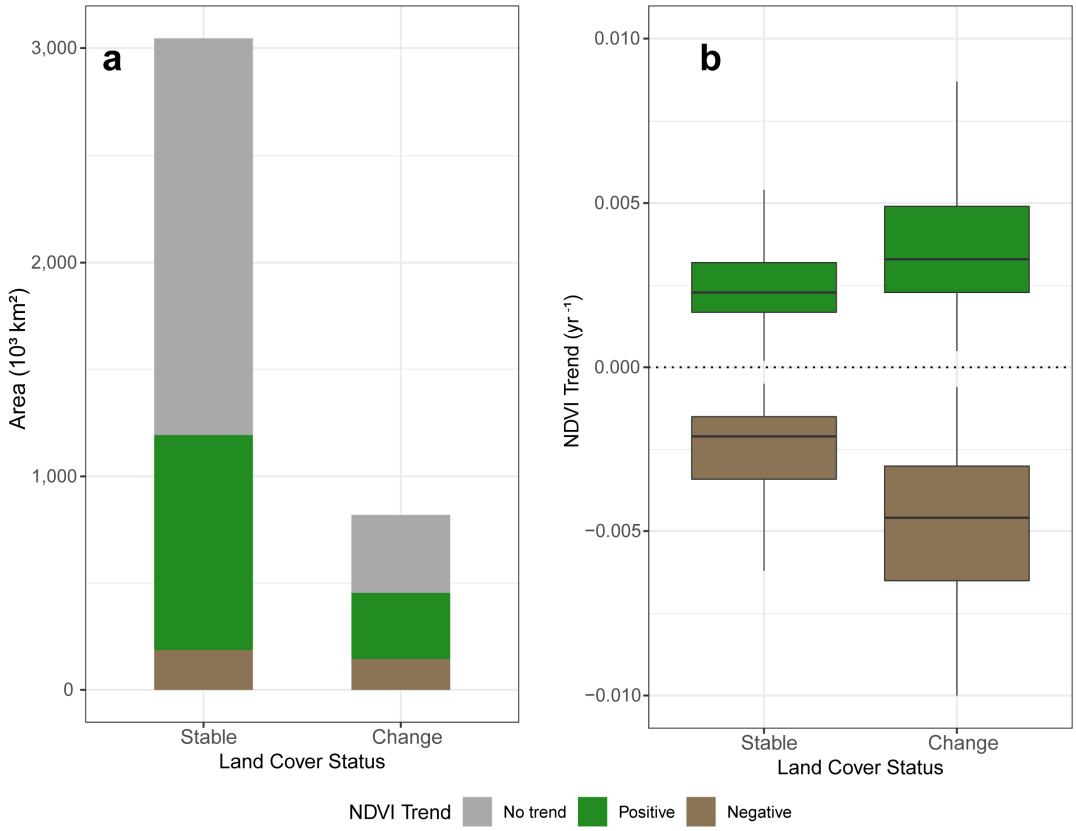

Figure 3.1 | Characterization of positive, negative, and non-significant NDVI trends as a function of land cover status across the ABoVE Core Study Domain. a) Total areas of NDVI trends by land cover change status. b) Distributions of positive and negative trend magnitudes as a function of land cover

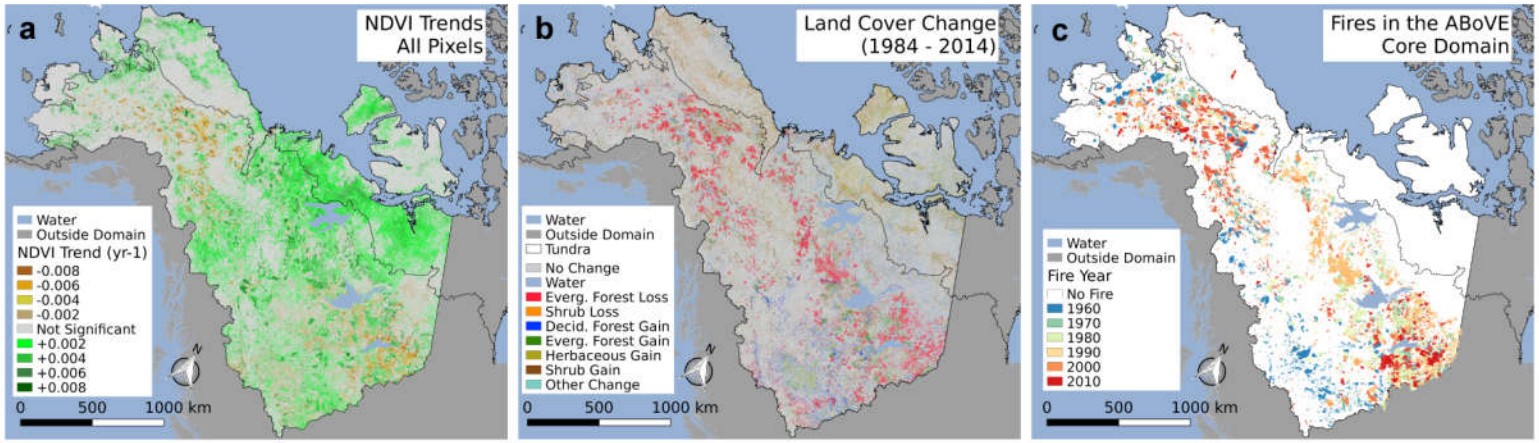

Figure 3.2 | Spatial distribution of NDVI trends and fires in the ABoVE Core Study Domain. a) Landsat-based NDVI trends from Ju and Masek (2016). b) Mapped areas of land cover change between 1984 and 2014 for key land cover transitions. c) Fires from the Canadian Fire Database and the Alaskan Large Fire Database.

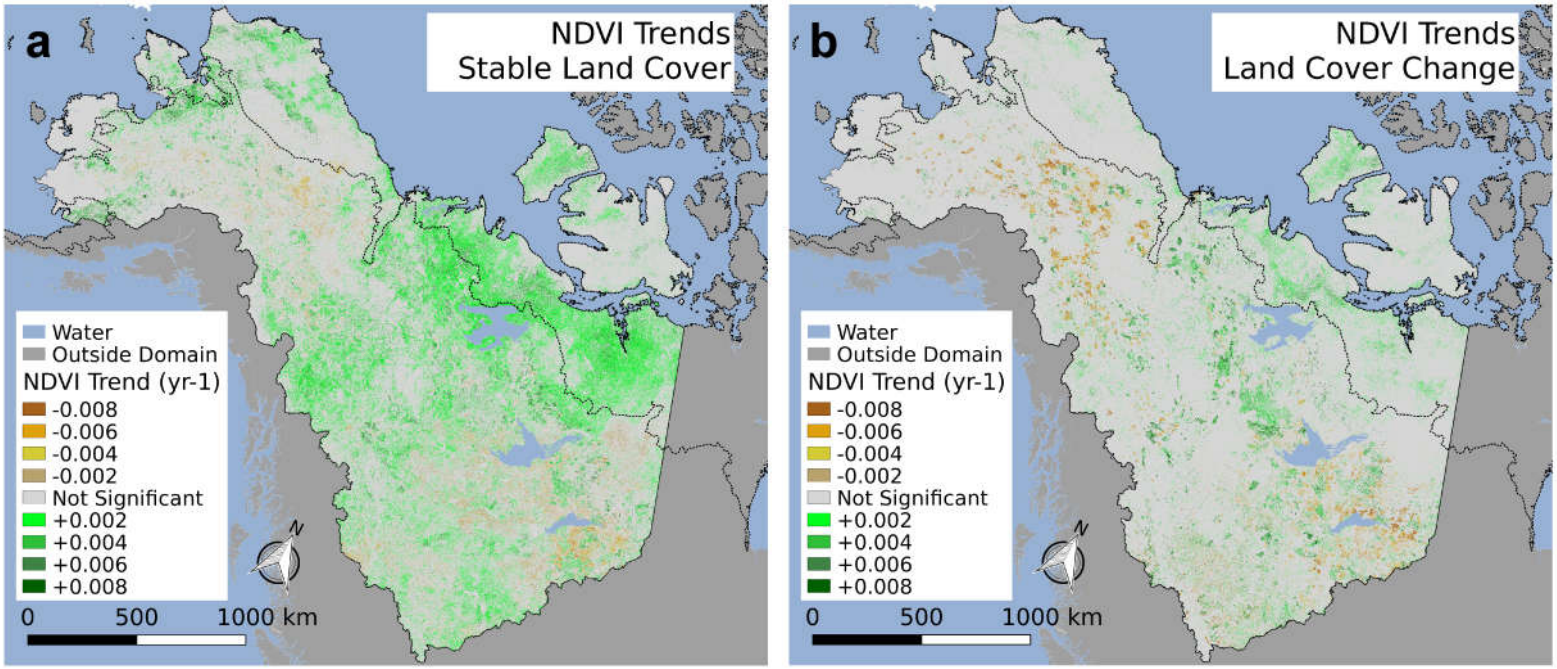

Figure 3.3 | Comparison of spatial distribution of land cover change and Landsat-based NDVI trends specific to land cover change status. a) Landsat-based trends in NDVI in areas with stable land cover. b) Landsat-based trends in NDVI in areas with changing land cover

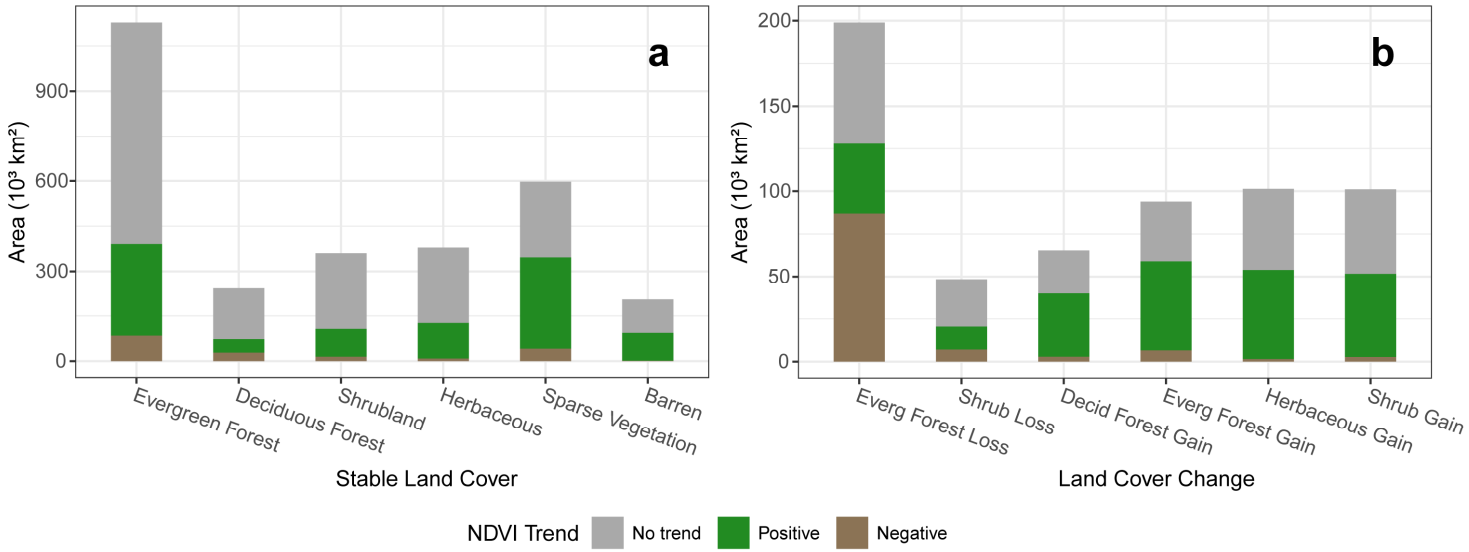

Figure 3.4 | Area distributions of NDVI trends as a function of land cover class and land cover change types. a) Area distributions for trends in areas of specific stable land covers. b) Area distributions of trends in areas of specific land cover change types.

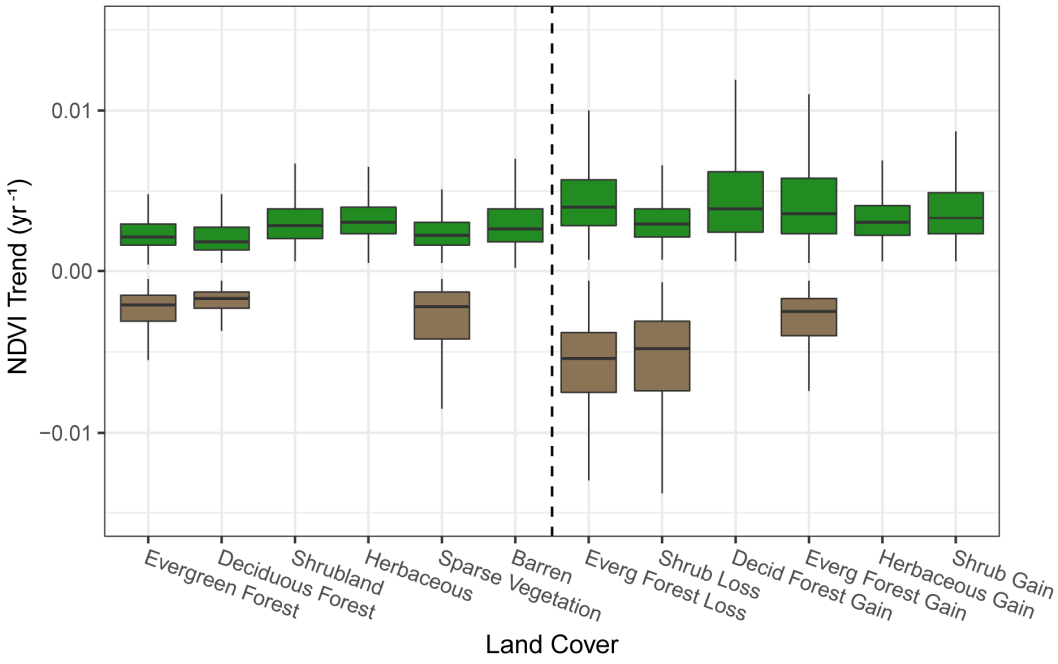

Figure 3.5 | Distribution of trend magnitudes as a function of both land cover type, land cover change type, and trend sign. Boxplots indicate median and interquartile range of a random sample of pixels across the domain (n = 2,626,923). Box plots are shown for a given NDVI trend sign if those NDVI trends accounted for a substantial (at least 5%) of the mapped land cover or land cover change area. Vertical dashed line indicates separation between stable land cover types (to the left) and land cover change types (to right right).

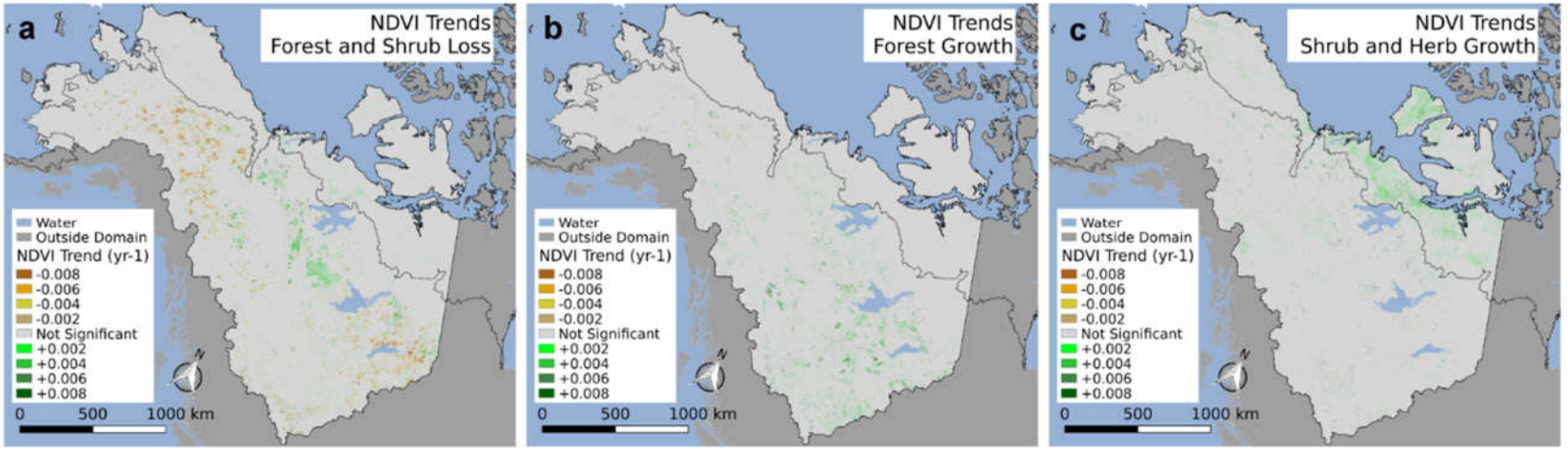

Figure 3.6 | Spatial distribution of NDVI trends as a function of aggregated land cover change types. a) NDVI trends associated with vegetation loss classes, including Evergreen Forest Loss and Shrub Loss. b) NDVI trends associated with forest growth classes, including Evergreen Forest Gain and Deciduous Forest Gain classes. c) NDVI trends associated with short vegetation gain, including Herbaceous Gain and Shrub Gain.

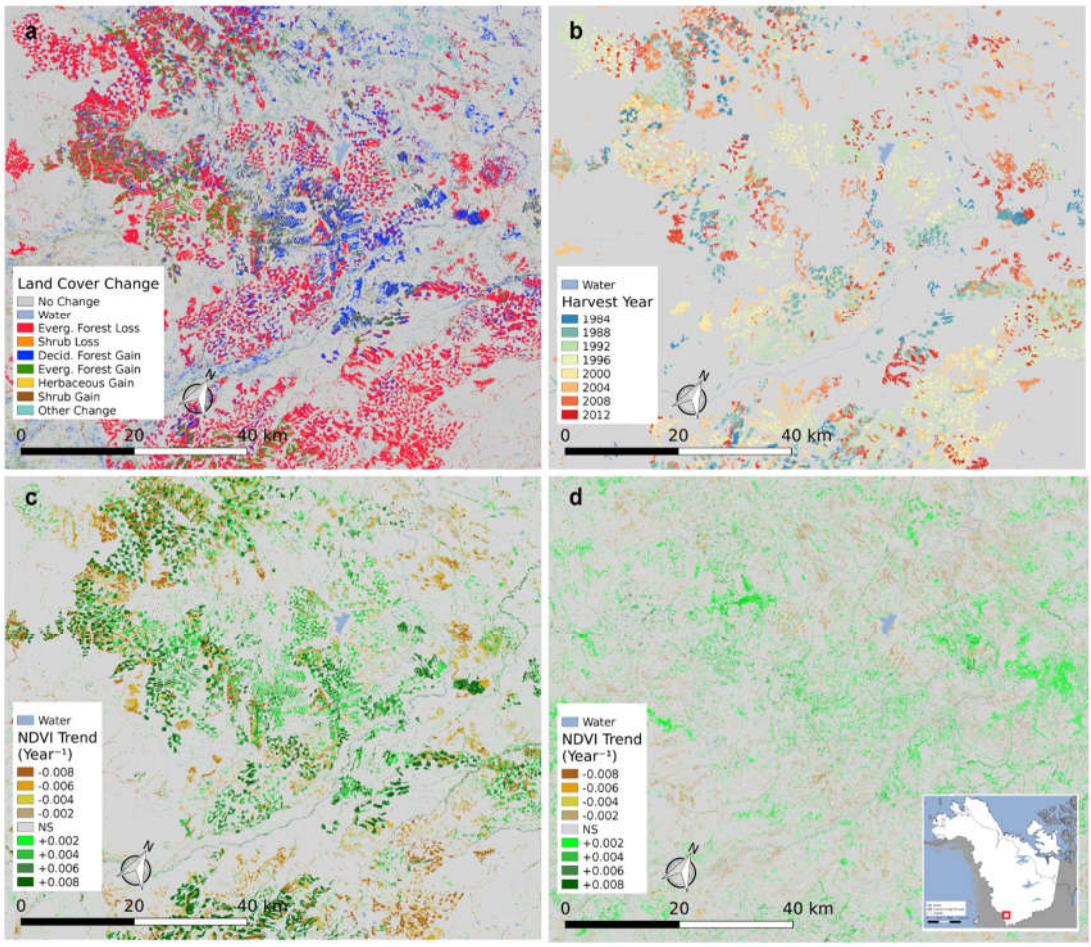

Figure 3.7 | Landscape-scale timber harvesting in British Columbia. Inset demonstrates the approximate area shown. a) Land cover change between 1984 and 2014 for the area. b) Timing of harvest events occurring between 1984 and 2012 in the region. Harvest data are drawn from the maps of White et al. (2017). c) NDVI trends associated with areas of land cover change. High magnitude trends are spatially associated with areas of timber harvest, with browning occurring in areas harvested late in the time series (i.e. after 2000) and greening occurring in areas recovering after being harvested earlier in the time series. d) NDVI trends associated with areas of stable land cover.

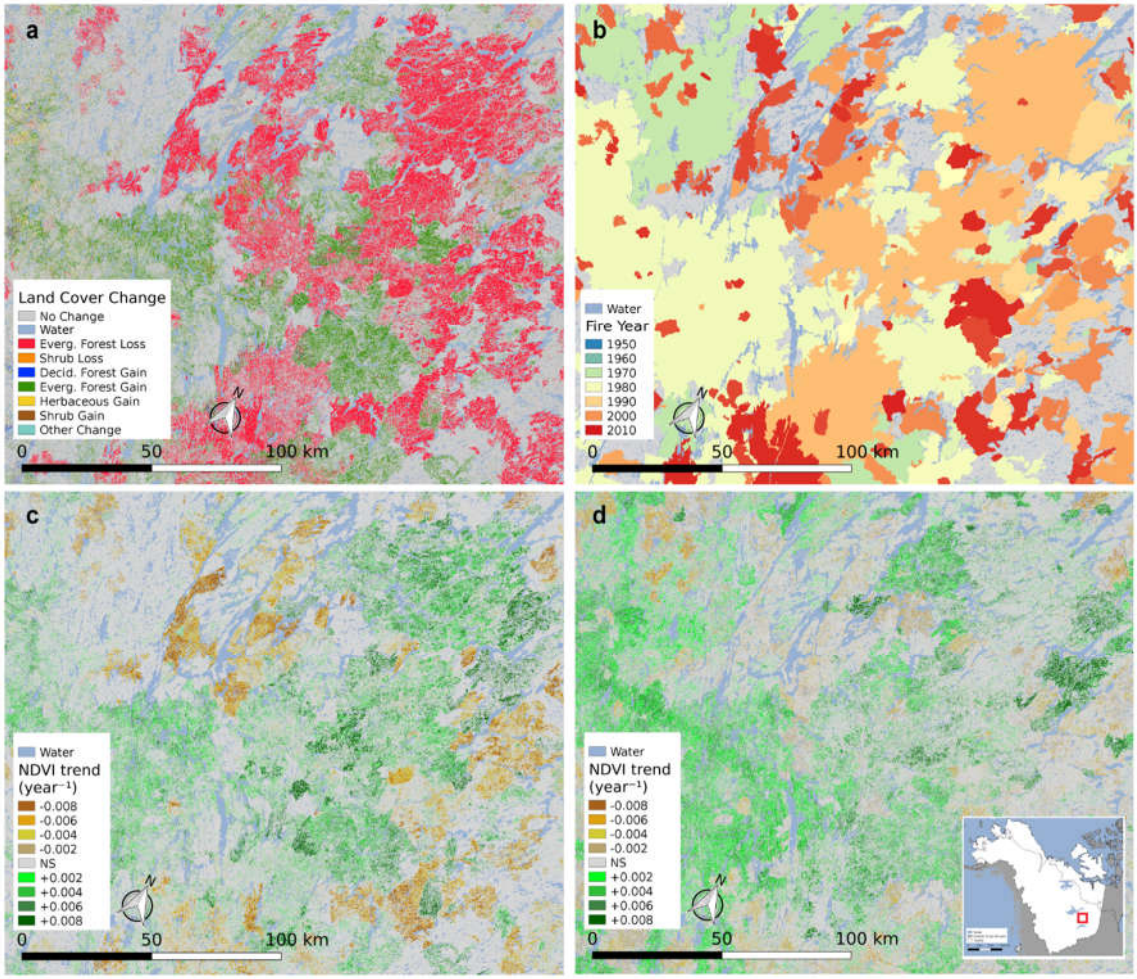

Figure 3.8 | Landscape-scale mosaics of fire-induced browning and greening in the Northwest Territories. Inset indicates approximate area shown. a) Land cover change occurring between 1984 and 2014. b) Fire perimeters from the Canadian Fire Database, with colors indicating year of fire. c) NDVI trends associated with areas of land cover change, including substantial browning from recent fires and greening from older fires. d) NDVI trends associated with areas of stable land cover.

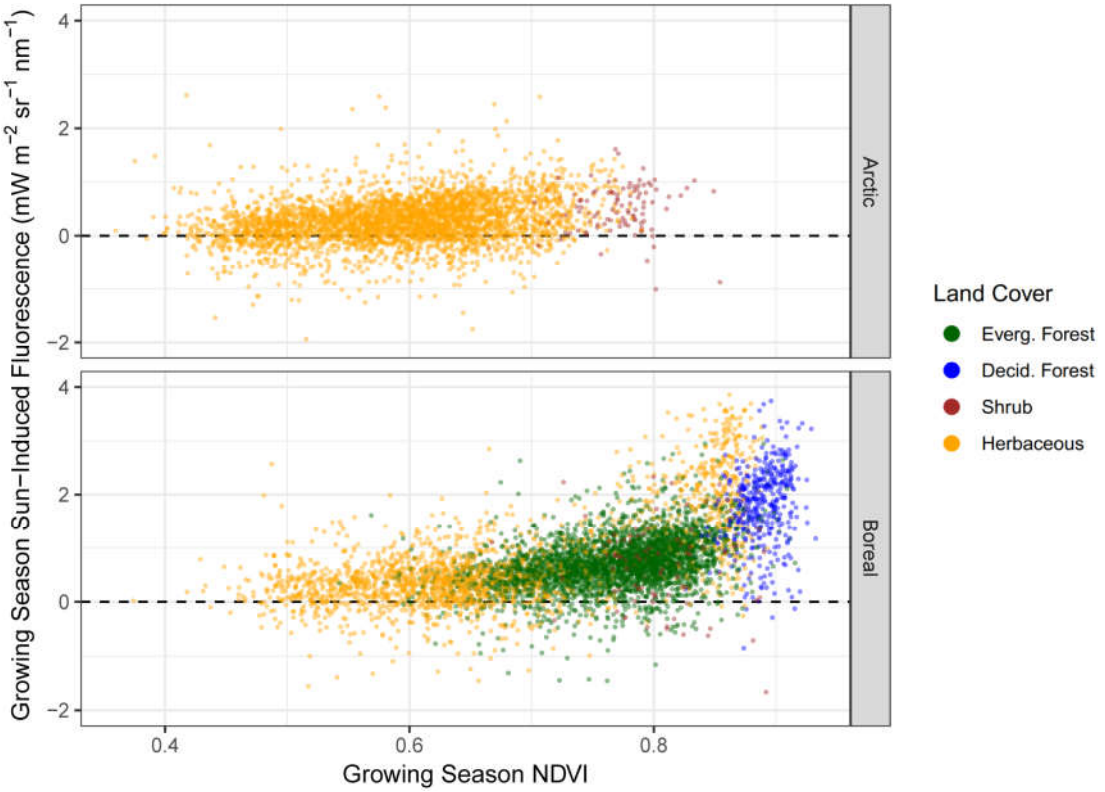

Figure 3.9 | Scatterplot showing relationship between normalized difference vegetation index (NDVI) and sun-induced fluorescence (SIF) across land cover and biome. Top panel: Herbaceous and Shrub pixels in the Arctic Biome. Bottom Panel: Forest, herbaceous, and shrub pixels in the Boreal biome. The delineation between Arctic and Boreal biomes were defined by the tundra ecoregions from the EPA Ecoregion Level 1 designations. SIF pixels were included if their underlying land cover distributions were relatively homogenous (at least 67% one class).

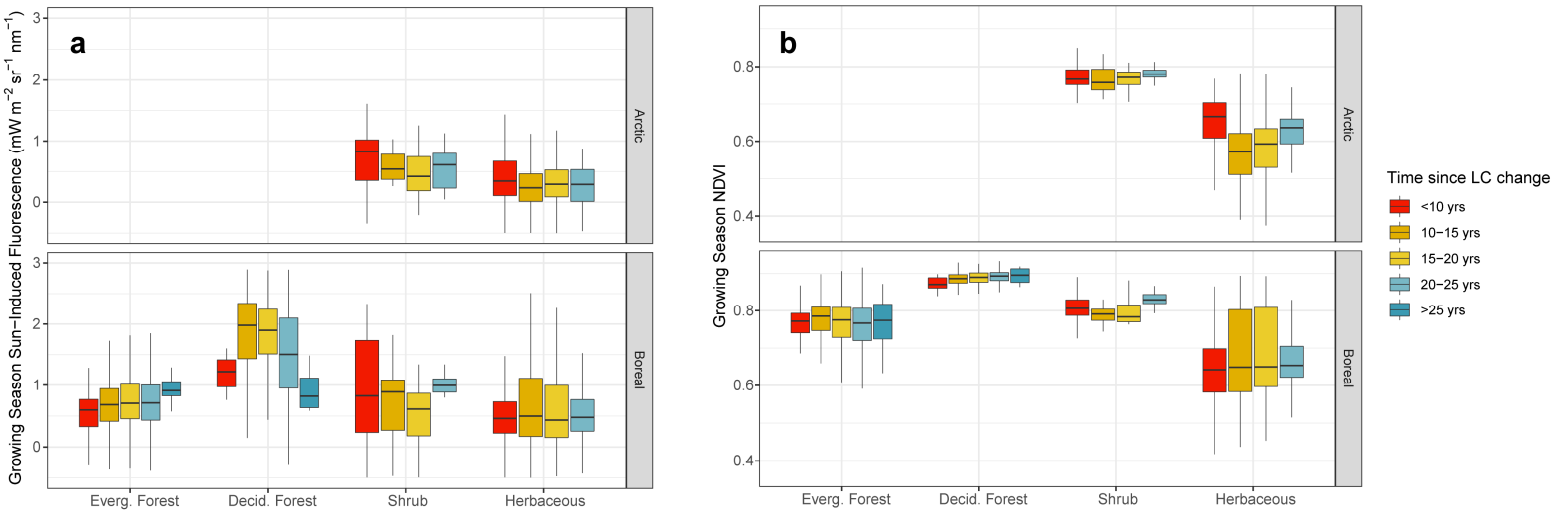

Figure 3.10 | Distributions of remotely-sensed indicators of growing-season productivity as a function of land cover, biome, and time since disturbance. a) Distributions for sun-induced fluorescence, showing substantial age-dependent relationships. b) Distributions for NDVI, which does not show age-dependent relationships. Top and bottom panels refer to Arctic and Boreal biomes, respectively, as defined by the tundra ecoregions from the EPA Ecoregion Level 1 designations.

DISTURBANCE-DRIVEN DYNAMICS OF ABOVEGROUND BIOMASS IN BOREAL FORESTS ACROSS NORTHWESTERN NORTH AMERICA

4.1 Introduction

Boreal forests are a critical component of the global carbon cycle due to their vast extent, climate sensitivity, and the immense amount of carbon they store in aboveground biomass and soil (Malhi et al., 1999). Changes in Arctic and Boreal productivity via CO_2 fertilization, warming, and land cover change have been linked to observed increases in high latitude productivity (Zhu et al., 2016). Therefore, understanding variability in Boreal and Arctic productivity is crucial to understanding changes in global carbon-climate feedbacks (Forkel et al., 2016; Graven et al., 2013; Zhu et al., 2016). Further, the annual carbon balance of Boreal forests is highly sensitive to climate forcing because both direct (e.g. drought) and indirect (e.g. fires) impacts of climate warming may induce tree mortality and cause the Boreal forest to transition from a carbon sink to a carbon source (Bond-Lamberty et al., 2007; Bradshaw and Warkentin, 2015; Kasischke et al., 1995). However, there is considerable uncertainty in the sign, magnitude, and nature of the most important drivers of change in Boreal forest carbon budgets (Magnani et al., 2007) due to the competing influences of climate-driven growth, disturbances, and post-disturbance recovery (Bond-Lamberty et al., 2007).

Repeat observations from remote sensing have long been used to characterize changes in ecosystem properties at synoptic scale. NDVI trends, in particular, have been

heavily used to describe changes in productivity and biomass resulting from fires and climate change (Beck and Goetz, 2011; Myneni et al., 2001, 1997a; Park et al., 2016). However, NDVI is an index with only indirect physical relationships to ecological properties such as leaf area or productivity, and hence, is difficult to interpret. In particular, NDVI values depend on land cover type, time since disturbance, spatial resolution, and sensor characteristics, and NDVI signals are sensitive to sub-pixel mixtures of land cover in coarse imagery (Alcaraz-Segura et al., 2010; Guay et al., 2014). NDVI trends are therefore particularly difficult to interpret in areas with extensive land cover change and high spatial heterogeneity, such as Boreal forests and Arctic tundra (White et al., 2017).

In contrast, aboveground woody biomass and its annual increment is a direct measure of carbon accumulation that can be easily compared across land cover types, ecoregions, and algorithms. Accurate tracking of biomass allows detection of gradual changes resulting from forest growth as well as subtle “press” disturbances that arise from drought, insect infestation, or forest degradation at sub-pixel scale (Eamus et al., 2013; Hogg et al., 2008; Ma et al., 2012; Volney and Fleming, 2000). Typically, forest biomass is estimated from forest surveys, relying heavily on allometric equations that convert forest structural properties to biomass per unit area (Zianis and Mencuccini, 2004). However, sampling plots that track long-term changes in forest structure are resource intensive, especially in geographically expansive and remote northern high-latitude systems. As a result, high quality information on forest structural characteristics are rare in Boreal forests. For example, the ForestGEO database of forest plots only has

one plot in the taiga of Canada, limiting the ability of researchers to generalize forest structural characteristics across Boreal Canada (https://www.forestgeo.si.edu/sites-all). Hence, remote sensing provides an important tool for monitoring biomass change over large areas in the Boreal biome (Lu, 2006).

The use of lidar remote sensing, an active remote sensing technique that measures forest structural properties by tracking the returned energy from a laser shot propagated at the surface, has become increasingly utilized for estimation of Boreal forest structural properties and, by extension, Boreal forest biomass via allometric equations (Bolton et al., 2017; Lefsky et al., 2002; Matasci et al., 2018a). Airborne and satellite-based lidar remote sensing have been used to simulate forest survey plots (so-called 'lidar plots'), thereby substantially increasing the amount of information on forest structure that is available across large areas relative to conventional forest surveys. Using plot data from both traditional and lidar-based sources in combination with time series of satellite-based surface reflectance data, total forest carbon stocks and changes in stocks in both the tropics and Boreal forests have been estimated (Baccini et al., 2004; Matasci et al., 2018b). These hierarchical, multi-source approaches to forest biomass estimation allow results from non-mapping lidar sensors with limited temporal coverage (e.g., the Geoscience Laser Altimeter Sensor (GLAS) onboard the Ice, Cloud, and Elevation Satellite (ICESat)) to be extended across vast regions over long timespans, revealing relationships between changes in forest biomass and trends in climate, disturbance, and land use. For example, Baccini et al. combined GLAS data with surface reflectance from the Moderate Resolution Imaging Spectroradiometer (MODIS) to map carbon density

maps in the tropics (Baccini et al., 2012). This approach was then extended to map time series of biomass and show that tropical forests, through repeated net losses of biomass, are a net source of carbon due to extensive logging (Baccini et al., 2017).

In contrast, efforts to estimate aboveground biomass (AGB) specifically in Boreal forests have focused on single points in time. Neigh et al. (2013) developed an estimate of circumBoreal forest AGB for a single year using MODIS data. Similarly, Matasci et al. (2018) developed annual estimates of Canadian Boreal forest AGB by combining airborne lidar with time series of Landsat data, but did not explicitly characterize any changes across time. Further, Matasci et al. did not include land cover or forest type (e.g. deciduous versus evergreen forest), which has been shown to be an important factor in estimating biomass from allometric equations (Asner et al., 2009; Drake et al., 2003; Wang et al., 2013). Field studies demonstrate that disturbance, drought, and land use exert first-order control on the carbon budget of Boreal forests through time. By analyzing permanent sampling plots, Ma et al. (2012) concluded that regional droughts have been reducing the biomass carbon sink in Canada's southern Boreal forest. Hogg et al. (2008) also found significant reductions in productivity and biomass resulting from drought in western Canada's deciduous forest. These studies, however, only represent small portions of Canada's Boreal forests and cannot be easily generalized across the domain. Because Boreal forests are geographically extensive, remote, and prone to disturbance, comprehensive information related to large-scale dynamics and trends in Boreal forest AGB remain poorly quantified.

Here we use an extensive inventory of forest lidar plots derived from GLAS data to estimate machine learning models that predict AGB from time series of Landsat surface reflectance data, and then use these models to create large scale maps of AGB dynamics in Boreal forests. Our study domain includes all forested ecoregions within the Core Study Domain of NASA's Arctic-Boreal Vulnerability Experiment (ABoVE), which extends from Alaska to northwestern Canada. Lidar plot data from GLAS provide extensive and unbiased geographic coverage that captures a wide array of forest types and disturbance histories that are not available at this scale from traditional forest inventory plots. When coupled to Landsat data via machine learning models, our maps provide spatially continuous estimates of AGB and their changes at a spatial resolution that resolves individual forest disturbance and regrowth trajectories. By extension, these maps provide new insights related to net changes in AGB carbon stocks and the landscape-scale processes that are causing these changes. Using these datasets, the research presented in this paper was designed to address the following research questions:

(1) What are the spatial and land cover-based patterns of AGB stocks and AGB changes across Boreal ecosystems in northwestern North America?

(2) How do different disturbance processes such as fire, harvest, and recovery control long term trends and interannual variability in carbon accumulation across different ecoregions?

(3) Which ecoregions are experiencing net losses of AGB? Which are experiencing gains?

(4) What are the strengths and weaknesses of NDVI as a metric for characterizing disturbance and regrowth dynamics in Boreal forests?

4.2 Methods

4.2.1 Overview

Our methodology includes three main elements: (1) estimation of a machine learning-based model to predict AGB over Boreal forests from time series of Landsat surface reflectance data, (2) application of this model to ecoregions within the ABoVE Core Study Domain that include Boreal forests, and (3) analysis of the biogeographic patterns and temporal trends in accumulation of AGB throughout the study domain. Our analysis focuses on aboveground live woody biomass in trees and shrubs (hereafter simply referred to as AGB), and does not include other carbon stocks (e.g., in soils and foliage). We therefore exclude Arctic ecoregions (e.g. tundra), which have relatively low amount of woody AGB. Ecoregions were based on the level 2 ecoregion designations from the Environmental Protection Agency (EPA), which capture spatial variability in Boreal forest density, soil types, and disturbance regimes (http://www.cec.org/tools-and-resources/map-files/terrestrial-ecoregions-level-ii).

4.2.2 GLAS Global Biomass Inventory

We utilized a recently developed global inventory of AGB plots estimated from GLAS data to calibrate our AGB models (Farina et al., 2019). We briefly overview its

generation here. The global AGB inventory was derived using GLAS/ICESat Version 33 data downloaded from the National Snow and Ice Data Center (NSIDC). GLAS is a full-waveform sampling lidar that generates 70 m diameter samples with 127 m along-track spacing. The full-waveform nature of GLAS allows it to be used to estimate multiple lidar metrics (e.g., quantile height or canopy height). Lidar waveform data from GLAS were used to replicate forest structural metrics using equations provided in existing literature. For each GLAS footprint, plot-scale AGB was estimated using lidar-based forest structural metrics in combination with allometric equations that varied by broad ecological region. Specifically, Boreal region AGB in GLAS footprints was estimated using height-biomass equations published by Neigh et al. (2013) and by Nelson et al. (2017). Land cover data from the National Land Cover Database (NLCD) for Alaska (Jin et al., 2017) and from the Earth Observation for Sustainable Development (EOSD) land cover data for Canada circa 2000 (Jin et al., 2017; Wulder et al., 2008), fractional tree cover data derived from the version 1.2 Global Forest Change dataset (Hansen et al., 2013), burned area from the MODIS MCD45 burned area data (Roy et al., 2006), and from SRTM v3 elevation data (Farr et al., 2007) were used to select, for each GLAS observation, the most appropriate empirical relationship to derive AGB.

For the ABoVE Core Study Domain, 230,880 values of GLAS-AGB were available between 2004 and 2008. To train machine learning models that predict GLAS-AGB from Landsat surface reflectance values, we filtered the GLAS-AGB data for quality based on several criteria. Because land cover is a fundamental part of the GLAS-AGB relationship, we sought to minimize bias due to sub-plot land cover variation and

only used GLAS-AGB plots in locations where 3 x 3 pixel windows of 30 m land cover information derived from Landsat (see below) centered in each 70 m diameter GLAS shot was homogeneous. In addition, because sloped surfaces introduce significant bias to GLAS waveforms, we removed GLAS plots in locations that had elevational slope greater than 10 degrees. After applying these two constraints, the final GLAS-AGB plot dataset included 80,673 values.

4.2.3 Landsat Reflectance, Land Cover, and Ancillary Data

Land cover is a fundamental ecosystem property that both influences GLAS-AGB data and explains a substantial proportion of spatio-temporal variation in AGB (Farina et al., 2019). Because climate change and disturbance are both active agents of land cover change in the ABoVE study domain, accurate information related to land cover and land cover change is essential for realistically capturing biogeographic patterns, temporal dynamics, and climate feedbacks in Boreal AGB. We therefore used the land cover dataset developed for chapter one of this dissertation to provide annual information spanning the period 1984 – 2014 for the ABoVE Core Study Domain.

We utilized time series of Landsat surface reflectance data from the Landsat 5 Thematic Mapper and the Landsat 7 Enhanced Thematic Mapper+. Prior to analysis, these data were masked for cloud and snow cover using the *Fmask* algorithm (Zhu and Woodcock, 2012), and time series at each pixel were evaluated for land cover changes using CCDC. To do this, CCDC fits harmonic models to time series of surface reflectance values, modeling seasonal and interannual variability in surface reflectance as

a function of time. These models are then used to identify statistically significant "breaks" in reflectance time series and to generate smooth time series of synthetic land surface reflectance data based on fitted models. Our AGB machine learning model utilizes seasonal-spectral features derived from these synthetic reflectance data as predictors. The synthetic reflectance data allow us to model trends in surface reflectance and fill gaps even under conditions where Landsat data are missing (e.g., due to cloud cover). Specific inputs to the machine learning model included the mean growing season and non-growing season synthetic values each year at each pixel in each Landsat band. Because the CCDC models can be unstable when growing seasons are short (i.e., less than 100 days), we normalized the snow-free growing season to the 5th and 95th percentiles of the snow-free days of year at each pixel. Peak growing season values were then based on values falling within the central 20% through the growing season (i.e. the middle of the snow-free season ± 10% of the length of the snow-free season), and the non-peak growing season values were based on those falling outside the central 20% of the snow-free season.

In addition to surface reflectance from Landsat, we included several additional variables in our models. Specifically, to capture broad geographic variability due to climate and topography, we included annual mean temperature and precipitation from the Worldclim dataset (Fick & Hijmans, 2017), elevation and slope data derived from ASTER (Tachikawa et al., 2011), surface water status (Pekel et al., 2016), ecoregion, and permafrost status from the Permafrost Zonation Index (PZI) (Gruber, 2012). In addition,

using the land cover change dataset described above, we included the time since disturbance at each pixel as a predictor.

4.2.4 Gradient Boosted Machine Model Estimation

Following the methodology employed by Baccini et al. (2012), we used GLAS-AGB data to calibrate machine learning models that predict AGB using time series of pixel-level synthetic surface reflectance values from Landsat, in association with the ancillary data, as described above, as predictors. Baccini et al. (2012) used the *Random Forest* machine learning model to predict biomass. However, initial assessments in our study domain revealed that *Random Forest* tended to under-predict in regions with high biomass and had relatively poor sensitivity to variability within forest classes. To address this bias, we tested a variety of alternative machine learning methods and found that Gradient Boosted Machines (GBM), an ensemble machine learning model that iteratively estimates a series of weak tree-based learners, did not suffer from these drawbacks (Friedman, 2001). Specifically, we used the GBM algorithm implemented in the *gbm* package in R (Greenwell et al., 2019). Like many machine learning algorithms, GBM has a number of hyperparameters that require tuning, which we accomplished using the R package *mlr* (Bischl et al., 2016).

We randomly selected 20% of the GLAS-AGB data to provide an independent sample for estimating error in our AGB predictions. The estimated model was applied to annual values of Landsat reflectance and land cover data, which resulted in 31-year stacks of AGB data over each tile. Because our primary research questions involve forest

disturbances and the loss of woody biomass, we include training data and predictions for non-treed classes as well as treed classes (i.e., which supports model predictions after stand-removing disturbances). Non-treed vegetation classes, such as Herbaceous, were generally predicted as 0 biomass without manual intervention.

4.2.5 Piecewise Linear Models

Initial time series of predicted AGB at each pixel show non-negligible interannual variation, resulting in many instances of spurious changes in AGB. Following the methodology of Baccini et al. (2017), we resolved this using a temporal change point algorithm that applies temporal segmentation to time series of AGB at each pixel, estimates piecewise linear models to each segment, and identifies statistically significant breaks in the time series (Appendix Figure A.5.1). This approach provides a means to reduce interannual noise, estimate AGB trends, and evaluate significance and uncertainty related to the linear model fit. We evaluate pixel-level changes in AGB on the basis of the temporal segmentation and linear model fits, rather than the *GBM* predicted biomass values themselves.

4.2.6 Ecoregions

The analysis of predicted AGB and its changes throughout the domain was organized into the ecoregions derived from the overlap of the ABoVE Core Study Domain and EPA Level 2 ecoregion designations for North America. The ABoVE-

overlapping ecoregions varied widely in their total area coverage, rates of fire and harvest areas, and total area of each ecoregion actually represented in our domain (Table 4.1). For example, while the Taiga Shield represents a relatively large portion of the study domain (12.6%), the study domain only contains about a third (30.3%) of the entire Taiga Shield. For certain ecoregions, AGB patterns we observe may be suggestive, but not necessarily representative, of AGB dynamics for these ecoregions. In particular, the Marine West Coast Forest, Western Cordillera, Taiga Shield, and Softwood Shield had a minority of their areas represented in the ABoVE Core Study Domain.

There was considerable variability in the rates of areas burned and areas harvested in each of the ecoregions. For example, the Softwood Shield experienced extremely low rates of harvest (0.1% of the mapped area), but very high rates of burned area (46.3% of the mapped area). In contrast, the Western Cordillera experiences noticeable harvesting (7.3%) and limited fires (2.5%). The Marine West Coast Forest in the ABoVE domain experienced almost no disturbance at all.

4.2.7 Analysis

To characterize temporal and spatial variability in modeled AGB time series, we drew a random sample of pixels from each tile that encompassed a wide range of variability in land cover, disturbance regime, and elevation. We sampled 0.1% of pixels in each tile, resulting in a sample of 36,000 pixels representing 32.4 km^2 in each tile and 3,636,000 pixels (3,272.4 km^2) across the study domain. At each randomly sampled

pixel, we analyzed the annual, 31-year time series of predicted AGB to explore four main features.

First, for pixels with no land cover change (i.e. stable forests), we used the Mann-Kendall test (Kendall, 1948) to detect statistically significant trends at $p \leq 0.05$, and then estimated the magnitude of detected trends using Theil-Sen linear regression (Sen, 1968; Theil, 1992). This analysis was designed to characterize trends in productivity via changes in AGB as a function of time in undisturbed forests, and so was limited to pixels with stable land cover across the time series.

Second, we characterized ecoregion-specific variability in cumulative and interannual biomass changes. To do this we calculated annual changes in AGB to create time series of annual biomass increment at each pixel. By summing the biomass increment across all pixels, we estimated interannual variability in AGB growth or loss for each ecoregion. These annual biomass increments provide estimates of net biomass accumulation rates in the Boreal forests that we mapped.

Third, we explored the nature and magnitude of how fire and timber harvest affect the net carbon budget of Boreal forests in the ABoVE study domain. To isolate fire-driven biomass losses, we incorporated information from historical fire databases from both the Canadian Fire Database and the Alaska Large Fire Database (Kasischke et al., 2002). To isolate biomass losses from timber harvest, we used data that catalogues the location and timing of forest harvest within Canada compiled by (White et al., 2017). Using these data we labelled the biomass increment in each pixel in each year as being associated with a fire or with harvest if the pixel-year's biomass increment occurred on or

after the year of a fire or harvest. The sum of fire- or harvest-related biomass increments across a tile therefore represents the change in AGB that occurred as a result of each disturbance process, including both losses in AGB caused by disturbance directly and gains in AGB associated with post-disturbance recovery. The difference between the total mapped biomass increments and the disturbance-specific increments were classified as "residual" biomass increment, which generally refers to natural growth or to growth arising from other disturbances processes but may in fact encompass a wide range of other processes for which we do not have reliable spatial data.

Fourth, we compared the influence of disturbance on both AGB dynamics and NDVI using a sample of time series of biomass and growing season NDVI that had an occurrence of either fire (n = 153,993) or harvest (n = 19,996). We normalized the dates of these time series by subtracting the year of the disturbance from the set of years in the time series, so that the year of disturbance was 0 and other years indicated time before or after the disturbance. We aggregated a set of these disturbance-labelled and normalized time series sampled across the study domain and, creating a general, characteristic post-disturbance trajectory of AGB, NDVI, and NBR.

4.3 Results

4.3.1 Model Assessment

The GBM model was trained using 64,537 GLAS AGB plots that were randomly selected across the geographic range of the study domain. Based a held-out test dataset of independent GLAS SGB plots, the model predicted AGB with an $R^2 = 0.801$ and a root

mean square error (RMSE) of 20.75 Mg/ha (Figure 4.1). The model fit varied substantially as a function of land cover, with notably lower predictive accuracy in the Woodland and Shrub classes, and higher predictive accuracy in Evergreen Forest, Deciduous Forest, and Mixed Forest. The GLAS-AGB biomass generally lacks observations less than 20 Mg/ha, which constrained our ability to predict AGB in areas with low-stature or sparse vegetation (e.g., shrub tundra). This lack of sensitivity may result from lack of sensitivity of GLAS lidar data over low stature vegetation (± 2m). The training and test data did include measurements with 0 Mg/ha of AGB, the vast majority of which represented areas with a land cover with no woody aboveground biomass (e.g., barren or water), some of which were predicted by the GBM model to have AGB values up to 50 Mg/ha. These errors arise from a combination of uncertainty in the GLAS-AGB data or GBM model uncertainty that bias some predictions towards higher biomass over sparse forests and unvegetated lands.

Land cover is the most important predictor in the model, suggesting that land cover information is crucial for predicting forest AGB from optical remote sensing. More specifically, analysis of variable influence estimated from the GBM model shows that the land cover provides 53.4% of the model explanatory power, followed by growing season green reflectance (12.6%), growing season tasseled cap wetness (5.7%), growing season shortwave infrared 1 (4.8%), and annual mean temperature (2.5%). Because land cover is defined based on plant functional type and density, this is intuitively reasonable.

4.3.2 Land Cover and Ecoregion Patterns

AGB shows a strong latitudinal gradient in AGB density (Figure 4.2), with the southern Boreal forests in the Boreal Plain, Boreal Cordillera, and Western Cordillera ecoregions showing the highest AGB values, and the Taiga Plain, Taiga Shield, and Taiga Cordillera ecoregions showing lower AGB density. Select tundra areas that were mapped north of the tree line have, as expected, near zero AGB (results not shown). High elevation areas, such as the Mackenzie Mountain Range in the Taiga Cordillera, have near zero AGB as a result sparse vegetation and relatively poor growing conditions at high altitudes.

The magnitude and variability in predicted AGB varied widely as a function of both ecoregion and land cover class and broadly reflect the spatial patterns of AGB described above (Figure 4.3). Median AGB by land cover and ecoregion was generally less than 100 Mg/ha, with the exception of forests in the Western Cordillera, Taiga Plain, and the Boreal Plain, which had Evergreen Forests with a median AGB density up to 125 Mg/ha. There is considerable variation in AGB across ecoregions and classes, with the Western Cordillera exhibiting by far the highest AGB density across all land cover classes. As expected, Herbaceous land showed near zero AGB density, which suggests that the GBM model is sensitive to a wide range of biomass densities and can capture large biomass changes caused by stand replacing disturbances. Among the land cover classes dominated by woody vegetation, Shrub generally had the lowest AGB (median 4.3 to 23.7 Mg/ha), Woodland had moderate AGB (median 35.3 to 55.7 Mg/ha), and Forests had the highest and most variable AGB (medians 52.7 to 119.1 Mg/ha for

Evergreen Forest, 47.0 to 83.4 Mg/ha for Deciduous Forest, and 55.8 to 95.4 Mg/ha for Mixed Forest). The land cover class with the highest biomass density varied by ecoregion. For example, while the Western Cordillera Evergreen Forests had the highest biomass, the Boreal Plain, Taiga Shield, and Taiga Plain Deciduous Forests and Mixed Forests had the highest biomass.

To characterize long-term trends in AGB, which reflect long term patterns of productivity, we isolated pixels where no land cover change occurred during the study period according to the land cover dataset from Chapter Two. Results from this analysis show that Deciduous and Mixed Forests consistently had the highest trends in AGB (median +0.01 to +0.47 Mg/ha/year) across all ecoregions (Figure 4.3), and that Evergreen Forests and Woodlands tended to have lower rates of growth (median +0.006 to +0.20 Mg/ha/year). AGB trends in areas with Shrubs were highly variable across ecoregions, and in most ecoregions, AGB trends in Shrublands (median +0.002 Mg/ha/year to +0.202 Mg/ha/year) were higher than in Evergreen forests and Woodlands. Generally speaking, there was less variability in the AGB trends in stable forests across ecoregions than there was for standing AGB density, and patterns in AGB density and trends were broadly consistent when aggregated to land cover across ecoregions (Appendix Figure A.6.1).

4.3.3 Biomass Dynamics in Logged Areas

Boreal forest carbon dynamics are largely driven by disturbances and post-disturbance recovery. However, depending on the mechanisms, disturbance often occurs

over small areas (e.g. 100s of m), particularly in areas of heavy land use. Hence, the ability of map AGB and changes in AGB at the spatial resolution provided by Landsat is desirable because it supports analysis of how disturbance processes like logging impact landscape scale carbon dynamics across multiple decades. For example, Figure 4.4 shows results from analysis of change in AGB arising from timber harvest near Prince George, British Columbia in the Western Cordillera ecoregion that illustrates the high spatial variability in both biomass density and biomass trends across this landscape. Over the 31 year span presented in this figure, areas that were recently logged at the start of the time series have accrued large amounts of AGB (roughly 90 Mg/ha), while other areas have lost large amounts of biomass (> 100 Mg/ha) as a result of logging. Importantly, post-harvest growth does not compensate entirely for biomass lost to timber harvest over the time period examined, largely because harvest typically occurs in the densest forests and results in near-complete removal of biomass, and growth rates in the Boreal forests are relatively slow. Across the area as a whole, post-disturbance recovery creates a heterogeneous landscape mosaic composed of vegetation communities with a wide range of stand ages and plant functional type composition.

Time series of AGB increments and resulting cumulative change in AGB show that timber harvests substantially impact the carbon balance in this area. In general, harvests imposed a steady release of carbon over time and interannual variability in biomass increment is mostly controlled by external factors such as climate. For the region as a whole, harvest-based losses more or less balance the combined effects of

post-fire regrowth and forest growth in undisturbed areas. As a result, the cumulative AGB balance across the time series for the area shown in Figure 4.4 is close to zero.

4.3.4 Biomass Dynamics in Fire Disturbed Areas

In contrast to the steady losses imposed by timber harvest, wildfires are highly stochastic and dominate the interannual variability in AGB across ecoregions outside of areas where logging is prevalent. For example, Figure 4.5 shows a forested area near Pelly Crossing, Yukon in the Boreal Cordillera ecoregion that has experienced many fires. Forests in this area generally show steadily increasing AGB. When large fires occur (e.g., 1990, 1995, 1998, and 2004), they exert first-order control on interannual changes in net biomass and result in significant decreases in AGB for the area as a whole. Fire scars are evident in Landsat imagery throughout the Boreal biome in both recently burned areas of low biomass and older burns with areas of slowly regenerating forest. The impact of fires in 1990, 1995, 1998, and 2004 near Pelly Crossing are also evident in plots showing annual biomass increments and cumulative biomass change for the area; AGB increments are strongly negative in fire years and moderately positive in post-fire years. As a result, fires counteract accumulation of AGB in surrounding undisturbed forest. The losses and gains in this area are relatively low in magnitude on a per-area basis when compared to the logged area in British Columbia (Figure 4.4). However, fires are more extensive in the Boreal Cordillera than logging is in the Western Cordillera, making it unclear what the relative total impact is between fires and harvesting.

In some areas, fires are rare but severe, and so have a large punctuated impact on local-to-regional carbon budgets. For example, Figure 4.6 shows an area of sparse Woodland in the Taiga Plain near Yellowknife where a severe fire occurred in 1995, resulting in the loss of nearly 20 Tg of AGB. For context, the decrease in AGB associated with the 1995 fire year was larger than the cumulative fire-related change in AGB the 31-year time series in the Pelly Crossing area, which experienced several fires. Post-fire recovery was relatively slow, and the area never recovers the lost carbon during the time series. This is exemplified by the map, as well, which shows that losses immediately following the fire (Figure 4.6d) are moderate in magnitude and extensive in area, yet regrowth over the decades following the fire is low in magnitude and sparse in extent (Figure 4.6e). Not all areas experience the same degree of biomass loss or regrowth due to disturbances. The cumulative AGB change shown in Figure 4.7f suggests that, over the course of twenty years, only about a quarter of the carbon released through this fire event was sequestered in post-fire recovery. Severe, episodic fire events dominate carbon dynamics of the Taiga Plain, and regrowth is slow. These results highlight the high level of variability in carbon dynamics across the ABoVE study domain, even when the disturbance agent (i.e. fires) is the same. Certain areas are more likely to recover after a large fire, while others may not recover and hence represent a net source of carbon to the atmosphere over multidecadal timescales.

4.3.5 Biomass Dynamics by Ecoregion

The examples presented above show landscape-scale variability in carbon gains and losses as a function of two drivers: fire and logging. In this section, we explore ecoregion-specific processes and regimes that control the nature and magnitude of disturbance impacts on AGB. Figure 4.7 presents the cumulative change in AGB for each ecoregion, summarizing the net impact of logging and fire on ecoregion-wide AGB budgets. The cumulative AGB changes reveal substantial variability in the relative influence of fires and logging on the aggregate carbon balance of each ecoregion. For example, while the Alaska Interior Boreal, Boreal Cordillera, Taiga Cordillera and Taiga Plain ecoregions experienced widespread and frequent fires, the net increase in AGB in unburned areas more than compensated for fire-induced losses across the time series. Consequently, these ecoregions show a net increase in AGB over the time series. The Taiga Plain, in particular, experienced considerable accumulation in AGB from post-fire growth in the latter part of the time series. As a result, the net balance in AGB over the time series due to fires in the Taiga Plain is close to 0. In the Taiga Shield and the Softwood Shield, on the other hand, the influence of fire was less episodic and more continuous, with limited growth in AGB outside of disturbed areas that did not compensate for AGB loss from fires. Hence, these ecoregions experienced net losses in AGB.

Despite the fact that logging events represent a small area (Table 4.1), timber harvest was consistently responsible for substantial AGB losses in areas where it occurred. Both the Boreal Plain and Western Cordillera showed losses from timber

harvest that were considerably larger than the impacts of fires, which were generally modest. In both of these ecoregions, the net balance in AGB plateaued or even decreased in the latter part of the time series, while harvest-based losses continuously accrued. These harvest-based losses counteracted much of the growth in undisturbed forests elsewhere.

Aggregated across all of the ecoregions included in our analysis, the ABoVE Core Study Domain shows widespread and substantial increases in AGB that appear to be slowing in the latter part of the time series (Figure 4.8). The aggregate time series also shows substantial variability at interannual time scales in both net and fire-driven AGB. In this context, we note that although fires primarily result in losses of AGB, there are cases where the long-term impact of fires results in modest net accumulation of AGB as a result of post-burn regrowth. Summed over the time series, both harvest and fires contributed substantial AGB losses, with harvest being a smaller, but steadier, driver of carbon loss while fire imposed steady growth with episodic large losses. Over the study region as a whole, harvest-driven losses were about half the magnitude of fire-driven losses, despite accounting a considerably smaller area of disturbed forest (Table 4.1). In total, including all AGB growth and loss processes, the aggregate result is a substantial net gain in AGB. Net change in AGB was sharply positive in the first twenty years of the time series (i.e., 1984 – 2005) (Figure 4.8), declines modestly in the late 2000s following a large fire year, and then increases again in the 2010s. This suggests that the Boreal forests in the ABoVE domain have undergone decadal-scale periods of both net gains and

losses of AGB, where dynamics during any given period depend on short term fire dynamics and longer-term climate processes.

4.3.6 Post-Disturbance Dynamics in Biomass and Greenness

Both harvest and fires stimulate accumulation of AGB through post-disturbance recovery processes. From the above analysis, we see increases in AGB in areas that were harvested or burned. In this context, recovery trajectories in disturbed forests have been extensively studied using time series of spectral vegetation indices by tracking temporal metrics that describe how these indices return to pre-disturbance values. Results from these studies suggest that the rate of forest recovery depends on the ecoregion, but generally requires at least 10-20 years for forests to re-establish (White et al., 2017). However, our analysis of recovery dynamics in AGB following disturbance suggest that post-disturbance recovery is much slower and requires more time relative to recovery based on spectral indices like NDVI or the normalized burn ratio (NBR) (Figure 4.9). Harvested areas experienced near complete loss of AGB and tend to have median AGB values at 0 and 4 years after disturbance that are lower than AGB values in burned areas. Harvested areas also typically have higher AGB densities prior to disturbance than burned areas. In burned areas, where AGB losses are less severe but are more geographically extensive, fires do not always completely remove trees and often occur in low biomass woodlands that occur throughout the Taiga ecoregions. In either case, it does not appear that either harvested or burned areas recover to their pre-disturbance AGB densities during the 30-year record. There is substantial variability in net recovery

in both disturbance regimes. However, in the median, recovering forests regained 2/3 of their pre-disturbance biomass after disturbance over the thirty-year time series. At the same time, recovery of both NDVI and NBR after disturbance is rapid and suggests a return to pre-disturbance conditions within 10-20 years, and sometimes exceeds the pre-disturbance values. Compared to the relatively slow regrowth of AGB, it is unclear what the meaning is for a forest to have recovered with respect to its spectral indices (e.g. NBR or NDVI).

4.4 Discussion

4.4.1 Overview

In this study, we combined data from satellite-borne lidar with time series of Landsat surface reflectance to generate annual estimates of AGB at 30 m spatial resolution across a large region of Boreal forest in northwestern Canada and Alaska. The results from this work provide a physically-interpretable characterization of changes in AGB across the study region that reveal landscape-scale information related to how different agents of change affect AGB budgets across multiple decades. We found that the AGB across the study domain was highly variable. The magnitude, frequency, and type of disturbance varied considerably across ecoregions, with southern ecoregions experiencing steady losses in AGB to harvest, and northern ecoregions experiencing episodic fluctuations in AGB caused by extensive wildfire.

Most previous studies that attempt to spatially estimate AGB using remote sensing exploit active remote sensing, such as radar or lidar, and use physically-based,

semi-empirical, and/or allometric models that relate forest structural properties to AGB. However, these studies have generally been limited in regard to their spatial or temporal scale of analysis in ways that preclude systematic analysis of changes in AGB over large areas across time (Harrell et al., 1995; Rauste, 2005; Rignot et al., 1994; Saatchi and Moghaddam, 2000). Here, we employ a methodology that combines information from spaceborne lidar data with long time series of surface reflectance data in a manner that allowed us to map AGB at high spatial resolution across more than 3 million km^2 over three decades. By estimating changes in AGB over time, our analysis provides a more physically interpretable estimate of changes in productivity than other widely used sources of remote sensing data that are widely used to infer productivity such as time series of NDVI or sun-induced fluorescence (Guay et al., 2014; Ju and Masek, 2016; Walther et al., 2016).

4.4.2 Disturbance-driven Dynamics of Forest Biomass

Consistent with results from other field and modeling studies, the Boreal forest of Canada and Alaska is a net sink of woody biomass carbon with substantial losses and gains of AGB being driven by disturbances such as fire, insects, and harvest (Bond-Lamberty et al., 2007; Kasischke et al., 2010; Stinson et al., 2011). While the geographic extents are not identical (e.g. managed versus all forests, or all of Canada versus ABoVE Core Study Domain), we found both that rates of biomass loss due to harvest and the overall rate of biomass accumulation were of similar magnitude (e.g. 10s of Tg AGB per year) to those of other studies, suggesting our methodology provides realistic estimates of

disturbance-driven Boreal forest carbon dynamics in the ABoVE Core Study Domain (Kurz et al., 2013; Stinson et al., 2011). Similarly, the timing of a substantial loss of live AGB in the southern portion of the domain coincides with the timing of reports of pathogen attacks in British Columbia, suggesting that our methodology is sensitive to drivers of biomass loss such as insect infestation that are not explicitly mapped in the fire and harvest databases (Kurz et al., 2008).

Characterizing the sensitivity of Boreal forest carbon to climate change requires understanding of disturbance regimes and the ensuing land changes that they create (Van Bellen et al., 2010). In this context, we found that the nature and magnitude of carbon losses due to disturbance varied substantially by ecoregion. Areas with extensive harvest experienced very little fire, and vice versa. This may be explained by fire suppression in areas with heavy land use such as commercial logging and by the incidental reduction in fire fuel load following harvest. On a per-area basis, AGB loss and recovery caused by timber harvest tended to be larger than losses caused by fires, largely because timber harvest tends to be most prevalent in highly productive forests with large trees. Harvest typically involves complete removal of trees, while fires have considerable variability in their severity, which can result in only partial burns. On balance, the area of harvest was exceedingly small in our domain, yet was comparable to fires (about half) for magnitude of AGB losses.

This methodology provides estimates of AGB stocks that are comparable across land cover types, ecoregions, and time. Further, by generating annual estimates of AGB, along with their change over time, we can characterize average AGB and changes in

AGB for key land cover types and over entire ecoregions based on units (Mg/ha) that can be directly related to ecosystem properties. Deciduous Forests and Mixed Forests, regardless of ecoregion, generally showed rates of AGB accumulation that were substantially higher than those observed over Evergreen Forests, and rates of AGB accumulation in Deciduous Forests were consistent with long term field studies that track accumulation of woody biomass in Boreal deciduous forests (Chen and Luo, 2015; Pare and Bergeron, 1995). This finding is consistent with results from field studies showing that Deciduous Forests have higher productivity than Evergreen Forests (Augusto et al., 2015), which also implies that recent shifts in forest demography and succession may be driving increases in Boreal productivity and carbon cycling (Pugh et al., 2019; Zimov et al., 1999). This increased rate of AGB accumulation is evident in all undisturbed areas, regardless of ecoregion, despite varying biogeographic and climatic conditions that influence the productivity of these forests across space.

4.4.3 Limitations in Disturbance Information

Information on the timing and location of forest disturbance events is crucial to understanding Boreal forest biomass changes, but this information is generally lacking in precision and availability, limiting our understanding of what drives Boreal biomass changes (Liu et al., 2011; Stinson et al., 2011). For example, to explore the role of fire disturbance, we used two widely used ancillary sources of data: the Canadian and Alaska fire databases (Kasischke et al., 2002; Stocks et al., 2002). These databases provide highly useful and important information, but are also limited by their simplified

representation fire disturbance. These databases only provide information related to the perimeter and timing of fires, and include no information related to spatial variability in the intensity of disturbance within fire perimeters or in the uncertainty in the total perimeter of each fire. However, a large body of evidence clearly shows that areas affected by fire events include substantial variability regarding tree mortality, combustion of fuel, and the net impact of each fire event (Rogers et al., 2015). The 30 m spatial resolution imagery can be used to evaluate the magnitude of AGB change within individual fire perimeters with high spatial heterogeneity, providing a means of estimating the severity of fires using relative AGB loss. Burn severity provides useful information for modeling carbon dynamics, biophysical climate feedbacks, successional processes (Johnstone et al., 2010; Rogers et al., 2015, 2013; Van Bellen et al., 2010). By analyzing changes in biomass, it may be possible to provide richer information on burn information and impacts beyond area and spectral response.

In addition, it's important to note that incomplete information related to disturbance agents and the causes of AGB gains and losses limits our ability to fully characterize and attribute observed dynamics in AGB. It is generally not well understood which disturbance processes are the most important to scale up from smaller scale events to continental scale dynamics, as well as finer-scale mechanistic understanding of the impact of forest disturbance on various pools of carbon (Liu et al., 2011). Reports of forest mortality (and, therefore, AGB loss) as a result of drought, insects, and permafrost degradation are increasingly common in the literature (Carpino et al., 2018; Helbig et al., 2016; Hogg et al., 2008; Ma et al., 2012; Volney and Fleming, 2000), but were not

included here due to lack of accurate information. These additional sources of disturbance are partly captured in the "other" category for biomass change. For example, AGB in the Western Cordillera exhibits a notable inflection point around 2005 (Figure 4.7), which coincides with the period when the "residual" source of AGB change becomes strongly negative. Reports have identified an extensive Mountain Pine Beetle infestation that occurred in the same region around the same time, resulting in a loss of ecosystem carbon stocks that was on the order of 20-25 Mt C yr^{-1} (Kurz et al., 2008). However, because our analysis did not explicitly include the effect of pest disturbance, we were unable to quantify the impact of this process on regional AGB budgets.

4.4.4 Rates of Forest Recovery

We note that, in addition to mapping and quantifying the impact of disturbance, understanding and quantifying the magnitude and rate of recovery in AGB after disturbance events is also of interest. Previous studies have used spectral vegetation indices such as the NDVI or normalized burn ratio (NBR) to characterize forest recovery after disturbance (Frazier et al., 2018; Kennedy et al., 2010). However, the use of such indices tends to overestimate rates of forest recovery (White et al., 2017) because NDVI and NBR changes may reflect understory growth and key forest structural parameters such as cover and height recover to pre-burn states over much longer time scales than do indices such as the NBR or NDVI (Bartels et al., 2016; Bolton et al., 2017). Thus, relying on spectral indices alone to characterize forest growth in heavily disturbed biomes like the Boreal forest is likely to overestimate growth and productivity because changes in

spectral indices may reflect changing characteristics on the land surface that are not directly related to woody biomass growth, such as the growth of Herbaceous vegetation or changing surface water status. This question requires more investigation, but the results presented here suggest that if extensive and high-quality training data are available, then it should be possible to directly and reliable estimate rates of recovery in AGB from time series of optical imagery using more sophisticated approaches than univariate correlations with spectral vegetation indices (e.g., machine learning approaches).

4.4.5 Non-Biomass Carbon

This study does not account for dynamics in below ground carbon (e.g., in soils and roots) or in other pools of carbon beyond live aboveground woody biomass, which all represent important and dynamic pools of carbon in Boreal ecosystems (Post et al., 1982). Although it is beyond the scope of our study, understanding changes in Boreal soil carbon is a crucial element of Boreal carbon balance, since their stores are large and sensitive to climate warming (Bradshaw & Warkentin, 2015; Post et al., 1982). Our analysis only provides information on net carbon uptake stored as wood, and does not account for substantial fluxes of carbon into the soil via litterfall and out of the soil by respiration. Furthermore, disturbance factors that may lead to forest mortality, but not immediate combustion or decomposition of woody biomass, are not explicitly accounted for by our methodology. For example, insect infestation or drought that kills trees generates standing dead trees that are considered biomass losses by our methodology, but

would not contribute to atmospheric carbon until they eventually decompose or are burned. Thus, our results provide information that is necessary, but not sufficient, to estimate a complete accounting of Boreal carbon dynamics and interannual-to-decadal time scales.

4.5 Conclusions

Recent advances in the availability of remote sensing information as well as computational techniques are making possible more detailed analyses of large and remote areas like Boreal forests. Changes in the ecosystems of high northern latitudes have substantial potential to alter global climate-carbon feedbacks, particularly as climate change alters disturbance regimes and the distribution of vegetation types. Here we demonstrate the ability of time series of optical remote sensing to characterize and quantify long-term dynamics in Boreal forest AGB. This type of analysis provides a considerable improvement over studies relying on spectral vegetation indices alone, which have no biophysical interpretation, or mapping gains and losses of forest cover, which fail to detect subtler changes in forests due to forest degradation or environmental stressors. We find substantial spatio-temporal variability in the accumulation rate of aboveground forest carbon stocks, suggesting that the nature and impact of disturbance regimes varies strongly by ecoregion. Hence, to accurately project changes in Boreal forest dynamics it will be necessary to characterize disturbance regimes and land cover change at regional and continental scales. While previous studies have also found fire to

be the primary driver of carbon balance on an interannual basis (Bond-Lamberty et al., 2007; Kasischke et al., 2010; Van Bellen et al., 2010), we find that harvest imposes a comparable impact on overall carbon budgets over time despite their limited area due to their relatively high per-area biomass density. The Boreal forests of the ABoVE Core Study Domain appear to be a net carbon sink with respect to live AGB, but that sink is modulated substantially by variable disturbance and regrowth occurring throughout space and time.

Table 4.1 | Summary of ecoregions mapped, including the proportional area experiencing fire or harvest and the proportion of the total ecoregion that lies within the study domain. The study domain only includes areas considered in the Boreal biome, which excludes Arctic and Tundra ecoregions with limited data AGB density.

Ecoregion	Area (km^2)	Proportion of domain	Percent burned	Percent harvested	Proportion of ecoregion
Alaska Boreal Interior	422,135	12.6	32.7	0.0	98.8
Boreal Cordillera	567,075	21.4	16.0	0.2	95.1
Boreal Plain	337,940	11.7	20.9	4.2	56.2
Marine West Coast Forest	51,402	3.9	1.0	0.0	21.7
Softwood Shield	86,801	4.9	46.3	0.1	10.8
Taiga Cordillera	302,976	8.7	14.8	0.2	96.2
Taiga Plain	633,262	17.5	23.1	0.2	92.1
Taiga Shield	381,311	12.6	26.0	0.0	30.3
Western Cordillera	85,454	6.8	2.5	7.3	17.9

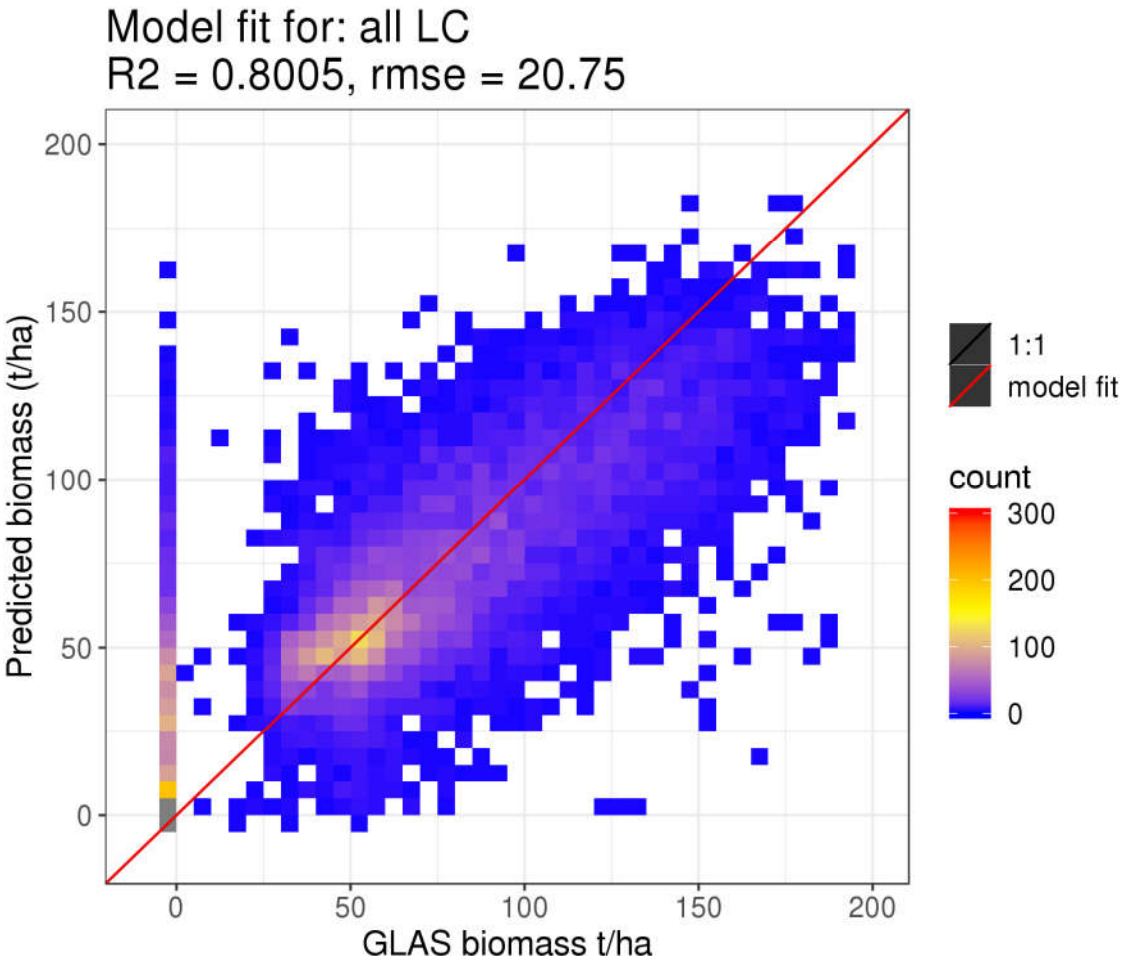

Figure 4.1 | Two-dimensional histogram indicating the correspondence between Gradient Boosted Machine model fit and independent test data set on predictions of aboveground biomass (GLAS-AGB) from Landsat reflectance. The grey boxes located at the origin indicates a large collection of points near zero that go beyond the scale.

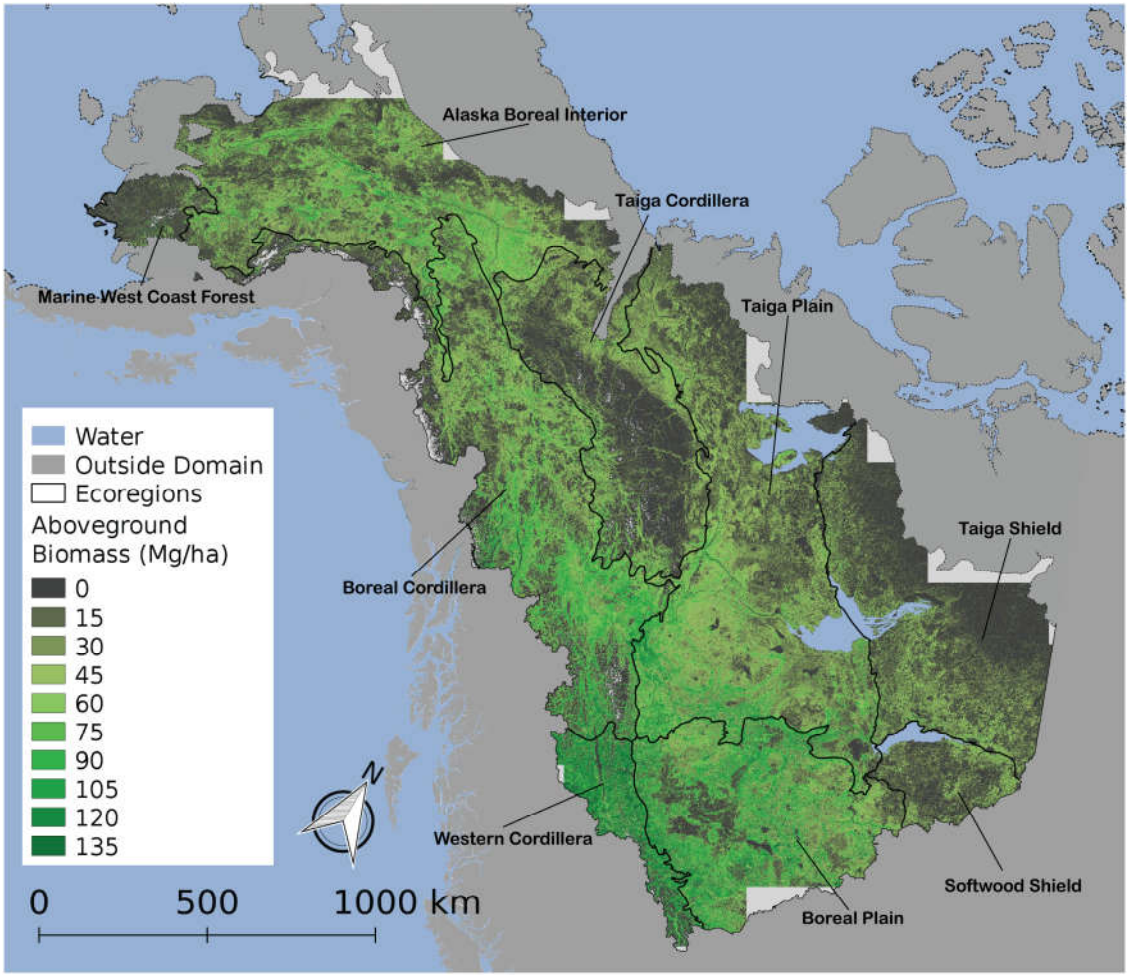

Figure 4.2 | Domain-wide map of mapped aboveground biomass (AGB) across Boreal biome in the study domain. Lines indicate ecoregion boundaries derived from the EPA North American Level 2 ecoregions. Shown is the predicted AGB for the year 2007 to demonstrate the spatial variability; 2007 was chosen as it lies within the years of observations for GLAS.

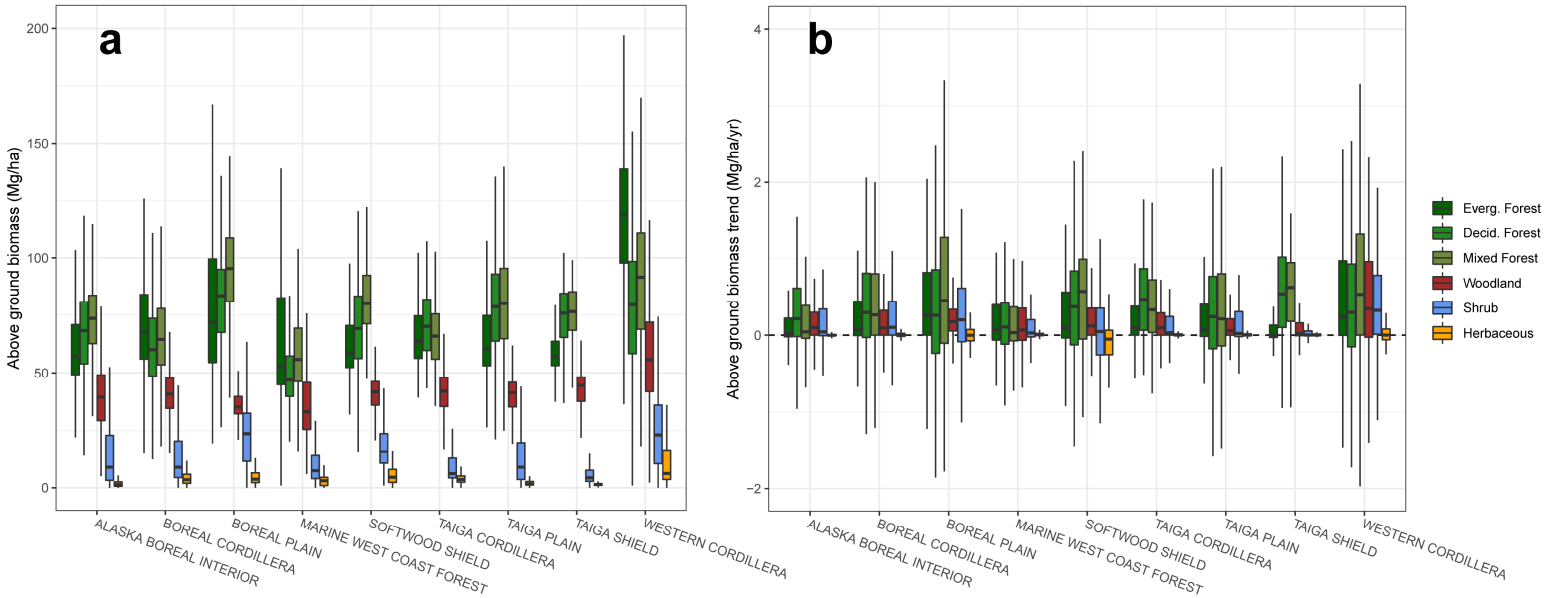

Figure 4.3 | Distribution of aboveground biomass (AGB) and trends taken from a sample across the ABoVE Core Study Domain. Shown are only the land covers that include woody biomass (e.g. Forest and Shrubs) and one non-woody land cover (Herbaceous) for comparison. a) Land cover and ecoregion-specific distributions of AGB in a sample of pixels. b) Land cover and ecoregion-specific distributions of trends in AGB in a sample of pixels that do not experience land cover change between 1984-2014.

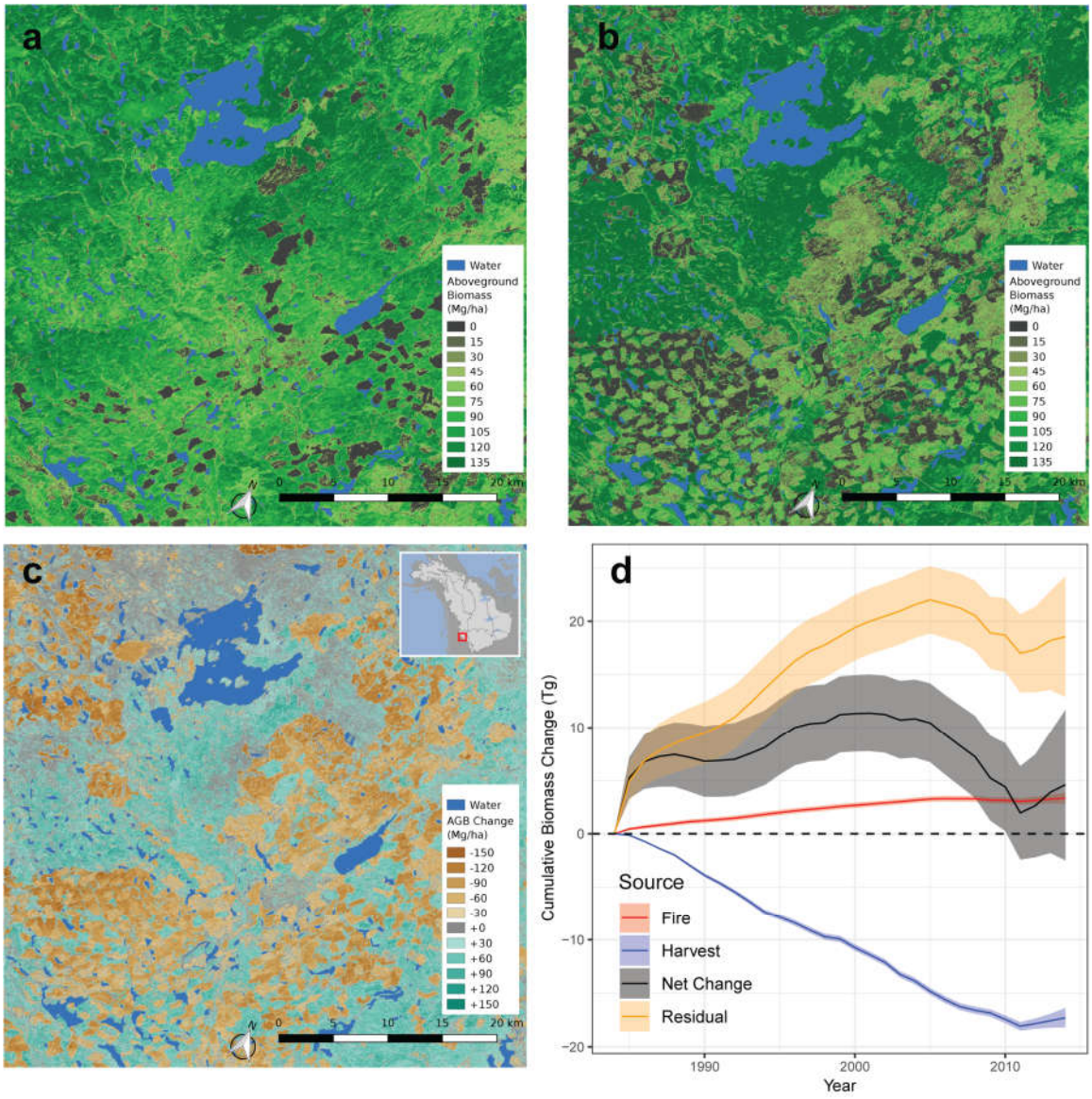

Figure 4.4 | Spatiotemporal dynamics of aboveground biomass (AGB) and its changes over an area of intensive timber harvest and other land use in British Columbia. a) AGB across the area in 1984. b) AGB across the area in 2014. c) The difference in AGB between 2014 and 1984, indicating areas of net gain and loss. d) Area-wide accounting of the total net cumulative changes in AGB overall as well as due to fire, harvest, and other. Cumulative accounting shown here is indicative of a larger region than shown, but the shown area is representative of the area analyzed. Uncertainty indicates the 95% confidence interval around the cumulative sum. Residual is determined as the difference between net change and the sum of fire and harvest changes. Disturbance-related changes that are positive indicate post-disturbance regrowth.

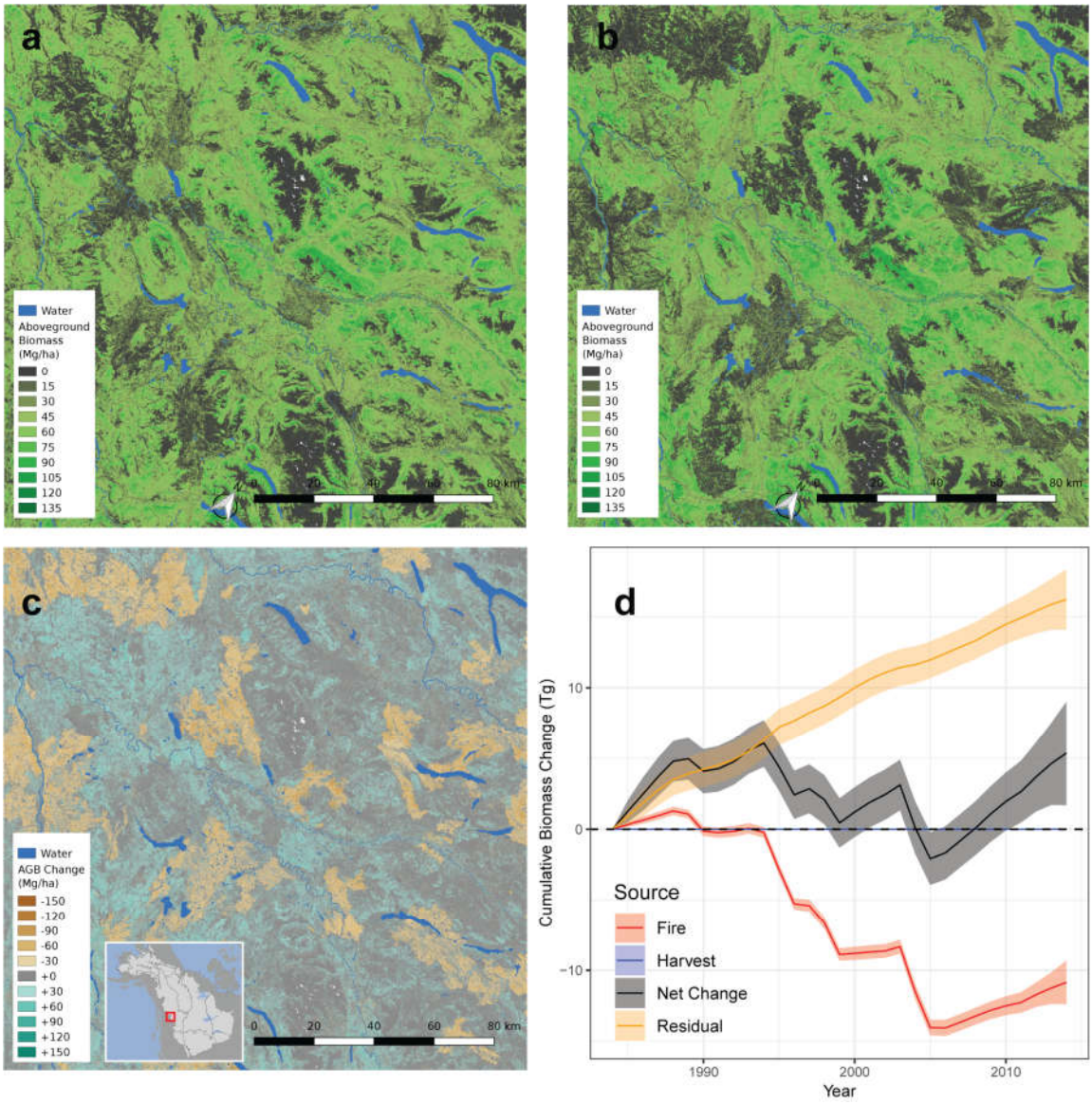

Figure 4.5 | Spatiotemporal dynamics of aboveground biomass (AGB) and its changes over an area of repeated fires near Pelly Crossing, the Yukon. a) AGB across the area in 1984. b) AGB across the area in 2014. c) The difference in AGB between 2014 and 1984, indicating areas of net gain and loss. d) Area-wide accounting of the total net cumulative changes in AGB overall as well as due to fire, harvest, and other. Uncertainty indicates the 95% confidence interval around the cumulative sum. Residual is determined as the difference between net change and the sum of fire and harvest changes. Disturbance-related changes that are positive indicate post-disturbance regrowth.

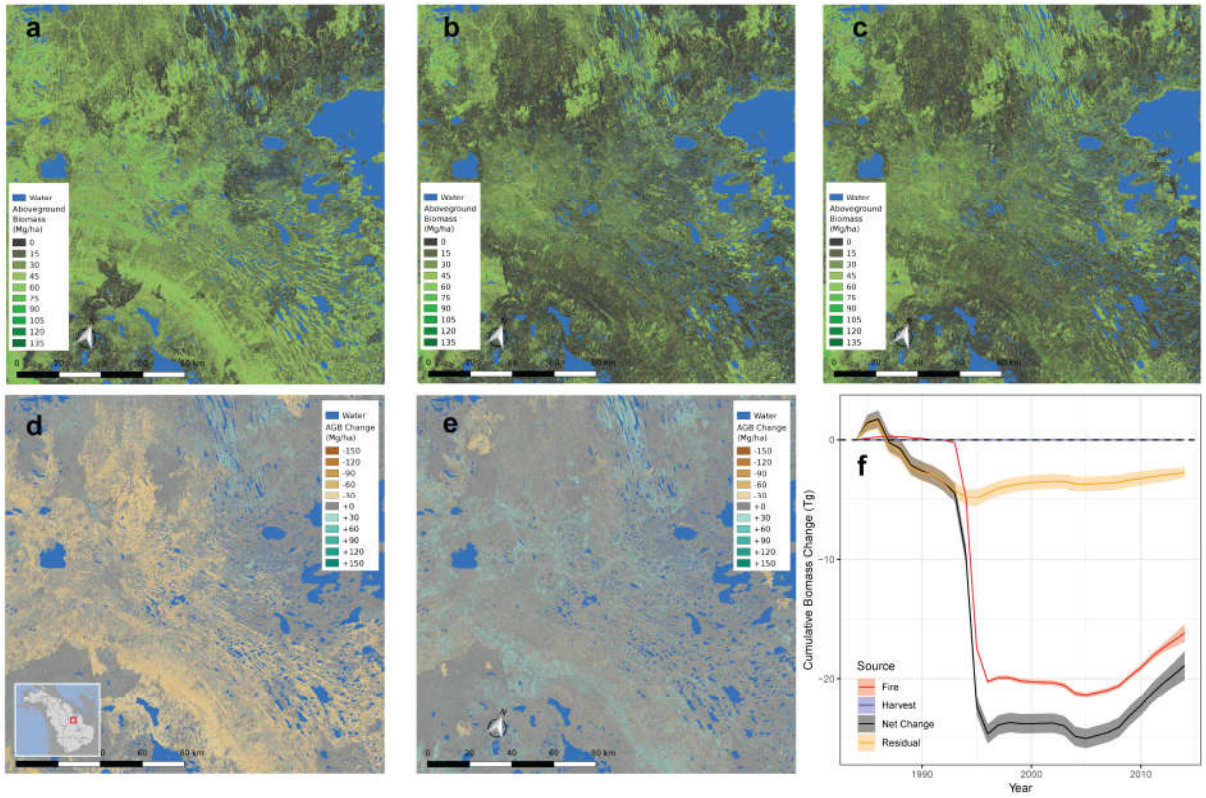

Figure 4.6 | Spatiotemporal dynamics of aboveground biomass (AGB) and its changes over an area with a single large fire in the time series in the Taiga Plain in the Northwest Territories. a) AGB across the area in 1984. b) AGB across the area in 1996, immediately following the major fire. c) AGB across the area in 2014, at the end of the time series. d) The difference in AGB between 1996 and 1984, indicating areas of AGB loss due to the fire. e) The difference in AGB between 2014 and 1996, indicating areas of slight AGB recovery 19 years after the fire. f) Area-wide accounting of the total net cumulative changes in AGB overall as well as due to fire, harvest, and other. Uncertainty indicates the 95% confidence interval around the cumulative sum. Residual is determined as the difference between net change and the sum of fire and harvest changes. Disturbance-related changes that are positive indicate post-disturbance regrowth.

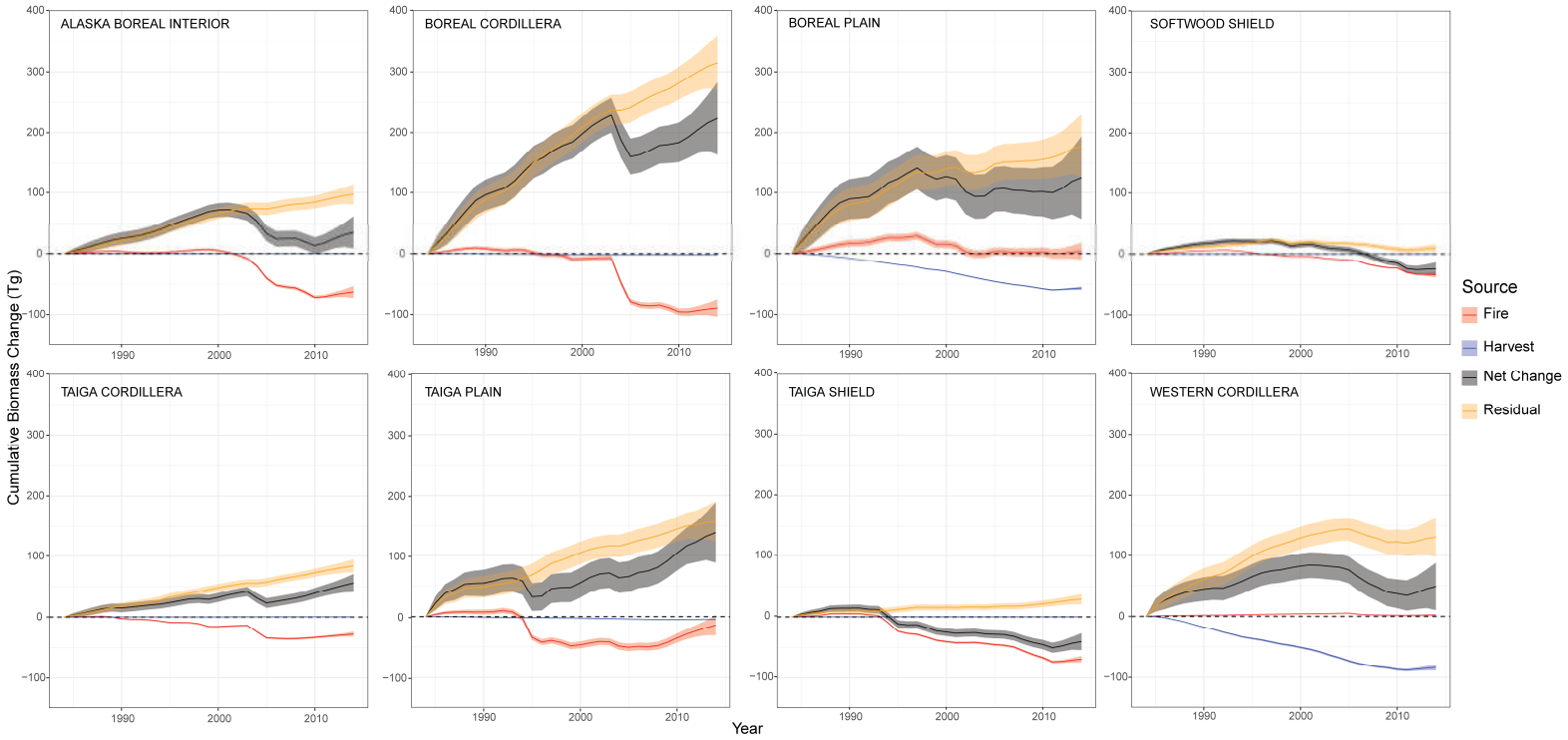

Figure 4.7 | Temporal dynamics of cumulative aboveground biomass (AGB) change due to disturbance over each ecoregion. Fire and Harvest related losses are derived from the Canadian Fire Database, Alaskan Large Fire Database, and the dataset of White et al. (2017) that catalogs timing and location of harvest events in Canada. The Residual source is determined as the difference of the Net AGB change and the sum of the Fire and Harvest changes. Lines indicate the mean cumulative change and shading indicates the 95% confidence interval determined from the change point algorithm. Not shown is the ecoregion MARINE WEST COAST FOREST, which had negligible changes in AGB within the ABoVE Core Study Domain.

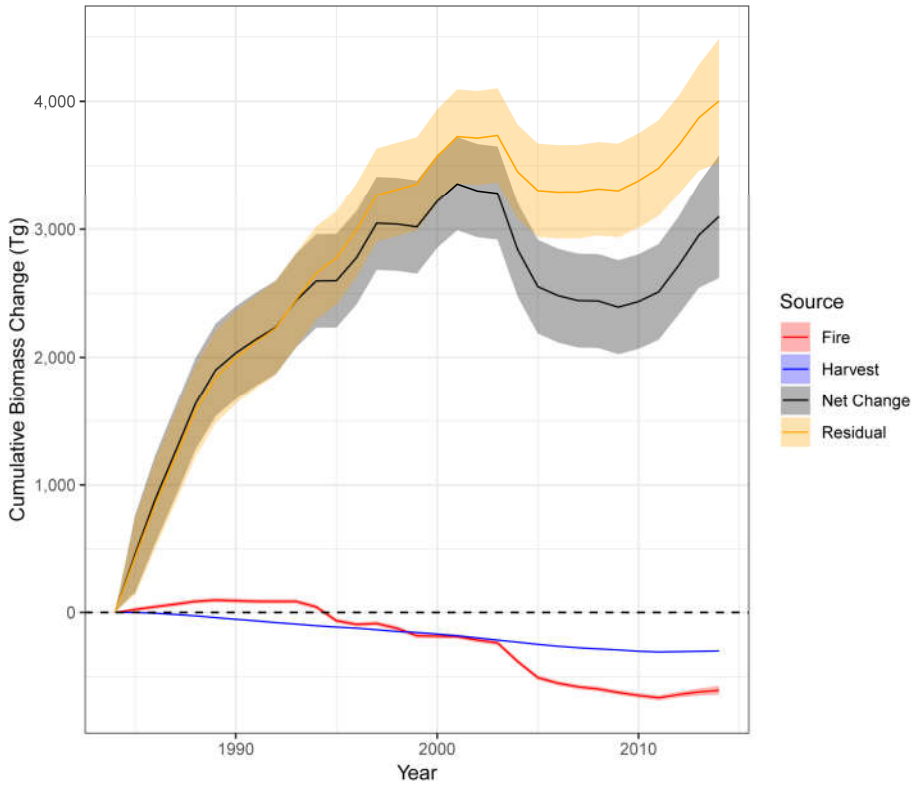

Figure 4.8 | Cumulative aboveground biomass (AGB) change totals and change due to disturbance aggregated across the entire study domain. Fire and Harvest related losses are derived from the Canadian Fire Database, Alaskan Large Fire Database, and the dataset of White et al. (2017) that catalogs timing and location of harvest events in Canada. The Residual source is determined as the difference of the Net AGB change and the sum of the Fire and Harvest changes. Lines indicate the mean cumulative change and shading indicates the 95% confidence interval determined from the change point algorithm.

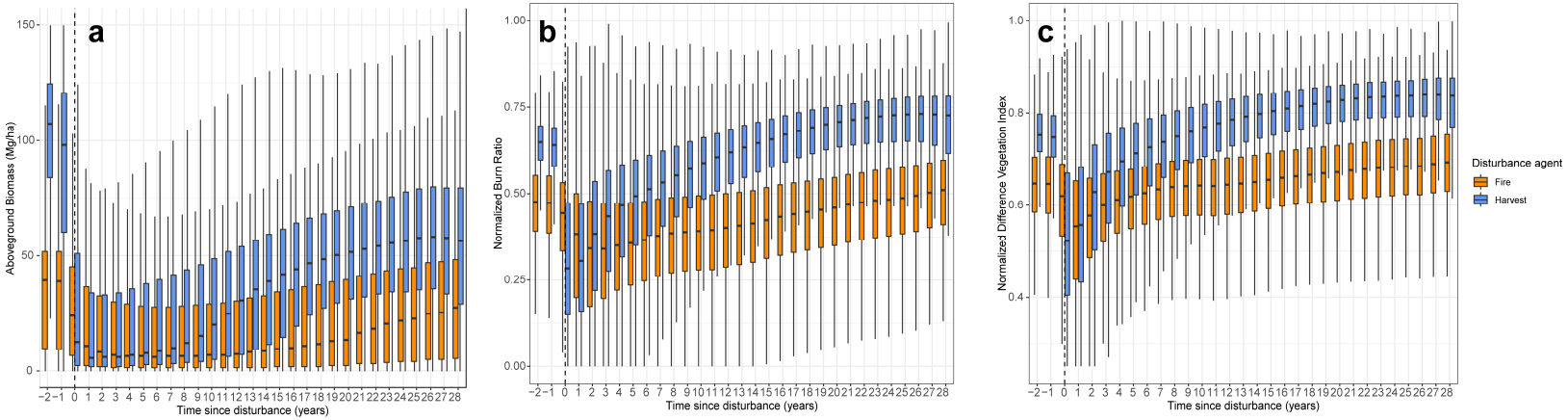

Figure 4.9 | Temporal dynamics of post-disturbance recovery for both aboveground biomass (AGB), and spectral indices including the normalized burn ratio (NBR) and the normalized difference vegetation index (NDVI) across a sample of pixels in the domain. The vertical dashed line indicates Year 0, the time of disturbance, while Years < 0 indicate times before disturbance, for context. a) Yearly distributions of AGB following fires and harvest b) Yearly distributions of NBR following fires and harvest. c) Yearly distributions of NDVI following fires and harvest. Temporal patterns when evaluated using the normalized burn ratio (NBR) were very similar to those

CONCLUSIONS

5.1 Overview

In this dissertation, we describe a series of analyses designed to characterize land cover change and its consequences for remote sensing of productivity across the study domain of NASA's ABoVE project in Alaska and northwestern Canada. Arctic and Boreal regions of North America are hypothesized to play a critical role in the global carbon-climate feedbacks (Chapin et al., 2000), yet understanding of these dynamics is incomplete (Fisher et al., 2018). Advances in this field have been stymied by the expansive, heterogeneous, and remote nature of these ecosystems, which makes field work resource intensive and scaling from limited sites challenging. Remote sensing plays a key role in understanding Arctic-Boreal systems due to its ability to repeatedly characterize ecosystem properties at synoptic scale.

This work is the product of many advances in the availability of spaceborne satellite remote sensing data and computational techniques that enable the processing of dense, multidecadal time series (Farina et al., 2019; Sun et al., 2017; Woodcock et al., 2008). Using these advances, we provide new insights relating how the complex disturbance regimes of Arctic-Boreal North America, including fires and logging, dramatically alter regional land cover and, by extension, remotely sensed measures of productivity at continental and decadal spatiotemporal scales. Specifically, by incorporating complementary streams of data from a variety of remote sensing platforms and other gridded datasets, we characterize the extent and nature of land cover change in

the ABoVE Core Study Domain, quantify the impacts these changes on remotely-sensed observations of productivity, and estimate the degree to which disturbances, and their associated land cover changes, impact biomass accumulation rates over time. Land cover is a fundamental ecosystem property that influences much of how carbon cycle science measures and understands climate change impacts. Without understanding the nature of land cover change at multiple spatial and temporal scales, it is impossible to accurately characterize carbon-climate feedbacks in the context of extensive global climate and ecosystem change. This work significantly advances our understanding of Arctic-Boreal land cover change and adds nuance to the interpretation of remotely-sensed measures of ecosystem properties.

5.2 Summary of Key Findings

The work presented here includes three separate, but related, chapters. They all incorporate heavy use of remote sensing data and computational analysis to characterize Arctic-Boreal land cover changes, how they intersect with observed trends in land surface greenness, and how they inform estimates of Boreal forest carbon balance. In the first chapter, we described the background of Arctic-Boreal ecosystem change, remote sensing applications, and greening trends that provide the context and motivation for this work.

In the second chapter, we utilize dense time series of Landsat surface reflectance measurements in combination with extensive high-resolution imagery to map 31 years of land cover across the ABoVE domain. We sought to quantify rates of various key land cover transitions that define important land surface characteristics in Arctic-Boreal

biomes. We found land cover change occurring extensively in two primary modes – one of Boreal biomes losing substantial Evergreen Forest (relative to 1984 area, -14.8 ± 3.0 %) while gaining Deciduous Forest substantially (+15.4 ± 5.2 %), and one of Arctic biomes experiencing substantial Shrub Gain and Herbaceous Gain (+7.3 ± 2.0 %) over previously Sparse Vegetation or Barren land. Boreal forest changes occurred due to disturbances, such as fires and logging, removing Evergreen Forests and spurring Deciduous Forest and Shrub Gain, while Arctic tundra changes occurred due to climate warming expanding shrubs. These changes are consistent with increased northern high-latitude productivity trends implied by atmospheric observations.

In the third chapter, we compared the land cover change information generated from the previous chapter with mapped trends in NDVI in the ABoVE Core Study Domain, a widely observed phenomenon referred to as “greening” and “browning”. We found that nearly a third of areas with significant greening or browning were associated with land cover change, implying a potential bias in the interpretation of these greening and browning areas if viewed without an understanding of their land cover history. Boreal patterns included the highest magnitude greening and browning within fire scars and logging, which largely reflected gains and losses in forest cover of various types, while Arctic patterns were widespread and showed lower magnitude greening trends often associated with shrub expansion. Sun-induced fluorescence, a proxy for productivity, captures age-dependent relationships in land cover and productivity that NDVI does not. This work provides a quantification of the degree to which land cover change influences Arctic-Boreal greening and browning trends in both extent and

magnitude, and begins to explore alternative measures of satellite-based productivity that are sensitive to dynamic land cover histories. More advanced studies will require an analysis of how these satellite-based measures can be understood with greater mechanistic detail and how the sparser datasets, such as SIF, can be extended in space and time.

For the fourth chapter, we generated a dataset of annual, 30 m maps of aboveground live woody biomass in the Boreal biome of the ABoVE Core Study Domain by combining data from time series of Landsat data, information on land cover and disturbance history, and extensive GLAS lidar data with advanced machine learning techniques. We used this data to characterize differences in woody biomass stocks and biomass accumulation rates across land covers and ecoregions, as well as to characterize the dynamics of disturbance-related loss and regrowth across ecoregions in the Boreal forests of the ABoVE domain. In most ecoregions, total carbon accumulation was highly correlated with the occurrence of fire, though harvests also imposed a large, cumulative loss of carbon via consistent losses. Despite these disturbances, the Boreal forest is overall accumulating biomass, although the sink appears to be slowing in the latter part of the time series. While it has long been known that fires drive much of Boreal forest carbon, here we present a quantification of these dynamics based on extensive observations, rather than limited field plots or model-based studies.

5.3 Future Directions

The work presented in this dissertation represents a significant advance in Earth Systems Science and remote sensing by analyzing how time series data can be used to characterize disturbance history and its impacts on ecosystem function. However, significant gaps still remain. Here, we discuss several potential future directions that can further improve the insights generated by this dissertation.

First, while the domain of this dissertation is large, it does not encompass the entirety of Arctic-Boreal regions, or even the entire Arctic-Boreal region of North America. The climate and disturbance regimes of eastern Canada are substantially different from those of Arctic-Boreal Eurasia, or even of western Canada (Gauthier et al., 2015; Soja et al., 2007; Sulla-Menashe et al., 2018). For example, eastern Canada tends to be substantially wetter and more heavily harvested than western Canada, which impacts the patterns of NDVI trends in different ways than in western Canada (Sulla-Menashe et al., 2018). The results here may not generalize across the continent without further study. Expanding the land cover change, productivity, and AGB analysis employed here will greatly improve understanding of the unique dynamics of other Arctic-Boreal regions.

Second, the disturbance agents that drive land cover change throughout Arctic-Boreal biomes are numerous. However, here we focus only on disturbance agents for which data are readily available and of high quality (wildfire and timber harvest) (Kasischke et al., 2002; Stocks et al., 2002; White et al., 2017), but which do not characterize any of the variety of other subtler, but potentially important, disturbances.

For example, permafrost degradation results in substantial forest loss, potentially at rates equivalent to those of fire-based losses (Carpino et al., 2018; Helbig et al., 2016), and the ensuing wetland expansion likely results in different carbon dynamics and biophysical than fires (Helbig et al., 2017). Insect infestation is a well-documented phenomenon in some parts of the Boreal forest and exhibit a potentially severe feedback with climate change (Kurz et al., 2008; Volney and Fleming, 2000), but data on the spatial variability of insect infestation is lacking. Other disturbance agents, like droughts, resource exploration, and changes in Arctic herbivory, are likely to impact land cover and carbon dynamics in distinct ways (Gough et al., 2012; Hogg et al., 2008; Ma et al., 2012; Park Williams et al., 2012; Sjögersten et al., 2008; Williams et al., 2013), and additional information on the location and timing of these different disturbance agents is required to accurately characterize these impacts.

Third, more sophisticated statistical methods for evaluating trends in NDVI are needed. Simple linear models based on time fail to capture interannual variability and are relatively insensitive to disturbances, resulting in simplified or biased understanding of land surface changes (Sulla-Menashe et al., 2018). Methods that fit piecewise linear trends are more sensitive to disturbances and are more likely to characterize realistic changes in land surface characteristics due to global change (Cohen et al., 2018; Forkel et al., 2013; Kennedy et al., 2010).

Fourth, we demonstrate that NDVI is not a sensitive indicator of changes in productivity in mid-successional forests, thus missing important demography-dependent variability in carbon exchange (Pugh et al., 2019). It is well-known that NDVI saturates

at relatively high values of LAI, suggesting a loss of sensitivity that may hamper its utility as a metric for productivity (Curran, 1983) . Additional information, such as SIF demonstrated here or other spectral indices that capture light use efficiency or water status (Crist and Cicone, 1984; Gamon et al., 1992; Garbulsky et al., 2011), may provide complementary information on ecosystem function. Dynamic and heterogeneous land surface characteristics, including open canopies and understory reflectance, often confound interpretation of NDVI in Arctic and Boreal ecosystems, such as the incidence of seasonally variable and extensive surface water (Cooley et al., 2019; Raynolds et al., 2012).

APPENDIX 1: LANDSAT-BASED SPECTRAL MEASURES USED FOR CLUSTERING AND MAPPING

Appendix Table A.1.1 | List and descriptions of the Landsat-based spectral features used for clustering and land cover mapping. Difference metrics (i.e. Tasseled Cap Wetness – Tasseled Cap Greenness) were because previous studies concluded that they improved accuracy for mapping wetlands (Huang et al., 2014). Coefficients for calculation of tasseled cap indices are taken from Crist & Cicone (1984).

Band or Index	Description
Blue	Landsat Band 1, wavelength 0.45 – 0.52 μm
Green	Landsat Band 2, wavelength 0.52 – 0.60 μm
Red	Landsat Band 3, wavelength 0.63 – 0.69 μm
Near Infrared	Landsat Band 4, wavelength 0.76 – 0.90 μm
Shortwave Infrared 1	Landsat Band 5, wavelength 1.55 – 1.75 μm
Shortwave Infrared 2	Landsat Band 7, wavelength 10.40 – 12.50 μm
Brightness Temp.	Landsat Band 6, wavelength 2.08 – 2.35 μm
Norm. Diff. Veg. Ind.	$\mathrm{NDVI} = \frac{\rho_{\mathrm{NIR}} - \rho_{\mathrm{red}}}{\rho_{\mathrm{NIR}} + \rho_{\mathrm{red}}}$
Enhanced Veg. Ind.	$\mathrm{EVI} = 2.5 * \frac{\rho_{\mathrm{NIR}} - \rho_{\mathrm{red}}}{\rho_{\mathrm{NIR}} + 6 * \rho_{\mathrm{red}} - 7.5 * \rho_{\mathrm{blue}} + 1}$
Norm. Burn Ratio	$\mathrm{NBR} = \frac{\rho_{\mathrm{NIR}} - \rho_{\mathrm{SWIR2}}}{\rho_{\mathrm{NIR}} + \rho_{\mathrm{SWIR2}}}$
TC Brightness	$\mathrm{TCB} = 0.2043 * \rho_{\mathrm{blue}} + 0.4158 * \rho_{\mathrm{green}} + 0.5524 * \rho_{\mathrm{red}} + 0.5741 * \rho_{\mathrm{NIR}} + 0.3124 * \rho_{\mathrm{SWIR1}} + 0.2303 * \rho_{\mathrm{SWIR2}}$
TC Greenness	$\mathrm{TCG} = -0.1603 * \rho_{\mathrm{blue}} - 0.2819 * \rho_{\mathrm{green}} - 0.4934 * \rho_{\mathrm{red}} + 0.7940 * \rho_{\mathrm{NIR}} + 0.0002 * \rho_{\mathrm{SWIR1}} + 0.1446 * \rho_{\mathrm{SWIR2}}$
TC Wetness	$\mathrm{TCW} = 0.0315 * \rho_{\mathrm{blue}} + 0.2021 * \rho_{\mathrm{green}} + 0.3102 * \rho_{\mathrm{red}} + 0.1594 * \rho_{\mathrm{NIR}} + 0.6806 * \rho_{\mathrm{SWIR1}} + 0.6109 * \rho_{\mathrm{SWIR2}}$
TC Wetness-Greenness Difference	$\mathrm{TCWGD} = \mathrm{TCW} - \mathrm{TCG}$
Red Chromatic Coordinate	$\mathrm{RCC} = \frac{\rho_{\mathrm{red}}}{(\rho_{\mathrm{blue}} + \rho_{\mathrm{green}} + \rho_{\mathrm{red}})}$
Green Chromatic Coordinate	$\mathrm{GCC} = \frac{\rho_{\mathrm{green}}}{(\rho_{\mathrm{blue}} + \rho_{\mathrm{green}} + \rho_{\mathrm{red}})}$
Blue Chromatic Coordinate	$\mathrm{BCC} = \frac{\rho_{\mathrm{blue}}}{(\rho_{\mathrm{blue}} + \rho_{\mathrm{green}} + \rho_{\mathrm{red}})}$

APPENDIX 2: EXTENDED LAND COVER LEGEND

Appendix Table A.2.1 | Land cover legend labels and descriptions for the extended legend. The land cover maps were originally created with this legend; they were then converted to the simplified legend (Table 2.1) for the change analysis.

Label	Description
Evergreen Forest	Area dominated by tall woody vegetation (> 3m tall) and over 60% canopy coverage with primarily (>75%) evergreen phenological habit (canopy maintains green foliage year-round).
Deciduous Forest	Area dominated by tall woody vegetation (> 3m tall) and over 60% canopy coverage with primarily (>75%) deciduous phenological habit (annual cycle of leaf-on and leaf-off periods).
Mixed Forest	Area dominated by tall woody vegetation (> 3m tall) and over 60% canopy coverage with neither forest type (deciduous or evergreen) exceeding over 60% of the area.
Woodland	Area dominated by tall woody vegetation (> 3m tall) with between 30-60% canopy coverage. Frequently co-exists with peatlands and typically, but not always, evergreen in phenological habit.
Low Shrub	Area dominated by dense hemi-prostrate to low-erect shrubs (5-30cm in height) with >60% area coverage. Analogous to "prostrate dwarf-shrub" occurring in tundra areas.
Tall Shrub	Area dominated by woody vegetation between 50cm and 3m tall and shrub canopy coverage >60% coverage. Typically, but not always, deciduous phenological habit.
Open Shrubs	Area with woody vegetation less than 3m tall and between 30-60% canopy coverage. Shrubs typically underlain by herbaceous or barren land cover.
Herbaceous	Area dominated by herbaceous land cover greater than 60% land cover and tree/shrub cover less than 10%.
Tussock Tundra	Tundra-specific herbaceous land dominated by *Eriophorum vaginatum* and other tussock-forming herbaceous species, coverage over 60%.
Sparsely Vegetated	10-30% canopy coverage, any vegetation but typically herbaceous/bryophyte, with rock underneath
Fen	hydrologically connected, sedge/grass dominated wetland
Bog	ombrotrophic, peat and shrub dominated wetland
Shallows/littoral	lakes <1 m deep with some vegetation or shoreline mixed with water/land
Barren	<10% vegetation, mostly rock
Water	Oceans, lakes, and rivers, either salt-water or freshwater.

APPENDIX 3: AREA ESTIMATION STRATA DEFINITION AND BIAS CORRECTION

Appendix Table A.3.1 | Matrix of mapped transitions and change strata definitions. For each box, the row indicates the starting land cover in 1984 and the column indicates the ending land cover in 2014. The boxes on the diagonal indicates the proportions of each stable land cover (e.g. experiencing no change in land cover). Due to space constraints, Evergreen Forest is abbreviated as EF, Deciduous Forest as DF, Shrub as SH, Herbaceous as Herb, Shallows as Shall., and Barren as Bare. Numeric values indicate the percent of the ABoVE Core Study Domain that is mapped as experiencing a land cover change defined by its row and column. The boxes are color coded according to the inclusion of each land cover transition in the definition of a given land cover change class (see Table 2.1). Strata weights are determined by the sums of the mapped areas across all land cover transitions within a certain land cover change class. White indicates stable classes (total 82.8%), red indicates Evergreen Forest Loss (4.98%), blue indicates Deciduous Forest Gain (1.40%), green indicates Evergreen Forest Gain (2.56%), orange indicates Shrub Loss (1.57%), brown indicates Shrub Gain (2.62%), yellow indicates Herbaceous Gain (2.2%), and pale blue indicates Other Change (1.932%). Deciduous Forest Loss was mapped as 0.53%, which was deemed negligible and thus not explicitly estimated.

Ends as…

Starts as…	EF	DF	SH	Herb	Sparse	Bare	Fen	Bog	Shall.	Water
EF	24.9	0.467	1.22	0.34	2.45	0.10	0.80	0.05	0.01	0.01
DF	0.26	5.4	0.24	0.17	0.03	0.01	0.08	0.00	0.00	0.00
SH	0.81	0.53	8.6	0.77	0.28	0.02	0.47	0.01	0.01	0.01
Herb	0.08	0.27	1.5	8.8	0.35	0.02	0.10	0.00	0.00	0.00
Sparse	1.01	0.05	0.71	1.13	13.5	0.21	0.272	0.00	0.01	0.00
Bare	0.12	0.01	0.05	0.07	1.00	9.7	0.04	0.00	0.02	0.06
Fen	0.25	0.07	0.35	0.03	0.05	0.01	2.3	0.00	0.01	0.01
Bog	0.03	0.00	0.01	0.00	0.00	0.00	0.00	0.2	0.00	0.00
Shall.	0.01	0.00	0.01	0.00	0.01	0.01	0.02	0.00	0.6	0.02
Water	0.00	0.00	0.01	0.00	0.00	0.05	0.01	0.00	0.05	8.8

Appendix Table A.3.2 | Impact of bias correction on area of land cover and land cover change from 1984-2014. The mapped area is derived as the simple sum of areas mapped by our *Random Forest* algorithm. The estimated area is the area derived from the design-based sample. The difference shows the relative change between mapped area and estimated area, which demonstrates the class-specific bias introduced by classification errors in the maps. Due to space constraints, the table has been split into two parts. Evergreen Forest is abbreviated as EF, Deciduous Forest as DF, Shrub as SH, Herbaceous as Herb, Shallows as Shall., and Other as Oth. Reference data indicated in columns and mapped classification data indicated in rows, total n = 1299. Absolute areas presented in units of 1,000 km^2. Table is broken into two parts to fit the page.

	EF	DF	SH	Herb	Sparse	Bare	Fen	Bog	Shall.	Water
Mapped Area	1,155.10	251.1	394	433	634.1	461.4	106.8	10	29.7	421.9
Estimated Area	1051.2	328.4	483.5	512.6	606.1	419.9	178	27.6	89.4	415.8
Difference (%)	9.9	-23.5	-18.5	-15.5	4.6	9.9	-40.0	-63.8	-66.8	1.5

	EF Loss	SH Loss	DF Gain	EF Gain	Herb Gain	SH Gain	Oth.
Mapped Area	244.3	75.4	70.5	111	109.7	124.3	128.3
Estimated Area	259.9	42.2	50.6	64	104.9	75.8	49.9
Difference (%)	-6.0	78.7	39.3	73.4	4.6	64.0	157.1

APPENDIX 4: ADDITIONAL MAPS OF LAND COVER AND LAND COVER CHANGE

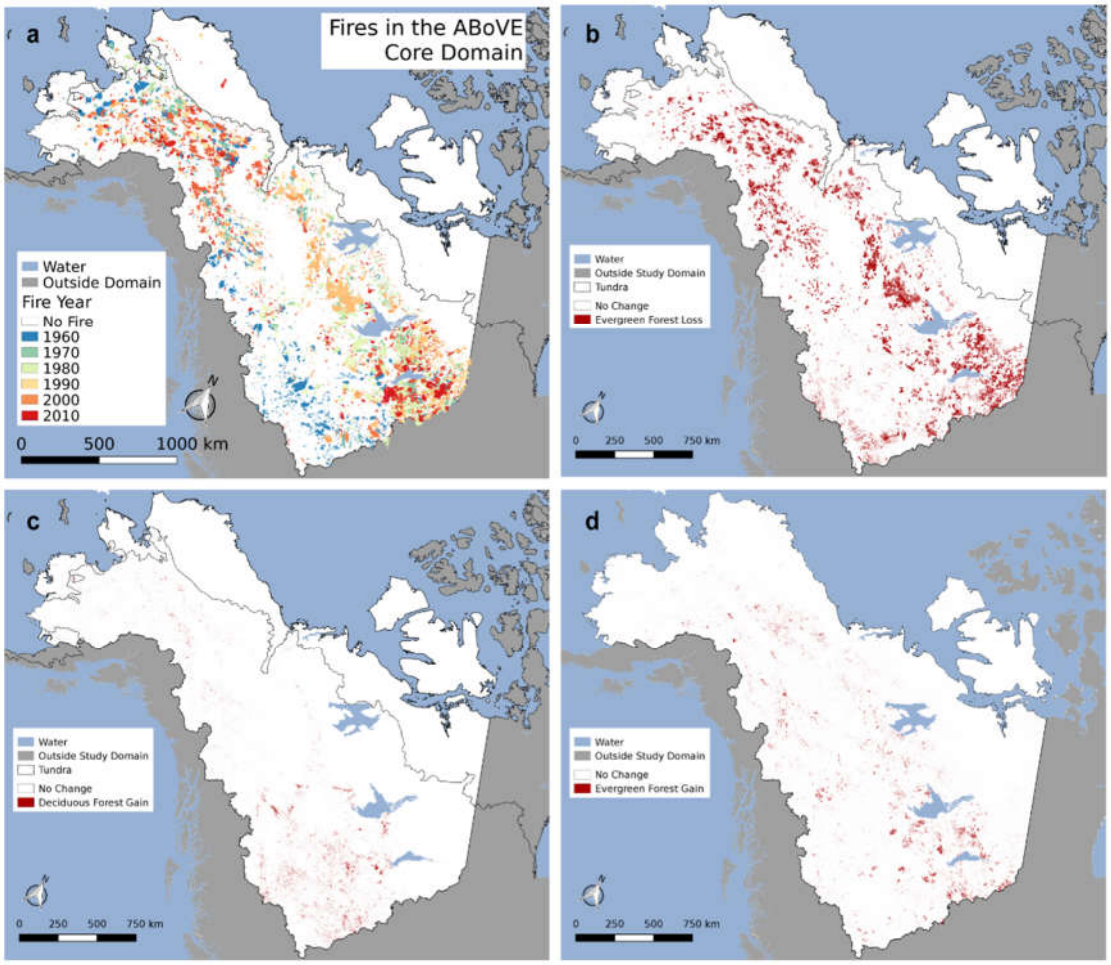

Appendix Figure A.4.1 | Domain-wide spatial coherence between forest change areas and historical fire perimeters. Comparison of maps of a) fire perimeters from the combined Alaska and Canadian large fire databases spanning 1960-2014 and land cover change, including b) evergreen forest loss, c) deciduous forest gain, and d) evergreen forest gain. Spatial patterns of forest loss and recovery are spatially coherent with fire perimeters, particularly for evergreen forests. Dotted line displays the treeline, which serves as our boundary between Boreal and Arctic biomes.

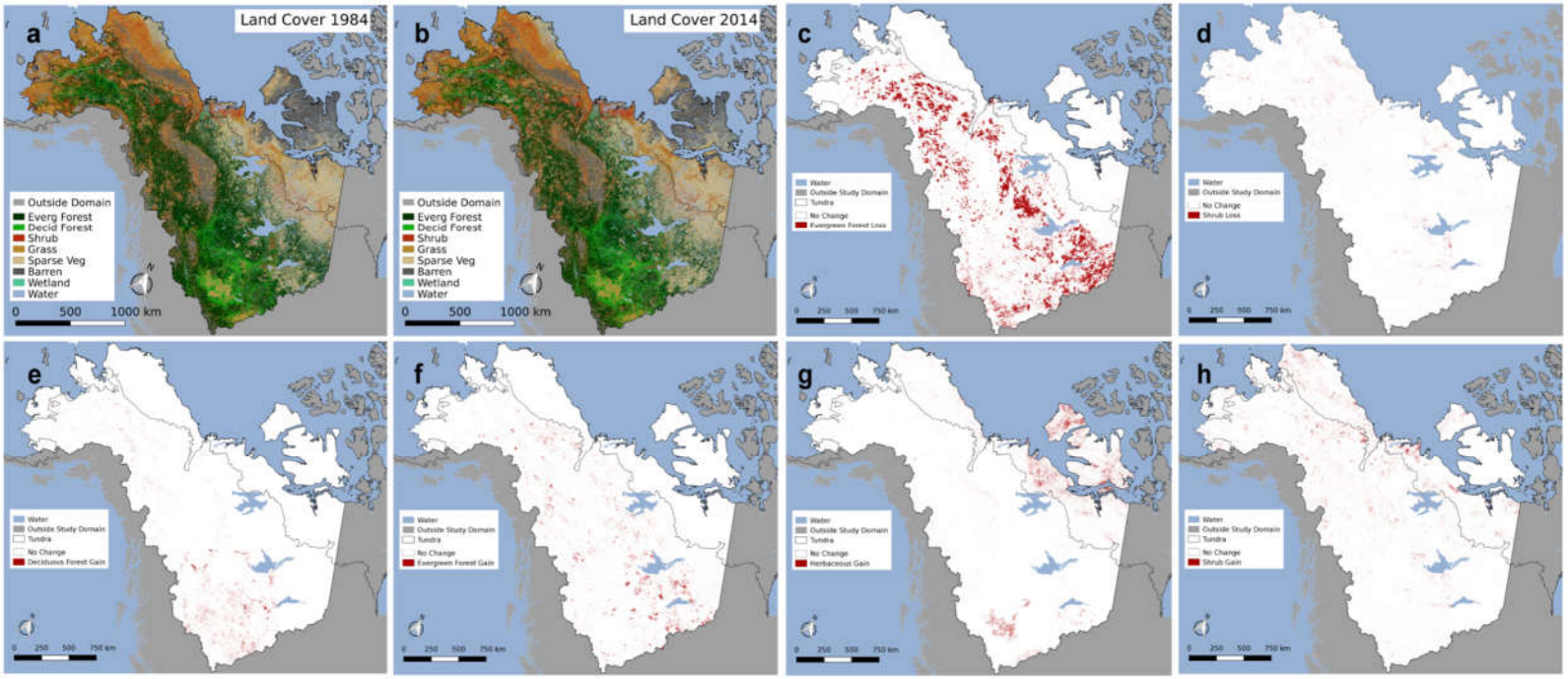

Appendix Figure A.4.2 | Additional maps of land cover and land cover change (1984-2014) in the ABoVE Core Study Domain. a) Land cover across the study domain in 1984; b) land cover across the study domain in 2014; c) Areas of Evergreen Forest Loss; d) areas of Shrub Loss; e) areas of Deciduous Forest Gain; f) areas of Evergreen Forest Gain; g) areas of Herbaceous Gain; h) areas of Shrub Gain. Dotted line displays the treeline, which serves as our boundary between Boreal and Arctic biomes. Mapped changes are presented as downscaled 900m pixels for display purposes.

APPENDIX 5: EXAMPLE OF CHANGE POINT FITTING ALGORITHM

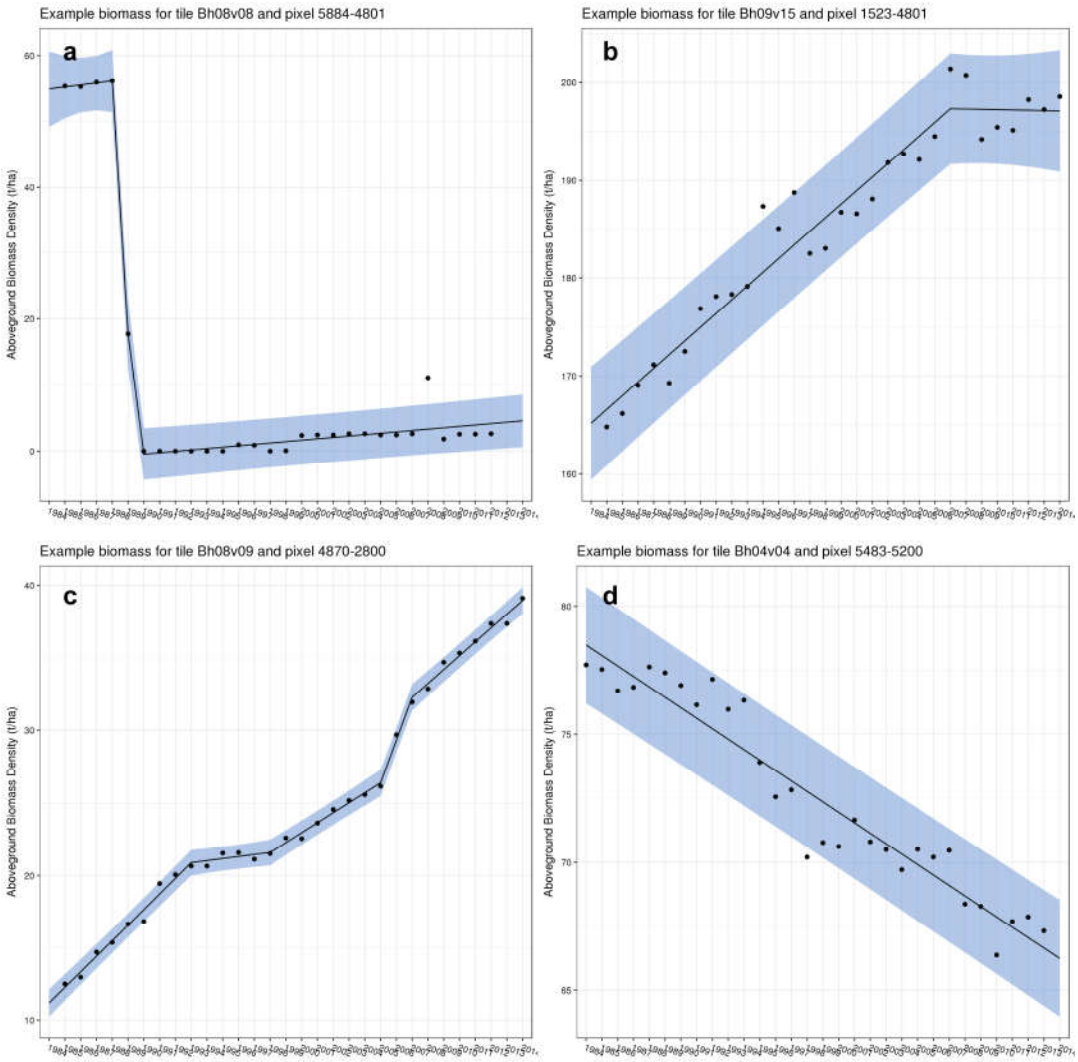

Appendix Figure A.5.1 | Example time series of changepoint algorithm and piece linear regression fitting procedure across four pixels. Points indicate the original AGB density predicted by the Gradient-Boosted Machine model. Lines indicate the fitted piecewise linear regressions and blue ribbons indicate the 95% confidence interval derived from the linear regressions. The algorithm captures carbon dynamics of various kinds, including a) sharp loss due to disturbance plus following regrowth, b) steady growth that plateaus, c) steady increases in AGB density in growing forests, and d) steady decreases of AGB in declining forests.

APPENDIX 6: LAND COVER-SPECIFIC DISTRIBUTIONS OF AGB AND AGB TRENDS

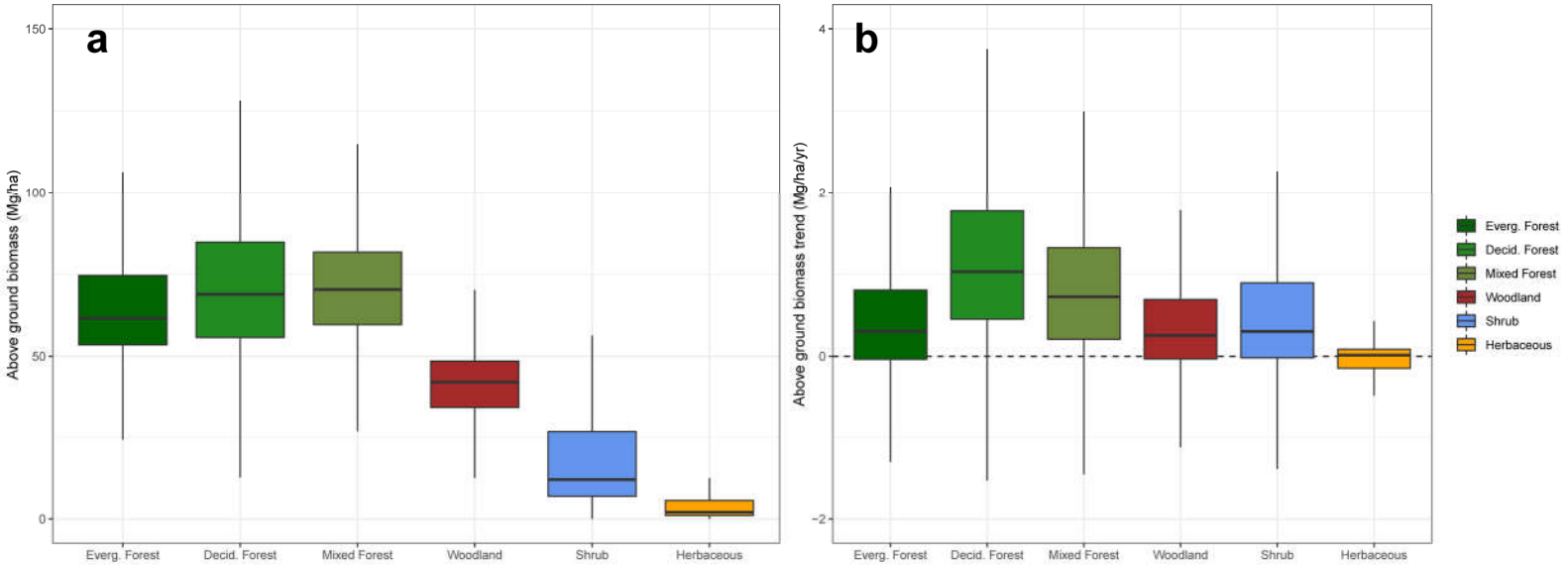

Appendix Figure A.6.1 | Distribution of aboveground biomass (AGB) and trends taken from a sample across the domain, aggregated across ecoregions. Shown are only the land covers that include woody biomass (e.g. Forest and Shrubs) and one non-woody land cover (Herbaceous) for comparison. a) Land cover specific distributions of AGB in a sample of pixels. b) Land cover specific distributions of trends in AGB in a sample of pixels that do not experience land cover change between 1984-2014

BIBLIOGRAPHY

Aber, J.D., Federer, C.A., 1992. A generalized, lumped-parameter model of photosynthesis, evapotranspiration and net primary production in temperate and boreal forest ecosystems. Oecologia 92, 463–474.

Alcaraz-Segura, D., Chuvieco, E., Epstein, H.E., Kasischke, E.S., Trishchenko, A., 2010. Debating the greening vs. browning of the North American boreal forest: differences between satellite datasets. Global Change Biology 16, 760–770.

Andela, N., Morton, D., Giglio, L., Chen, Y., Van Der Werf, G., Kasibhatla, P., DeFries, R., Collatz, G., Hantson, S., Kloster, S., others, 2017. A human-driven decline in global burned area. Science 356, 1356–1362.

Asner, G.P., Hughes, R.F., Varga, T.A., Knapp, D.E., Kennedy-Bowdoin, T., 2009. Environmental and biotic controls over aboveground biomass throughout a tropical rain forest. Ecosystems 12, 261–278.

Augusto, L., De Schrijver, A., Vesterdal, L., Smolander, A., Prescott, C., Ranger, J., 2015. Influences of evergreen gymnosperm and deciduous angiosperm tree species on the functioning of temperate and boreal forests. Biological reviews 90, 444–466.

Baccini, A., Friedl, M., Woodcock, C., Warbington, R., 2004. Forest biomass estimation over regional scales using multisource data. Geophysical research letters 31.

Baccini, A., Goetz, S., Walker, W., Laporte, N., Sun, M., Sulla-Menashe, D., Hackler, J., Beck, P., Dubayah, R., Friedl, M., others, 2012. Estimated carbon dioxide emissions from tropical deforestation improved by carbon-density maps. Nature climate change 2, 182.

Baccini, A., Walker, W., Carvalho, L., Farina, M., Sulla-Menashe, D., Houghton, R., 2017. Tropical forests are a net carbon source based on aboveground measurements of gain and loss. Science 358, 230–234.

Badgley, G., Field, C.B., Berry, J.A., 2017. Canopy near-infrared reflectance and terrestrial photosynthesis. Science Advances 3, e1602244.

Bartels, S.F., Chen, H.Y., Wulder, M.A., White, J.C., 2016. Trends in post-disturbance recovery rates of Canada's forests following wildfire and harvest. Forest Ecology and Management 361, 194–207.

Bartsch, A., Höfler, A., Kroisleitner, C., Trofaier, A., 2016. Land cover mapping in northern high latitude permafrost regions with satellite data: Achievements and remaining challenges. Remote Sensing 8, 979.

Beck, P.S., Goetz, S.J., 2011. Satellite observations of high northern latitude vegetation productivity changes between 1982 and 2008: ecological variability and regional differences. Environmental Research Letters 6, 045501.

Beget, M.E., Di Bella, C.M., 2007. Flooding: The effect of water depth on the spectral response of grass canopies. Journal of hydrology 335, 285–294.

Berner, L.T., Jantz, P., Tape, K.D., Goetz, S.J., 2018. Tundra plant above-ground biomass and shrub dominance mapped across the North Slope of Alaska. Environmental Research Letters 13, 035002.

Betts, A.K., Ball, J.H., 1997. Albedo over the boreal forest. Journal of Geophysical Research: Atmospheres 102, 28901–28909.

Black, T., Chen, W., Barr, A., Arain, M., Chen, Z., Nesic, Z., Hogg, E., Neumann, H., Yang, P., 2000. Increased carbon sequestration by a boreal deciduous forest in years with a warm spring. Geophysical Research Letters 27, 1271–1274.

Bolton, D.K., Coops, N.C., Hermosilla, T., Wulder, M.A., White, J.C., 2017. Assessing variability in post-fire forest structure along gradients of productivity in the Canadian boreal using multi-source remote sensing. Journal of Biogeography 44, 1294–1305.

Bonan, G.B., 2008. Forests and climate change: forcings, feedbacks, and the climate benefits of forests. science 320, 1444–1449.

Bonan, G.B., Pollard, D., Thompson, S.L., 1992. Effects of boreal forest vegetation on global climate. Nature 359, 716.

Bond-Lamberty, B., Peckham, S.D., Ahl, D.E., Gower, S.T., 2007. Fire as the dominant driver of central Canadian boreal forest carbon balance. Nature 450, 89.

Botkin, D.B., Simpson, L.G., 1990. Biomass of the North American boreal forest: A step toward accurate global measures. Biogeochemistry 161–174.

Boucher, Y., Auger, I., Noël, J., Grondin, P., Arseneault, D., 2017. Fire is a stronger driver of forest composition than logging in the boreal forest of eastern Canada. Journal of Vegetation Science 28, 57–68.

Bradshaw, C.J., Warkentin, I.G., 2015. Global estimates of boreal forest carbon stocks and flux. Global and Planetary Change 128, 24–30.

Breiman, L., 2001. Random forests. Machine learning 45, 5–32.

Buermann, W., Wang, Y., Dong, J., Zhou, L., Zeng, X., Dickinson, R.E., Potter, C.S., Myneni, R.B., 2002. Analysis of a multiyear global vegetation leaf area index data set. Journal of Geophysical Research: Atmospheres 107, ACL–14.

Bunn, A.G., Goetz, S.J., 2006. Trends in satellite-observed circumpolar photosynthetic activity from 1982 to 2003: the influence of seasonality, cover type, and vegetation density. Earth Interactions 10, 1–19.

Buttrey, S., 2016. treeClust: Cluster Distances Through Trees.

Carlson, T.N., Ripley, D.A., 1997. On the relation between NDVI, fractional vegetation cover, and leaf area index. Remote sensing of Environment 62, 241–252.

Carpino, O.A., Berg, A.A., Quinton, W.L., Adams, J.R., 2018. Climate change and permafrost thaw-induced boreal forest loss in northwestern Canada. Environmental Research Letters 13, 084018.

Chapin, F.S., Sturm, M., Serreze, M.C., McFadden, J.P., Key, J.R., Lloyd, A.H., McGuire, A.D., Rupp, T.S., Lynch, A.H., Schimel, J.P., Beringer, J., Chapman, W.L., Epstein, H.E., Euskirchen, E.S., Hinzman, L.D., Jia, G., Ping, C.-L., Tape, K.D., Thompson, C.D.C., Walker, D.A., Welker, J.M., 2005. Role of Land-Surface Changes in Arctic Summer Warming. Science 310, 657–660.

Chapin III, F., McGuire, A., Randerson, J., Pielke, R., Baldocchi, D., Hobbie, S., Roulet, N., Eugster, W., Kasischke, E., Rastetter, E., others, 2000. Arctic and boreal ecosystems of western North America as components of the climate system. Global Change Biology 6, 211–223.

Chasmer, L., Hopkinson, C., Veness, T., Quinton, W., Baltzer, J., 2014. A decision-tree classification for low-lying complex land cover types within the zone of discontinuous permafrost. Remote Sensing of Environment 143, 73–84.

Chen, C., Park, T., Wang, X., Piao, S., Xu, B., Chaturvedi, R.K., Fuchs, R., Brovkin, V., Ciais, P., Fensholt, R., others, 2019. China and India lead in greening of the world through land-use management. Nature Sustainability 2, 122.

Chen, H.Y., Luo, Y., 2015. Net aboveground biomass declines of four major forest types with forest ageing and climate change in western Canada's boreal forests. Global change biology 21, 3675–3684.

Cochran, W.G., 1977. Sampling techniques-3.

Cohen, W.B., Yang, Z., Healey, S.P., Kennedy, R.E., Gorelick, N., 2018. A LandTrendr multispectral ensemble for forest disturbance detection. Remote sensing of environment 205, 131–140.

Cooley, S.W., Smith, L.C., Ryan, J.C., Pitcher, L.H., Pavelsky, T.M., 2019. Arctic-Boreal lake dynamics revealed using CubeSat imagery. Geophysical Research Letters.

Crist, E.P., Cicone, R.C., 1984. A physically-based transformation of Thematic Mapper data—The TM Tasseled Cap. IEEE Transactions on Geoscience and Remote sensing 256–263.

Curran, P., 1983. Multispectral remote sensing for the estimation of green leaf area index. Philosophical Transactions of the Royal Society of London. Series A, Mathematical and Physical Sciences 309, 257–270.

Damm, A., Elbers, J., Erler, A., Gioli, B., Hamdi, K., Hutjes, R., Kosvancova, M., Meroni, M., Miglietta, F., Moersch, A., Moreno, J., Schickling, A., Sonnenschein, R., Udelhoven, T., Van Der LINDEN, S., Hostert, P., Rascher, U., 2010. Remote sensing of sun-induced fluorescence to improve modeling of diurnal courses of gross primary production (GPP): RS OF SUN-INDUCED FLUORESCENCE TO IMPROVE MODELING OF GPP. Global Change Biology 16, 171–186.

DeFries, R., Townshend, J., 1994. NDVI-derived land cover classifications at a global scale. International Journal of Remote Sensing 15, 3567–3586.

Drake, J.B., Knox, R.G., Dubayah, R.O., Clark, D.B., Condit, R., Blair, J.B., Hofton, M., 2003. Above-ground biomass estimation in closed canopy neotropical forests using lidar remote sensing: Factors affecting the generality of relationships. Global ecology and biogeography 12, 147–159.

Dunn, A.L., Barford, C.C., Wofsy, S.C., Goulden, M.L., Daube, B.C., 2007. A long-term record of carbon exchange in a boreal black spruce forest: Means, responses to interannual variability, and decadal trends. Global Change Biology 13, 577–590.

Eamus, D., Boulain, N., Cleverly, J., Breshears, D.D., 2013. Global change-type drought-induced tree mortality: vapor pressure deficit is more important than temperature per se in causing decline in tree health. Ecology and Evolution 3, 2711–2729.

Elmendorf, S.C., Henry, G.H., Hollister, R.D., Björk, R.G., Boulanger-Lapointe, N., Cooper, E.J., Cornelissen, J.H., Day, T.A., Dorrepaal, E., Elumeeva, T.G., others, 2012. Plot-scale evidence of tundra vegetation change and links to recent summer warming. Nature Climate Change 2, 453.

Farina, M., Baccini, A., Golcalves, F., Walker, W., 2019. Global Aboveground Biomass Estimates from ICESAT GLAS. In Prep.

Fick, S.E., Hijmans, R.J., 2017. WorldClim 2: new 1-km spatial resolution climate surfaces for global land areas. International Journal of Climatology 37, 4302–4315.

Fisher, J.B., Hayes, D.J., Schwalm, C.R., Huntzinger, D.N., Stofferahn, E., Schaefer, K., Luo, Y., Wullschleger, S.D., Goetz, S., Miller, C.E., others, 2018. Missing pieces to modeling the Arctic-Boreal puzzle. Environmental Research Letters 13, 020202.

Forkel, M., Carvalhais, N., Rödenbeck, C., Keeling, R., Heimann, M., Thonicke, K., Zaehle, S., Reichstein, M., 2016. Enhanced seasonal CO2 exchange caused by amplified plant productivity in northern ecosystems. Science 351, 696–699.

Forkel, M., Carvalhais, N., Verbesselt, J., Mahecha, M., Neigh, C., Reichstein, M., 2013. Trend change detection in NDVI time series: Effects of inter-annual variability and methodology. Remote Sensing 5, 2113–2144.

Fox, A.M., Huntley, B., Lloyd, C.R., Williams, M., Baxter, R., 2008. Net ecosystem exchange over heterogeneous Arctic tundra: Scaling between chamber and eddy covariance measurements. Global Biogeochemical Cycles 22.

Frankenberg, C., O'Dell, C., Berry, J., Guanter, L., Joiner, J., Köhler, P., Pollock, R., Taylor, T.E., 2014. Prospects for chlorophyll fluorescence remote sensing from the Orbiting Carbon Observatory-2. Remote Sensing of Environment 147, 1–12.

Frazier, R.J., Coops, N.C., Wulder, M.A., Hermosilla, T., White, J.C., 2018. Analyzing spatial and temporal variability in short-term rates of post-fire vegetation return from Landsat time series. Remote Sensing of Environment 205, 32–45.

Gamon, J.A., Field, C.B., Goulden, M.L., Griffin, K.L., Hartley, A.E., Joel, G., Penuelas, J., Valentini, R., 1995. Relationships between NDVI, canopy structure, and photosynthesis in three Californian vegetation types. Ecological Applications 5, 28–41.

Gamon, J.A., Huemmrich, K.F., Wong, C.Y., Ensminger, I., Garrity, S., Hollinger, D.Y., Noormets, A., Peñuelas, J., 2016. A remotely sensed pigment index reveals photosynthetic phenology in evergreen conifers. Proceedings of the National Academy of Sciences 113, 13087–13092.

Gamon, J.A., Penuelas, J., Field, C.B., 1992. A narrow-waveband spectral index that tracks diurnal changes in photosynthetic efficiency. Remote sensing of environment 41, 35–44.

Garbulsky, M.F., Peñuelas, J., Gamon, J., Inoue, Y., Filella, I., 2011. The photochemical reflectance index (PRI) and the remote sensing of leaf, canopy and ecosystem radiation use efficienciesA review and meta-analysis. Remote Sensing of Environment 115, 281–297.

Gauthier, S., Bernier, P., Kuuluvainen, T., Shvidenko, A.Z., Schepaschenko, D.G., 2015. Boreal forest health and global change. Science 349, 819–822.

Gibson, C.M., Chasmer, L.E., Thompson, D.K., Quinton, W.L., Flannigan, M.D., Olefeldt, D., 2018. Wildfire as a major driver of recent permafrost thaw in boreal peatlands. Nature communications 9, 3041.

Gislason, P.O., Benediktsson, J.A., Sveinsson, J.R., 2006. Random forests for land cover classification. Pattern Recognition Letters 27, 294–300.

Gough, L., Moore, J.C., Shaver, G.R., Simpson, R.T., Johnson, D.R., 2012. Above-and belowground responses of arctic tundra ecosystems to altered soil nutrients and mammalian herbivory. Ecology 93, 1683–1694.

Goulden, M.L., McMillan, A., Winston, G., Rocha, A., Manies, K., Harden, J.W., Bond-Lamberty, B., 2011. Patterns of NPP, GPP, respiration, and NEP during boreal forest succession. Global Change Biology 17, 855–871.

Grace, J., Nichol, C., Disney, M., Lewis, P., Quaife, T., Bowyer, P., 2007. Can we measure terrestrial photosynthesis from space directly, using spectral reflectance and fluorescence? Global Change Biology 13, 1484–1497.

Graven, H., Keeling, R., Piper, S., Patra, P., Stephens, B., Wofsy, S., Welp, L., Sweeney, C., Tans, P., Kelley, J., others, 2013. Enhanced seasonal exchange of CO2 by northern ecosystems since 1960. Science 1239207.

Graven, H.D., Keeling, R.F., Piper, S.C., Patra, P.K., Stephens, B.B., Wofsy, S.C., Welp, L.R., Sweeney, C., Tans, P.P., Kelley, J.J., Daube, B.C., Kort, E.A., Santoni, G.W., Bent, J.D., 2013. Enhanced Seasonal Exchange of CO2 by Northern Ecosystems Since 1960. Science.

Gray, J.M., Frolking, S., Kort, E.A., Ray, D.K., Kucharik, C.J., Ramankutty, N., Friedl, M.A., 2014. Direct human influence on atmospheric CO2 seasonality from increased cropland productivity. Nature 515, 398–401.

Greaves, H.E., 2017. Applying Lidar and High-Resolution Multispectral Imagery for Improved Quantification and Mapping of Tundra Vegetation Structure and Distribution in the Alaskan Arctic (PhD Thesis). University of Idaho.

Greenwell, B., Boehmke, B., Cunningham, J., Developers, G.B.M., 2019. gbm: Generalized Boosted Regression Models.

Grosse, G., Harden, J., Turetsky, M., McGuire, A.D., Camill, P., Tarnocai, C., Frolking, S., Schuur, E.A., Jorgenson, T., Marchenko, S., others, 2011. Vulnerability of high-latitude soil organic carbon in North America to disturbance. Journal of Geophysical Research: Biogeosciences 116.

Gruber, S., 2012. Derivation and analysis of a high-resolution estimate of global permafrost zonation. The Cryosphere 6, 221.

Guanter, L., Zhang, Y., Jung, M., Joiner, J., Voigt, M., Berry, J.A., Frankenberg, C., Huete, A.R., Zarco-Tejada, P., Lee, J.-E., others, 2014. Global and time-resolved

monitoring of crop photosynthesis with chlorophyll fluorescence. Proceedings of the National Academy of Sciences 111, E1327–E1333.

Guay, K.C., Beck, P.S., Berner, L.T., Goetz, S.J., Baccini, A., Buermann, W., 2014. Vegetation productivity patterns at high northern latitudes: a multi-sensor satellite data assessment. Global Change Biology 20, 3147–3158.

Hall, F.G., Hilker, T., Coops, N.C., Lyapustin, A., Huemmrich, K.F., Middleton, E., Margolis, H., Drolet, G., Black, T.A., 2008. Multi-angle remote sensing of forest light use efficiency by observing PRI variation with canopy shadow fraction. Remote Sensing of Environment 112, 3201–3211.

Hansen, M.C., Potapov, P.V., Moore, R., Hancher, M., Turubanova, S., Tyukavina, A., Thau, D., Stehman, S., Goetz, S., Loveland, T.R., others, 2013. High-resolution global maps of 21st-century forest cover change. science 342, 850–853.

Harrell, P., Bourgeau-Chavez, L., Kasischke, E., French, N., Christensen Jr, N., 1995. Sensitivity of ERS-1 and JERS-1 radar data to biomass and stand structure in Alaskan boreal forest. Remote Sensing of Environment 54, 247–260.

Helbig, M., Chasmer, L.E., Desai, A.R., Kljun, N., Quinton, W.L., Sonnentag, O., 2017. Direct and indirect climate change effects on carbon dioxide fluxes in a thawing boreal forest–wetland landscape. Global change biology 23, 3231–3248.

Helbig, M., Pappas, C., Sonnentag, O., 2016. Permafrost thaw and wildfire: Equally important drivers of boreal tree cover changes in the Taiga Plains, Canada. Geophysical Research Letters 43, 1598–1606.

Hermosilla, T., Wulder, M.A., White, J.C., Coops, N.C., Hobart, G.W., 2018. Disturbance-informed annual land cover classification maps of Canada's forested ecosystems for a 29-year Landsat time series. Canadian Journal of Remote Sensing 44, 67–87.

Hicke, J.A., Asner, G.P., Kasischke, E.S., French, N.H., Randerson, J.T., Collatz, G.J., Stocks, B.J., Tucker, C.J., Los, S.O., Field, C.B., 2003. Postfire response of North American boreal forest net primary productivity analyzed with satellite observations. Global Change Biology 9, 1145–1157.

Hilker, T., Hall, F.G., Coops, N.C., Collatz, J.G., Black, T.A., Tucker, C.J., Sellers, P.J., Grant, N., 2013. Remote sensing of transpiration and heat fluxes using multi-angle observations. Remote sensing of environment 137, 31–42.

Hogg, E., Brandt, J., Michaelian, M., 2008. Impacts of a regional drought on the productivity, dieback, and biomass of western Canadian aspen forests. Canadian Journal of Forest Research 38, 1373–1384.

Huang, C., Peng, Y., Lang, M., Yeo, I.-Y., McCarty, G., 2014. Wetland inundation mapping and change monitoring using Landsat and airborne LiDAR data. Remote Sensing of Environment 141, 231–242.

Huete, A., Didan, K., Miura, T., Rodriguez, E.P., Gao, X., Ferreira, L.G., 2002. Overview of the radiometric and biophysical performance of the MODIS vegetation indices. Remote sensing of environment 83, 195–213.

IPCC AR5 SPM, n.d.

Jin, S., Yang, L., Zhu, Z., Homer, C., 2017. A land cover change detection and classification protocol for updating Alaska NLCD 2001 to 2011. Remote Sensing of Environment 195, 44–55.

Johnstone, J.F., Hollingsworth, T.N., Chapin, F.S., Mack, M.C., 2010. Changes in fire regime break the legacy lock on successional trajectories in Alaskan boreal forest. Global Change Biology 16, 1281–1295.

Ju, J., Masek, J.G., 2016. The vegetation greenness trend in Canada and US Alaska from 1984–2012 Landsat data. Remote Sensing of Environment 176, 1–16.

Kasischke, E.S., Christensen Jr, N., Stocks, B.J., 1995. Fire, global warming, and the carbon balance of boreal forests. Ecological applications 5, 437–451.

Kasischke, E.S., Verbyla, D.L., Rupp, T.S., McGuire, A.D., Murphy, K.A., Jandt, R., Barnes, J.L., Hoy, E.E., Duffy, P.A., Calef, M., others, 2010. Alaska's changing fire regime—implications for the vulnerability of its boreal forests. Canadian Journal of Forest Research 40, 1313–1324.

Kasischke, E.S., Williams, D., Barry, D., 2002. Analysis of the patterns of large fires in the boreal forest region of Alaska. International Journal of Wildland Fire 11, 131–144.

Kaufman, L., Rousseeuw, P.J., 1990. Partitioning around medoids (program pam). Finding groups in data: an introduction to cluster analysis 68–125.

Keeling, C.D., Chin, J., Whorf, T., 1996. Increased activity of northern vegetation inferred from atmospheric CO2 measurements. Nature 382, 146.

Kelly, R., Chipman, M.L., Higuera, P.E., Stefanova, I., Brubaker, L.B., Hu, F.S., 2013. Recent burning of boreal forests exceeds fire regime limits of the past 10,000 years. Proceedings of the National Academy of Sciences 110, 13055–13060.

Kelso, N.V., Patterson, T., 2010. Introducing natural earth data-naturalearthdata. com. Geographia Technica 5, 82–89.

Kendall, M.G., 1948. Rank correlation methods.

Kennedy, R.E., Yang, Z., Cohen, W.B., 2010. Detecting trends in forest disturbance and recovery using yearly Landsat time series: 1. LandTrendr — Temporal segmentation algorithms. Remote Sensing of Environment 114, 2897–2910.

Kimball, J.S., Keyser, A.R., Running, S.W., Saatchi, S., 2000. Regional assessment of boreal forest productivity using an ecological process model and remote sensing parameter maps. Tree physiology 20, 761–775.

Kimball, J.S., Zhao, M., McGuire, A., Heinsch, F.A., Clein, J., Calef, M., Jolly, W.M., Kang, S., Euskirchen, S., McDonald, K., others, 2007. Recent climate-driven increases in vegetation productivity for the western Arctic: evidence of an acceleration of the northern terrestrial carbon cycle. Earth Interactions 11, 1–30.

Krause, G.H., Weis, E., 1991. Chlorophyll fluorescence and photosynthesis: the basics. Annual review of plant biology 42, 313–349.

Kurz, W.A., Dymond, C., Stinson, G., Rampley, G., Neilson, E., Carroll, A., Ebata, T., Safranyik, L., 2008. Mountain pine beetle and forest carbon feedback to climate change. Nature 452, 987.

Kurz, W.A., Shaw, C., Boisvenue, C., Stinson, G., Metsaranta, J., Leckie, D., Dyk, A., Smyth, C., Neilson, E., 2013. Carbon in Canada's boreal forest—a synthesis. Environmental Reviews 21, 260–292.

Lefsky, M.A., Cohen, W.B., Harding, D.J., Parker, G.G., Acker, S.A., Gower, S.T., 2002. Lidar remote sensing of above-ground biomass in three biomes. Global ecology and biogeography 11, 393–399.

Liu, S., Bond-Lamberty, B., Hicke, J.A., Vargas, R., Zhao, S., Chen, J., Edburg, S.L., Hu, Y., Liu, J., McGuire, A.D., others, 2011. Simulating the impacts of disturbances on forest carbon cycling in North America: Processes, data, models, and challenges. Journal of Geophysical Research: Biogeosciences 116.

Loranty, M.M., Goetz, S.J., 2012. Shrub expansion and climate feedbacks in Arctic tundra. Environmental Research Letters 7, 011005.

Lu, D., 2006. The potential and challenge of remote sensing-based biomass estimation. International journal of remote sensing 27, 1297–1328.

Luus, K., Commane, R., Parazoo, N., Benmergui, J., Euskirchen, E., Frankenberg, C., Joiner, J., Lindaas, J., Miller, C., Oechel, W., others, 2017. Tundra photosynthesis captured by satellite-observed solar-induced chlorophyll fluorescence. Geophysical Research Letters 44, 1564–1573.

Luus, K., Lin, J., 2015. The Polar Vegetation Photosynthesis and Respiration Model: a parsimonious, satellite-data-driven model of high-latitude CO 2 exchange. Geoscientific Model Development 8, 2655–2674.

Ma, Z., Peng, C., Zhu, Q., Chen, H., Yu, G., Li, W., Zhou, X., Wang, W., Zhang, W., 2012. Regional drought-induced reduction in the biomass carbon sink of Canada's boreal forests. Proceedings of the National Academy of Sciences 109, 2423–2427.

Maechler, M., Rousseeuw, P., Struyf, A., Hubert, M., Hornik, K., 2017. cluster: Cluster Analysis Basics and Extensions.

Mahadevan, P., Wofsy, S.C., Matross, D.M., Xiao, X., Dunn, A.L., Lin, J.C., Gerbig, C., Munger, J.W., Chow, V.Y., Gottlieb, E.W., 2008. A satellite-based biosphere parameterization for net ecosystem CO $_2$ exchange: Vegetation Photosynthesis and Respiration Model (VPRM): NET ECOSYSTEM EXCHANGE MODEL. Global Biogeochemical Cycles 22

Malhi, Y. al, Baldocchi, D., Jarvis, P., 1999. The carbon balance of tropical, temperate and boreal forests. Plant, Cell & Environment 22, 715–740.

Matasci, G., Hermosilla, T., Wulder, M.A., White, J.C., Coops, N.C., Hobart, G.W., Bolton, D.K., Tompalski, P., Bater, C.W., 2018a. Three decades of forest structural dynamics over Canada's forested ecosystems using Landsat time-series and lidar plots. Remote Sensing of Environment 216, 697–714.

Matasci, G., Hermosilla, T., Wulder, M.A., White, J.C., Coops, N.C., Hobart, G.W., Zald, H.S., 2018b. Large-area mapping of Canadian boreal forest cover, height, biomass and other structural attributes using Landsat composites and lidar plots. Remote sensing of environment 209, 90–106.

Meltzer, A., 2003. EarthScope Opportunities and challenges for earth-science research and education. The Leading Edge 22, 268–271.

Meroni, M., Rossini, M., Guanter, L., Alonso, L., Rascher, U., Colombo, R., Moreno, J., 2009. Remote sensing of solar-induced chlorophyll fluorescence: Review of methods and applications. Remote Sensing of Environment 113, 2037–2051.

Myers-Smith, I.H., In Press. Eighteen years of ecological monitoring reveals multiple lines of evidence for tundra vegetation change. Ecological Monographs.

Myers-Smith, I.H., Forbes, B.C., Wilmking, M., Hallinger, M., Lantz, T., Blok, D., Tape, K.D., Macias-Fauria, M., Sass-Klaassen, U., Lévesque, E., others, 2011. Shrub expansion in tundra ecosystems: dynamics, impacts and research priorities. Environmental Research Letters 6, 045509.

Myers-Smith, I.H., Grabowski, M.M., Thomas, H.J., Angers-Blondin, S., Daskalova, G.N., Bjorkman, A.D., Cunliffe, A.M., Assmann, J.J., Boyle, J.S., McLeod, E., others, 2019. Eighteen years of ecological monitoring reveals multiple lines of evidence for tundra vegetation change. Ecological Monographs e01351.

Myneni, R., Dong, J., Tucker, C., Kaufmann, R., Kauppi, P., Liski, J., Zhou, L., Alexeyev, V., Hughes, M., 2001. A large carbon sink in the woody biomass of northern forests. Proceedings of the National Academy of Sciences 98, 14784–14789.

Myneni, R.B., Keeling, C., Tucker, C.J., Asrar, G., Nemani, R.R., 1997a. Increased plant growth in the northern high latitudes from 1981 to 1991. Nature 386, 698.

Myneni, R.B., Ramakrishna, R., Nemani, R., Running, S.W., 1997b. Estimation of global leaf area index and absorbed PAR using radiative transfer models. IEEE Transactions on Geoscience and remote sensing 35, 1380–1393.

Neigh, C.S., Nelson, R.F., Ranson, K.J., Margolis, H.A., Montesano, P.M., Sun, G., Kharuk, V., N\a esset, E., Wulder, M.A., Andersen, H.-E., 2013. Taking stock of circumboreal forest carbon with ground measurements, airborne and spaceborne LiDAR. Remote Sensing of Environment 137, 274–287.

Olofsson, P., Foody, G.M., Herold, M., Stehman, S.V., Woodcock, C.E., Wulder, M.A., 2014. Good practices for estimating area and assessing accuracy of land change. Remote Sensing of Environment 148, 42–57.

Olofsson, P., Foody, G.M., Stehman, S.V., Woodcock, C.E., 2013. Making better use of accuracy data in land change studies: Estimating accuracy and area and quantifying uncertainty using stratified estimation. Remote Sensing of Environment 129, 122–131.

Pare, D., Bergeron, Y., 1995. Above-ground biomass accumulation along a 230-year chronosequence in the southern portion of the Canadian boreal forest. Journal of Ecology 1001–1007.

Parent, M.B., Verbyla, D., 2010. The browning of Alaska's boreal forest. Remote Sensing 2, 2729–2747.

Park, T., Ganguly, S., Tømmervik, H., Euskirchen, E.S., Høgda, K.-A., Karlsen, S.R., Brovkin, V., Nemani, R.R., Myneni, R.B., 2016. Changes in growing season duration and productivity of northern vegetation inferred from long-term remote sensing data. Environmental Research Letters 11, 084001.

Park Williams, A., Allen, C.D., Macalady, A.K., Griffin, D., Woodhouse, C.A., Meko, D.M., Swetnam, T.W., Rauscher, S.A., Seager, R., Grissino-Mayer, H.D., Dean, J.S., Cook, E.R., Gangodagamage, C., Cai, M., McDowell, N.G., 2012. Temperature as a

potent driver of regional forest drought stress and tree mortality. Nature Climate Change 3, 292.

Pasquarella, V.J., Holden, C.E., Woodcock, C.E., 2018. Improved mapping of forest type using spectral-temporal Landsat features. Remote Sensing of Environment 210, 193–207.

Pastick, N.J., Jorgenson, M.T., Goetz, S.J., Jones, B.M., Wylie, B.K., Minsley, B.J., Genet, H., Knight, J.F., Swanson, D.K., Jorgenson, J.C., 2019. Spatiotemporal remote sensing of ecosystem change and causation across Alaska. Global change biology 25, 1171–1189.

Pekel, J.-F., Cottam, A., Gorelick, N., Belward, A.S., 2016. High-resolution mapping of global surface water and its long-term changes. Nature 540, 418.

Piao, S., Ciais, P., Friedlingstein, P., Peylin, P., Reichstein, M., Luyssaert, S., Margolis, H., Fang, J., Barr, A., Chen, A., others, 2008. Net carbon dioxide losses of northern ecosystems in response to autumn warming. Nature 451, 49.

Pithan, F., Mauritsen, T., 2014. Arctic amplification dominated by temperature feedbacks in contemporary climate models. Nature Geoscience 7, 181.

Post, W.M., Emanuel, W.R., Zinke, P.J., Stangenberger, A.G., 1982. Soil carbon pools and world life zones. Nature 298, 156.

Pugh, T.A., Lindeskog, M., Smith, B., Poulter, B., Arneth, A., Haverd, V., Calle, L., 2019. Role of forest regrowth in global carbon sink dynamics. Proceedings of the National Academy of Sciences 116, 4382–4387.

Randerson, J., Field, C., Fung, I., Tans, P., 1999. Increases in early season ecosystem uptake explain recent changes in the seasonal cycle of atmospheric CO2 at high northern latitudes. Geophysical Research Letters 26, 2765–2768.

Randerson, J.T., Liu, H., Flanner, M.G., Chambers, S.D., Jin, Y., Hess, P.G., Pfister, G., Mack, M., Treseder, K., Welp, L., others, 2006. The impact of boreal forest fire on climate warming. science 314, 1130–1132.

Rauste, Y., 2005. Multi-temporal JERS SAR data in boreal forest biomass mapping. Remote Sensing of Environment 97, 263–275.

Raynolds, M.K., Walker, D.A., 2016. Increased wetness confounds Landsat-derived NDVI trends in the central Alaska North Slope region, 1985–2011. Environmental Research Letters 11, 085004.

Raynolds, M.K., Walker, D.A., Epstein, H.E., Pinzon, J.E., Tucker, C.J., 2012. A new estimate of tundra-biome phytomass from trans-Arctic field data and AVHRR NDVI. Remote Sensing Letters 3, 403–411.

Rignot, E., Way, J., Williams, C., Viereck, L., 1994. Radar estimates of aboveground biomass in boreal forests of interior Alaska. IEEE Transactions on Geoscience and Remote Sensing 32, 1117–1124.

Rogers, B.M., Soja, A.J., Goulden, M.L., Randerson, J.T., 2015. Influence of tree species on continental differences in boreal fires and climate feedbacks. Nature Geoscience 8, 228.

Rogers, B.M., Solvik, K., Hogg, E.H., Ju, J., Masek, J.G., Michaelian, M., Berner, L.T., Goetz, S.J., 2018. Detecting early warning signals of tree mortality in boreal North America using multiscale satellite data. Global change biology 24, 2284–2304.

Rogers, M., Randerson, T., Bonan, B., 2013. High-latitude cooling associated with landscape changes from North American boreal forest fires. Biogeosciences 10, 699–718.

Roy, D.P., Boschetti, L., Justice, C., 2006. Global mapping of fire-affected areas using multitemporal MODIS data: The MCD45 product, in: 2006 IEEE International Geoscience and Remote Sensing Symposium, Vols. 1. pp. 4165–4168.

Running, S.W., Nemani, R.R., Heinsch, F.A., Zhao, M., Reeves, M., Hashimoto, H., 2004. A continuous satellite-derived measure of global terrestrial primary production. Bioscience 54, 547–560.

Saatchi, S.S., Moghaddam, M., 2000. Estimation of crown and stem water content and biomass of boreal forest using polarimetric SAR imagery. IEEE Transactions on Geoscience and Remote Sensing 38, 697–709.

Schimel, D., Pavlick, R., Fisher, J.B., Asner, G.P., Saatchi, S., Townsend, P., Miller, C., Frankenberg, C., Hibbard, K., Cox, P., 2015. Observing terrestrial ecosystems and the carbon cycle from space. Global Change Biology 21, 1762–1776.

Sen, P.K., 1968. Estimates of the regression coefficient based on Kendall's tau. Journal of the American statistical association 63, 1379–1389.

Serreze, M., Barrett, A., Stroeve, J., Kindig, D., Holland, M., 2009. The emergence of surface-based Arctic amplification. The Cryosphere 3, 11–19.

Sjögersten, S., Van der Wal, R., Woodin, S.J., 2008. Habitat type determines herbivory controls over CO2 fluxes in a warmer arctic. Ecology 89, 2103–2116.

Smith, W.B., 2002. Forest inventory and analysis: a national inventory and monitoring program. Environmental pollution 116, S233–S242.

Soja, A.J., Tchebakova, N.M., French, N.H., Flannigan, M.D., Shugart, H.H., Stocks, B.J., Sukhinin, A.I., Parfenova, E., Chapin III, F.S., Stackhouse Jr, P.W., 2007. Climate-induced boreal forest change: predictions versus current observations. Global and Planetary Change 56, 274–296.

Song, X.-P., Hansen, M.C., Stehman, S.V., Potapov, P.V., Tyukavina, A., Vermote, E.F., Townshend, J.R., 2018. Global land change from 1982 to 2016. Nature 560, 639.

Stinson, G., Kurz, W., Smyth, C., Neilson, E., Dymond, C., Metsaranta, J., Boisvenue, C., Rampley, G., Li, Q., White, T., others, 2011. An inventory-based analysis of Canada's managed forest carbon dynamics, 1990 to 2008. Global change biology 17, 2227–2244.

Stocks, B., Mason, J., Todd, J., Bosch, E., Wotton, B., Amiro, B., Flannigan, M., Hirsch, K., Logan, K., Martell, D., others, 2002. Large forest fires in Canada, 1959–1997. Journal of Geophysical Research: Atmospheres 107, FFR–5.

Stow, D., Petersen, A., Hope, A., Engstrom, R., Coulter, L., 2007. Greenness trends of Arctic tundra vegetation in the 1990s: comparison of two NDVI data sets from NOAA AVHRR systems. International Journal of Remote Sensing 28, 4807–4822.

Sturm, M., Racine, C., Tape, K., 2001. Climate change: increasing shrub abundance in the Arctic. Nature 411, 546.

Sulla-Menashe, D., Woodcock, C.E., Friedl, M.A., 2018. Canadian boreal forest greening and browning trends: an analysis of biogeographic patterns and the relative roles of disturbance versus climate drivers. Environmental Research Letters 13, 014007.

Sun, Y., Frankenberg, C., Wood, J.D., Schimel, D.S., Jung, M., Guanter, L., Drewry, D., Verma, M., Porcar-Castell, A., Griffis, T.J., others, 2017. OCO-2 advances photosynthesis observation from space via solar-induced chlorophyll fluorescence. Science 358, eaam5747.

Tachikawa, T., Hato, M., Kaku, M., Iwasaki, A., 2011. Characteristics of ASTER GDEM version 2, in: Geoscience and Remote Sensing Symposium (IGARSS), 2011 IEEE International. IEEE, pp. 3657–3660.

Tape, K., Sturm, M., Racine, C., 2006. The evidence for shrub expansion in Northern Alaska and the Pan-Arctic. Global Change Biology 12, 686–702.

Team, R.C., others, 2013. R: A language and environment for statistical computing.

Theil, H., 1992. A rank-invariant method of linear and polynomial regression analysis, in: Henri Theil's Contributions to Economics and Econometrics. Springer, pp. 345–381.

Thomas, R.T., Prentice, I.C., Graven, H., Ciais, P., Fisher, J.B., Hayes, D.J., Huang, M., Huntzinger, D.N., Ito, A., Jain, A., others, 2016. Increased light-use efficiency in northern terrestrial ecosystems indicated by CO2 and greening observations. Geophysical Research Letters 43, 11–339.

Treat, C.C., Marushchak, M.E., Voigt, C., Zhang, Y., Tan, Z., Zhuang, Q., Virtanen, T.A., Räsänen, A., Biasi, C., Hugelius, G., others, 2018. Tundra landscape heterogeneity, not interannual variability, controls the decadal regional carbon balance in the Western Russian Arctic. Global change biology 24, 5188–5204.

Van Bellen, S., Garneau, M., Bergeron, Y., 2010. Impact of climate change on forest fire severity and consequences for carbon stocks in boreal forest stands of Quebec, Canada: a synthesis. Fire Ecology 6, 16–44.

Verbyla, D., 2011. Browning boreal forests of western North America. Environmental Research Letters 6, 041003.

Verma, M., Schimel, D., Evans, B., Frankenberg, C., Beringer, J., Drewry, D.T., Magney, T., Marang, I., Hutley, L., Moore, C., others, 2017. Effect of environmental conditions on the relationship between solar-induced fluorescence and gross primary productivity at an OzFlux grassland site. Journal of Geophysical Research: Biogeosciences 122, 716–733.

Volney, W.J.A., Fleming, R.A., 2000. Climate change and impacts of boreal forest insects. Agriculture, Ecosystems & Environment 82, 283–294.

Vourlitis, G.L., Oechel, W.C., 1999. Eddy covariance measurements of CO2 and energy fluxes of an Alaskan tussock tundra ecosystem. Ecology 80, 686–701.

Walker, D.A., Raynolds, M.K., Daniëls, F.J., Einarsson, E., Elvebakk, A., Gould, W.A., Katenin, A.E., Kholod, S.S., Markon, C.J., Melnikov, E.S., others, 2005. The circumpolar Arctic vegetation map. Journal of Vegetation Science 16, 267–282.

Walther, S., Voigt, M., Thum, T., Gonsamo, A., Zhang, Y., Köhler, P., Jung, M., Varlagin, A., Guanter, L., 2016. Satellite chlorophyll fluorescence measurements reveal large-scale decoupling of photosynthesis and greenness dynamics in boreal evergreen forests. Global change biology 22, 2979–2996.

Wang, X., Ouyang, S., Sun, O.J., Fang, J., 2013. Forest biomass patterns across northeast China are strongly shaped by forest height. Forest ecology and management 293, 149–160.

White, J.C., Wulder, M.A., Hermosilla, T., Coops, N.C., Hobart, G.W., 2017. A nationwide annual characterization of 25 years of forest disturbance and recovery for Canada using Landsat time series. Remote Sensing of Environment 194, 303–321.

Williams, T.J., Quinton, W.L., Baltzer, J.L., 2013. Linear disturbances on discontinuous permafrost: implications for thaw-induced changes to land cover and drainage patterns. Environmental Research Letters 8, 025006.

Woodcock, C.E., Allen, R., Anderson, M., Belward, A., Bindschadler, R., Cohen, W., Gao, F., Goward, S.N., Helder, D., Helmer, E., others, 2008. Free access to Landsat imagery. Science 320, 1011–1011.

Wright, M.N., Ziegler, A., 2017. ranger: A Fast Implementation of Random Forests for High Dimensional Data in C++ and R. Journal of Statistical Software 77, 1–17.

Wulder, M.A., White, J.C., Bater, C.W., Coops, N.C., Hopkinson, C., Chen, G., 2012. Lidar plots—A new large-area data collection option: Context, concepts, and case study. Canadian Journal of Remote Sensing 38, 600–618.

Wulder, M.A., White, J.C., Cranny, M., Hall, R.J., Luther, J.E., Beaudoin, A., Goodenough, D.G., Dechka, J.A., 2008. Monitoring Canada's forests. Part 1: Completion of the EOSD land cover project. Canadian Journal of Remote Sensing 34, 549–562.

Xia, J., Chen, J., Piao, S., Ciais, P., Luo, Y., Wan, S., 2014. Terrestrial carbon cycle affected by non-uniform climate warming. Nature Geoscience 7, 173.

Xiao, X., 2004. Modeling gross primary production of temperate deciduous broadleaf forest using satellite images and climate data. Remote Sensing of Environment 91, 256–270.

Yuan, W., Piao, S., Qin, D., Dong, W., Xia, J., Lin, H., Chen, M., 2018. Influence of vegetation growth on the enhanced seasonality of atmospheric CO2. Global Biogeochemical Cycles 32, 32–41.

Zeng, N., Zhao, F., Collatz, G.J., Kalnay, E., Salawitch, R.J., West, T.O., Guanter, L., 2014. Agricultural Green Revolution as a driver of increasing atmospheric CO 2 seasonal amplitude. Nature 515, 394.

Zhang, K., Kimball, J.S., Hogg, E., Zhao, M., Oechel, W.C., Cassano, J.J., Running, S.W., 2008. Satellite-based model detection of recent climate-driven changes in northern high-latitude vegetation productivity. Journal of Geophysical Research: Biogeosciences 113.

Zhang, W., Miller, P.A., Jansson, C., Samuelsson, P., Mao, J., Smith, B., 2018. Self-Amplifying Feedbacks Accelerate Greening and Warming of the Arctic. Geophysical Research Letters 45, 7102–7111.

Zhang, W., Miller, P.A., Smith, B., Wania, R., Koenigk, T., Döscher, R., 2013. Tundra shrubification and tree-line advance amplify arctic climate warming: results from an individual-based dynamic vegetation model. Environmental Research Letters 8, 034023.

Zhang, Y., Guanter, L., Berry, J.A., Joiner, J., van der Tol, C., Huete, A., Gitelson, A., Voigt, M., Köhler, P., 2014. Estimation of vegetation photosynthetic capacity from space-based measurements of chlorophyll fluorescence for terrestrial biosphere models. Global Change Biology 20, 3727–3742.

Zhu, Z., Piao, S., Lian, X., Myneni, R.B., Peng, S., Yang, H., 2017. Attribution of seasonal leaf area index trends in the northern latitudes with "optimally" integrated ecosystem models. Global change biology 23, 4798–4813.

Zhu, Z., Piao, S., Myneni, R.B., Huang, M., Zeng, Z., Canadell, J.G., Ciais, P., Sitch, S., Friedlingstein, P., Arneth, A., others, 2016. Greening of the Earth and its drivers. Nature Climate Change 6, 791–795.

Zhu, Z., Woodcock, C.E., 2014. Continuous change detection and classification of land cover using all available Landsat data. Remote sensing of Environment 144, 152–171.

Zhu, Z., Woodcock, C.E., 2012. Object-based cloud and cloud shadow detection in Landsat imagery. Remote Sensing of Environment 118, 83–94.

Zianis, D., Mencuccini, M., 2004. On simplifying allometric analyses of forest biomass. Forest Ecology and Management 187, 311–332.

Zimov, S., Davidov, S., Zimova, G., Davidova, A., Chapin, F., Chapin, M., Reynolds, J., 1999. Contribution of disturbance to increasing seasonal amplitude of atmospheric CO2. Science 284, 1973–1976.

CURRICULUM VITAE